Low Cost Sonar Based on Echolocation: An Embedded System Approach

Thiago Fernandes Moya Moreira

Dissertation presented to the School of Technology and Management of Bragança to obtain the Master Degree in Industrial Engineering under the double diploma with the Federal University of Technology – Paraná.

Work oriented by:

Professor PhD José Luis Sousa Magalhães Lima

Professor PhD Paulo José Cerqueira Gomes da Costa

Professor PhD Márcio Rodrigues da Cunha

Bragança

2019

Low Cost Sonar Based on Echolocation: An Embedded System Approach

Thiago Fernandes Moya Moreira

Dissertation presented to the School of Technology and Management of Bragança to obtain the Master Degree in Industrial Engineering under the double diploma with the Federal University of Technology – Paraná.

Work oriented by:

Professor PhD José Luis Sousa Magalhães Lima

Professor PhD Paulo José Cerqueira Gomes da Costa

Professor PhD Márcio Rodrigues da Cunha

Bragança

2019

Acknowledgement

First of all, I would like to thank God for giving me the strength and wisdom to conduct this dissertation. Sincerely, I thank my advisor Professor José Lima for the support, guidance and incentive in order to accomplish this work. Also, I would like to express my gratitude to my co-advisors, Paulo Costa and Márcio Cunha, for the availability and supervision during the development of this work. In particular, I thank my parents, Tadeu and Elaine, and my sister Thaysa for the reinforce and always telling me to move on, as well as my friends and colleagues. Finally, I would like to thank the Federal University of Technology — Paraná (UTFPR) and the Polytechnic Institute of Bragança (IPB) for giving me this opportunity.

Resumo

Um dos maiores desafios das aplicações de robôs móveis é a detecção de obstáculos e sua localização. A maioria dos sistemas aplicados para solucionar esse problema pode ser ramificada em dois segmentos: baseado em visão e em não visão. No primeiro, a detecção por câmera e o processamento de imagens são sensíveis as variações nas condições ambientais, além de possuírem alto custo. No segundo segmento, por outro lado, os sensores ultrassônicos se destacam por seus recursos atraentes a um custo acessível e, ao contrário de outros sistemas, são capazes de operar em uma variedade de ambientes. O principal problema do uso desses dispositivos é a dificuldade de manipular corretamente os dados adquiridos, limitando sua eficiência. O presente trabalho enfoca na melhoria e no emprego de um sistema de localização de baixo custo, baseado em sensores ultrassônicos, combinando técnicas trigonométricas e de processamento de sinais. O trabalho está dividido em duas partes: versão processada em MATLAB e aplicação do sistema embarcado. Para a versão em MATLAB, duas técnicas ótimas — detecção de envelope e correlação cruzada — foram avaliadas. Para a abordagem de sistema embarcado, foi implementada a técnica com o melhor desempenho. Em ambas as partes, a validação dos resultados obtidos ocorreu através de um conjunto de medidas com vários objetos em configurações variadas.

Palavras-chave: Sensor Ultrassônico; Detecção de Obstáculo; Robô Móvel; Processamento de Sinal; Sistema Embarcado; Baixo Custo.

Abstract

One of the greatest challenges of mobile robot applications is obstacle detection and its localization. Most systems applied to address this problem can be branched into two segments: vision-based and non-vision based. In the former, camera detection and image processing are sensitive to variations in environmental conditions as well as their high cost. For this reason, this option is not interesting. In the second segment, on the other hand, ultrasonic sensors stand out for their attractive features at an affordable cost and, unlike other systems, are capable of operating in a variety of environments. The main problem using these devices is the difficulty of correctly handling the data acquired, limiting their efficiency. The present work focuses on the improvement and employment of a low cost location system based on ultrasonic sensors, combining trigonometric and signal processing techniques. The work is divided into two parts: processed version in MATLAB and application of embedded system. For the version in MATLAB, two optimal techniques — envelope detection and cross-correlation — were evaluated. For the embedded system approach, the technique with the best performance was implemented. In both parts, the validation of results obtained occurred through a set of measurements with various objects in assorted configurations.

Keywords: Ultrasonic Sensor; Obstacle Detection; Mobile Robot; Signal Processing; Embedded System; Low Cost.

Contents

List of Tables

List of Figures

Acronyms

ADC Analog-to-Digital Converter.

CCR Cross-Correlation.

DC Direct Current.

DSP Digital Signal Processor.

FPGA Field-Programmable Gate Array.

GPIO General Purpose Input/Output.

GPS Global Positioning System.

I2C Inter-Integrated Circuit.

IC Integrated Circuit.

IMU Inertial Measurement Unit.

IoT Internet of Things.

LiDAR Light Detection and Ranging.

MCU Microcontroller Unit.

NCC Normalized Cross-Correlation.

PGA Programmable-Gain Amplifier.

PS Phase Shift.

SCI Serial Communications Interface.

SPI Serial Peripheral Interface.

ToF Time of Flight.

UART Universal Asynchrounous Receiver/Transmiter.

USART Universal Synchronous Asynchronous Receiver/Transmitter.

Chapter 1

Introduction

Ultrasonic sensors offers attractive features at an affordable cost. However, the main problem faced by the use of these devices is that the data obtained are not so easy to interpret, restricting their efficiency. Thus, the intention of the present work is to develop a sound navigation and ranging system, also known as sonar, based on the echolocation principle, which aims to provide accurate measurements and increase the system reliability. For that, mathematical and sophisticated signal processing techniques are exploited. In addition, the proposal is composed of low cost components, intending to demonstrate that their improvement is feasible.

1.1 Overview and Motivation

In mobile robot applications the knowledge of the environment in which the device is inserted and the objects that surround it are essential information for a successful navigation, avoiding collisions and increasing the system safety. For the purpose of achieve this goal, the use of sensors becomes indispensable and its features must be taken into account [1]. Among the different types of sensors, many researches have been exploring the ultrasonic sensors to deal with this problem, attracted by the flexibility in several environments and applications where vision based sensors fail due to some constraints as low visibility, mirrors or clear objects [2].

Typically, the employment of ultrasonic sensing in an industrial or commercial atmosphere is limited to simple tasks, that do not require optimal measurements. The leading reason for this scenario is due to the fact that the data obtained from the commercial ultrasonic range-finders are not easy to be interpreted. Therefore, the literature has shown a great interest in investigating the use of these sensors for complex applications [3]–[5]. The result of a measurement performed by a standard sensor occurs through an ultrasonic burst with a single frequency, which can range from 40 kHz to 50 kHz. The distance is calculated using the Time of Flight (ToF) when the echo emitted from the transmitter reflects an obstacle or object and returns back to the receiver [6]. In general, the reflected signal is detected by a predefined trigger level, however this method is not so efficient [7]. Thus, to improve the system accuracy, some enhanced approaches have combined advanced signal processing techniques [8], [9].

Conventional ultrasonic range-finders mostly are composed of a single transmitter and a single receiver or a transducer that acts as both. The main disadvantage of this system is the wide beam of the emitted signal, causing a very poor resolution. Furthermore, other phenomena like the multi-reflection effect may arise and cause false positives. In order to reduce these issues, a system that contains at least two receivers and a transmitter is needed [6].

The best known example that use ultrasonic navigation are the bats. They are able to avoid obstacles even at high speeds when flying in the dark [10]. The main difference between an ultrasonic range finder and the bat is that it has two ears, which allows them to detect which direction the echo comes from [6]. Inspired by the echolocation of the animals, this work proposes a binaural sonar based on accuracy techniques, addressing the issues associated with the use of ultrasonic measurements in indoor environments.

1.2 Objectives

The main objective of this work is to develop a solution based on low cost elements to provide with accuracy the detection and/or motion of objects, getting their coordinates in a two-dimensional space. Also, other objectives make up this work, as follows:

- Develop an algorithm in MATLAB addressing the envelope detection and Cross-Correlation (CCR) method;
- Analyze the typical behavior of an ultrasonic wave and verify the need to condition the signal;
- Evaluate and implement the designed versions in MATLAB using STM32;
- Perform the transition of the selected approach from MATLAB to ESP32 using the C++ programming language;
- Accomplish and evaluate a new set of measurements with the proposed methodology in assorted conditions.

1.3 Document Structure

This document is divided into six chapters, describing the study conducted during the dissertation. The first chapter introduces the challenge of objects detection and their location applied for mobile robots, and a low cost sonar based on mathematical and signal processing techniques is proposed.

The second chapter briefly analyzes the emergence of mobile robots and addresses their needs based on real applications. Next, is contextualized the related work to obstacle detection systems and the tools adopted to deal with this issue, focusing on ultrasonic applications. Lastly, an analysis about signal processing techniques and embedded system used in robotics is accomplished.

The third chapter presents the theoretical background and the study of tools enforced in this work. Initially is approached the basic principle of ultrasonic sensing and its characteristics, as well as the most typical arrangements. After that, the main distance methods based on ToF are discussed and evaluated. Following, necessary signal processing and mathematical techniques, such as filtering, sampling and interpolation are reviewed. Ultimately, the triangulation concept is explained highlighting essential aspects.

The fourth chapter discusses the implementation specifying the adopted elements that composes the hardware design. On the sequence, is elucidated the procedure of data acquisition, making clear the endorsed configuration. Then, the data management and how the data handle occurs is exposed. At last, the system settings described through particular features, such as angles and baselines, and the selected objects to act as target are expressed, followed by experimental tests process.

The fifth chapter is devoted to the exposition of results obtained through the experimental tests, intending to validate the proposed methodology. In addition, this chapter contains an assessment comparing possible approaches to be implemented in the final system. Finally, the sixth chapter presents a discussion about the results followed by conclusions. Additionally, ideas or suggestions for future work are drawn.

Chapter 2

Related Work

In this chapter will be analyzed the related work to sensing systems and its tools, focusing on mobile robot applications. Taking into account the developed work and the concern for successful prevention of obstacles, this chapter introduces the state of the art.

2.1 Mobile Robots and Obstacle Detection

Industrial manufacturing has an essential role in the success of robotics. Robotic arms, or manipulators, annually produces significant revenues for the industry. Attached to a specific position in the assembly line, these devices can move quickly and accurately to perform repetitive tasks such as spot welding and painting. Due to the fact of the manipulators are fixed, this implies in a limited range of motion that depends where it is screwed [11]. The ability to move indoors, collect surroundings information and adapt to environmental changes are factors that when combined provide flexibility for the robot, making its operation most effective. This type of robot is known as mobile robot [12].

Mobility enables the accomplishment of different types of actions in several types of environments, simplifying and helping human tasks. For this reason, researches has shown how mobile robots can be useful in areas other than industry, such as rehabilitation [13], rescue operations [14], [15] and surveillance [16]. When a robot or any other mobile platform needs to interact with the place which it is inserted, is expected it be able to

navigate, and for a reliable navigation, proper information about static and dynamic ambience are required [17].

Regardless of the area, safety is an important feature to consider when there is the presence of individuals and/or machines. Intending to ensure that all participants are safe, object prevention systems should be designed. In general, if an obstacle detection occurs, a warning is transmitted to the controller device to prevent a collision. After that, the robot is capable to recalculate its path and return to its routine [13]. The capacity to carefully travel through obstacles is a difficult task for autonomous mobile robots and is still a well-researched topic in robotics [18].

The presence of barriers and unknown environments become the path planning more difficult, then, aiming to deal with this problem detailed information are acquired from different sources. These information allows to find out the robot's position and obstacles location, using technologies such as Global Positioning System (GPS) [19], acoustic [20] and optical [21] systems.

2.1.1 Navigation Assistance Tools

A great challenge of mobile robot navigation is the detection of targets and their location. Thus, auxiliary devices have been widely exploited, and most systems employed to assist in this assignment are vision and non-vision based [22]. In vision based systems, the Light Detection and Ranging (LiDAR) is that is typically used. It is a remote sensing technology that emits light beams and measures the time it takes for reflections to be detected by the sensor. Then, from the collected data is possible to calculate the distance value of nearby objects [23].

An obstacle detection and obstacle avoidance algorithm based on visibility graph method is discussed in [24]. The authors justify choosing LiDAR due to its wide use, as well as some advantages such as accuracy, large detection range and fast sweep frequency. Experimental tests carried out outdoors provided satisfactory results using this method, though it was applied in a simple situation.

Alternatively there is the GPS, which was developed and is maintained by the U.S. Department of Defense based on satellite technology. The fundamental technique of this system is to measure the distance between the receiver and a few simultaneously observed satellites. The most important applications of GPS are positioning and navigation, although its operating is complex. It comprises the knowledge of electronics, orbital mechanics, atmosphere science, geodesy, relativity theory, mathematics, adjustment and filtering as well as software engineering [25].

GPS-based navigation has been successful in non-urban areas, while navigation in the urban ones is still a challenge. In these cases, GPS truthfulness drops sharply as result to multiple signal reflections. So, Maier and Kleiner [26] set up an improved GPS sensor model for mobile robots in urban terrain, generating a 3D representation of the surroundings of the robot and detecting obstructed satellites. The approach has been applied with an Unscented Kalman filter (UKF) fusing data from odometry, Inertial Measurement Unit (IMU) and GPS, using the new technique for improving pose estimation.

The acoustic sensors also are applied to deal with this problem, particularly that ones based on ultrasonic. Commonly, these sensors are composed by an emitter and a receiver. The transmitted signal is propagated with frequencies between 40 kHz, for piezoelectric transducers, to 50 kHz, for electrostatic transducers. Similar to LiDAR, its working principle is calculated by the time it takes for the emitted signal to be reflected back into the receiver [6]. Ultrasonic signal allows to provide particular information about detected objects, and it is one of the few types of emissions that can easily pass through blurred materials. Furthermore, ultrasonic has become an acknowledged and valuable tool for better comprehension the properties of solids and liquids [10]. However, these sensors are not restricted to robotics and are used for agriculture, archaeology, medicine and other fields.

A robot that can move flexibly, adjust its own movement speed and inclination angles in an adaptive manner requires appropriate architecture. Thus, Ruan and Li [27] built a two-wheeled self-balanced robot, adopting an ultrasonic ranging system combined with a fuzzy control method. Simulation and real tests have characterized that this proposal

can successfully perform independent obstacle prevention in an unknown environment.

2.1.2 Localization and Sensing Systems

The concern about techniques for moving a robot to a remote location and performing useful tasks autonomously, without human interaction, emerged many years ago. In 1977, Lewis and Johnston [28] published a technical report sponsored by National Aeronautics and Space Administration (NASA) describing the development of a laser range finder created in a robot research program, which the main purpose of this work was to locate and manipulate rock samples on the surface of a planet.

In 1998, a novel hardware system structure and digital signal processing algorithms for the localization of an autonomous mobile robot by fusing dead-reckoning and ultrasonic measurements was introduced. Some researchers tried to improve the accuracy of dead-reckoning, using encoded magnetic compass and IMU, nonetheless, these attempts were not promising. A suitable option was to use ultrasonic sensors, providing a highly robust and reliable orientation estimate, besides completely eliminating the cumulative location error caused by wheel slippage or surface roughness [29].

In 2001, Harper and McKerrow [30] presented a plant recognition technique using ultrasonic sensing for mobile robots. A system capable of recognizing plants is very useful for navigation, especially in agricultural applications. Systems based on others sensing technologies has succeeded navigating in these environments, but only in highly constrained scenarios. This research led to the conclusion that the correlation of echoes from many orientations show that plants can be recognized with sufficient accuracy for navigation.

In 2004, a self-location system able to operate in several places was developed by Lee, Lee, An, *et al.* [31]. The ultrasonic satellite system (U-SAT) for positioning of mobile robots adopts the distance measurement process of ultrasonic signal and the coordinate acquisition of GPS. The proposed method does not yield any accumulated estimation errors and obtains the exact position of the robot. The only constraint of this scheme is

the limited area of activity, though the cost of U-SAT is affordable.

When multiple robots are inserted into the same work space the complexity of their actions increases, to safely move or share its position information requires the ability to localize each other. Determining where the robots are located can be achieved through vision, i.e. cameras and optical gadgets, but the use of these devices is not cost effective. In this way, a mobile ultrasonic relative positioning system (URPS) to detect the distances and the angles of surrounding robots is proposed in 2008 by Rivard, Bisson, Michaud, *et al.* [32]. The system demonstrates proper performance for midsize robots in indoor applications, and having the system placed directly on the robots, make it interesting for search and rescue missions in hazardous locations.

Over the past decades, artificial intelligence researchers have developed many methodologies for the improvement of robotic software. One of these approaches, probabilistic robotics, has led to systems with exceptional levels of autonomy and robustness. Basically, probabilistic approach to robotics is represent information through mathematics. In this sense, Adiprawita, Ahmad, Sembiring, *et al.* [33] implemented in 2011 a localization algorithm using a particle filter, through a probabilistic technique for mobile robots. From the experiments, it can be concluded that the algorithm used had a good efficiency aided by ultrasonic sensors.

An important property that is expected from humanoid robots is their agile and flexible walking in an environment that is quite adapted to humans. For many years, sensors have been used to accomplish many tasks in robotic fields because they are easily integrable, inexpensive and accurate. In this context, Chassagne, Bruneau, Bialek, *et al.* [34] established a system composed of a set of ultrasonic emitters and receivers for direct sensing of 3D relative position and orientation of a humanoid robot feet. The operation of this arrangement is based on ultrasonic measurements and triangulation process. Experiments proved an accurate enforcement with resolution lower than 1 mm and the capability of the system to be executed in walking behaviour.

2.2 Signal Processing Applied in Robotics

Signal processing theory plays a fundamental role in the advancement of digital communication and automation systems. Numerical models are applied in signal processing, and in decision making of systems, for obtaining data from a signal that may be noisy, distorted or incomplete. Among the different signal processing methods, their applications include radio, speech recognition, telephony and those related to robotics, i.e. vision, radar, sonar and any system associated to communication or information processing [35].

In subsection 2.1.2, it is possible to notice that the use of sensors in localization and sensing systems is indispensable for mobile robot navigation. However, sensors are not perfect, and their estimation are subject to errors. Merging data from multiple sensors provides a general estimate of the position whose error is smaller than if a single sensor were used and, in most cases, a larger amount of sensor input data produces more accurate estimates. In 2015, Moore and Stouch [36] developed a software addressing the sensor fusion needs with the implementation of an Extended Kalman Filter (EKF) for the Robot Operating System (ROS). This filter acts like an estimator for the quadratic linear problem, which consists in reckoning the state of a linear dynamic system corrupted by noise and inaccuracy [37].

In order to prevent inconsistent data and maintain system reliability, Básaca, Rodríguez, Sergiyenko, *et al.* [38] modeled a Butterworth low pass filter on the input signal to improve the resolution of the dynamic triangulation method for the robot navigation 3D vision system. Also, Qi, Lam, Qian, *et al.* [39] resorted to some signal processing techniques, including Codomain, Average, Median and Chebyshev filtering to design an optimal arc tracking on an eight-axis robot system for welding industry.

Senses like vision and hearing are key elements in the development of mobile humanoids. Although robotic vision systems have evolved considerably in recent years, robotic audio perception, particularly binaural audition, is still under development. Thus, Keyrouz [40] introduced an advanced binaural sound localization in 3D for humanoid robots, applying sophisticated techniques of signal processing to increase the localization

resolution in a reverberant environment. This approach was able to accurately localize sound sources in three dimensions aiming the real-time implementation in robotic platforms.

Most systems focused on mobile robotics applications are designed for real-time purposes. Therefore, Shen [41] established an efficient Normalized Cross-Correlation (NCC) calculation method for stereo vision based robot navigation. The NCC is an important tool to support navigation systems, mainly that based on acoustic and vision devices, and in this research was possible generates the same results as the traditional NCC with a much lower computational cost.

2.3 Applications of Embedded Systems

Embedded system can be described as an information processing system integrated into a single product. In general, these systems presents several types of characteristics, including real-time constraints, low cost, reliability and efficiency requirements. Integrated system technology is indispensable for supplying comprehensive information, which is one of the major goals of the information technology field [42], [43].

A relevant analysis is performed in Malinowski and Yu [44], making the comparison of main embedded systems platform, such as Microcontroller Unit (MCU), Field-Programmable Gate Array (FPGA), Digital Signal Processor (DSP) and Integrated Circuit (IC) for specific applications. The authors defined three cases of study to accomplish the inquiry, containing an industrial control, a mobile robot navigation system and a computationally control system. Besides that, they states that embedded system when compared with computer platform presents a less power of computation, as well as a limited memory size. However, for solving real-time tasks, its disadvantages are offset, due to the fact of embedded systems are inexpensive and easier to design.

Kuo, Yeh, Wu, *et al.* [45] presents the development of an autonomous robotic wheelchair using embedded systems. The authors mention that in most research on autonomous wheelchair the personal computer is employed, nevertheless, this type of device is not

suitable to the users, as a result of improper size, lower reliability and high power consumption. On the other hand, an embedded system can provide a smaller size, better reliability and low power consumption. Similarly, an embedded system comprising a MCU and a network of ultrasonic sensors is proposed in [46], aiming to design an electronic navigation system for visually impaired and blind people.

Chapter 3

Study of Tools

This chapter will introduce the theoretical background and the methodology enforced to attain the established objectives. Important aspects about ultrasonic sensing, distance estimation and signal processing techniques are addressed.

3.1 Ultrasonic Sensing

Before choosing which approach is adopted, a brief overview is given about the main devices to deal with the obstacle detection issue. As previously mentioned, most detection systems are vision and non-vision based. In systems based on vision, the detection through cameras and image processing are sensitive to the variation in environmental conditions like darkness, foggy or low visibility [22]. As well, the computational consumption and the price of these systems are still high [6].

Systems based on acoustic sensors, particularly the ultrasonic sensors, have many advantages over other methods. As an example, in applications that requires reduced size the modules can be very small without interfering in their performance, and it is capable of operating in several environments in which other devices can not be used [47]. In addition, ultrasonic signal can easily penetrate opaque objects, whereas many other types of radiation such as visible light cannot [10].

Just like the visible spectrum, the audio spectrum is similar to the standard human

perception and reaches frequencies from 20 Hz to 20 kHz, although, according to age, the upper limit can be reduced considerably. In this context, ultrasonic is classified as a inaudible signal with band above 20 kHz, which can rises in the MHz band and when it reaches 1 GHz, become what is typically called the hypersonic regime [10]. However, in this work only the first phenomena is explored.

The operating principle used by this type of sensor is based on the ToF estimation. The transmitter generates an ultrasonic pulse which propagates through the air and when it detects a target the signal is reflected back to the receiver [48]. Equation 3.1 shows how the distance measurement is achieved from the estimated ToF.

$$d = \frac{c \cdot T_f}{2} \tag{3.1}$$

where c is the speed of sound and T_f is the ToF.

The determination of the speed of sound in air can be established as a function which depends on the temperature θ, and to a lesser extent, on the air humidity h

$$c = f(\theta, h) \tag{3.2}$$

Taking into account the humidity as a random variable uniformly distributed in the interval of 10% to 90% of Relative Humidity (RH), its influence on the speed of sound is about 0.15% at 20°C, becoming negligible. Following the analysis, Equation 3.3 describes the speed of sound estimate according to the temperature.

$$c \approx 20.0055 \cdot \sqrt{T} \tag{3.3}$$

where T is the absolute temperature (in Kelvin). For temperatures changes between 0 - 40°C is expected the speed of sound in the range of 330 - 360 m/s. Clearly, this event has a considerable impact on the measurements. Therefore, it is highly recommended to consider it.

3.2 Distance Estimation Methods

Estimating how far a target or object is, represents an important data which involves many fields of study, besides that, distance information is useful in locating, mapping, tracking, focusing on the camera lens and in various industrial applications [49].

The main approaches to determine the distance through ultrasonic waves are given by the Phase Shift (PS) and ToF. The first strategy comprises the continuous calculation of the PS between the transmitted and received signal. In this case, it is only possible establish, without ambiguity, distances up to a wavelength (λ). This happens due to the fact that a phase variation from 0 to 2π is equal to a distance variation from 0 to λ. As an example, an ultrasonic system that is operating at 40 kHz, at 20°C, would only be able to determine, without uncertainty, distances up to 8.6 mm, which is a very narrow measurable range for most applications. The second strategy, unlike the first one, allows to measure greater distances and consists in determining the time that a wave takes to reach the receiver [50], [51].

There are several methods for estimating the ToF, in the following subsections the most common techniques are presented.

3.2.1 Threshold Detection

This form is the simplest and fastest way to calculate the ToF. It involves transmitting and detecting the arrival of an ultrasonic wave when the received signal exceeds, for the first time, a predefined threshold level, as seen in Figure 3.1. There are some benefits to using this method, it requires no complex computation and can be performed with simple circuitry. The main problem of this method is that it typically estimates a higher ToF compared to the actual one. This happens due to the long rise time of the signal, added to other factors, such as low signal-to-noise ratio (SNR) and inherent bias [8], [51].

As noise increases the likelihood of incorrect readings also increases, and systems that use threshold as a reference value are vulnerable to this type of error. In low SNR conditions, it is recommended to amplify the signal, or equivalently, adjust the detection

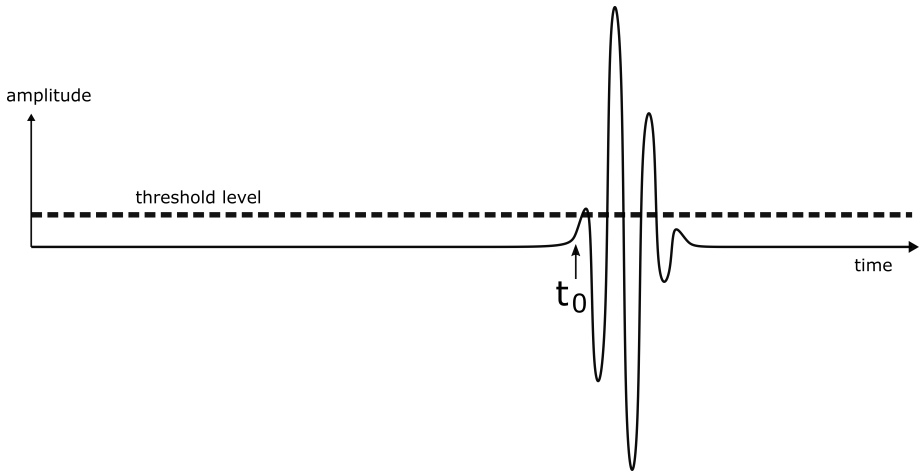

Figure 3.1: Threshold detection method. Adapted from [52].

threshold in order to reduce the system uncertainty. According to [8], the inherent bias occurs for two reasons: the first is that no matter how good the transducer performance is, there will always be a rise time when a signal is detected; the second and most crucial is the threshold level setting, this is a critical factor for the bias, because if a low threshold is set the occurrence of false positives tends to increase.

3.2.2 Cross-Correlation

Supposing two real functions $f(x)$ and $g(x)$, if CCR is applied it will produce a new function $c_{f,g}$ also in the x domain. Basically, the CCR function indicates the relative amount of agreement between two given functions for all possible degrees of displacements; i.e. this function is a estimation of similarity between $f(x)$ and a moving copy of $g(x)$, which gets its maximum value at the point representing the displacement of g for which its similarity with f is the highest. Although its operation is similar to convolution, there is an important difference: the function $g(x)$ is not rotated as in convolution [53].

Assuming ToF estimation as a time delay issue, it is possible to imagine that when a generated ultrasonic signal $s_T(t)$ propagates in the air and is reflected, the time between the transmission and the reception of the signal is established by a delay τ. Thus, techniques for calculate the time delay should be employed. Among them, CCR, has been

highlighted [54]. As an example, when the CCR is used in the transmitted and received signal the result is a peak at the time delay t_0 (Figure 3.2) which allows to determine the ToF measurement. In this case, the CCR $c(t)$ can be defined by:

$$c(t) = \int_{-\infty}^{+\infty} s_T(t) s_R(t+\tau)\ d(\tau) \tag{3.4}$$

where $s_T(t)$ is the transmitted signal, $s_R(t+\tau)$ is the signal received and shifted in time.

Graphically, this operation can be represented using a move and multiply interpretation. So, Equation 3.4 can be rewritten as two sequences of sampled signals in order to simplify its application, as follows:

$$c(t) = \sum_{n=-\infty}^{\infty} s_T(n) s_R(n+\tau) \qquad \tau = 0, \pm 1, \pm 2, ... \tag{3.5}$$

This approach has noise reduction properties, because the CCR of random noise is almost zero, thus additive noise is decreased with its application. Furthermore, CCR can be improved depending on the signal design, i.e., a frequency-modulated (FM) signal yields a limited cross-correlated peak (Fig. 3.2) than that acquired by a single frequency tone-burst [8].

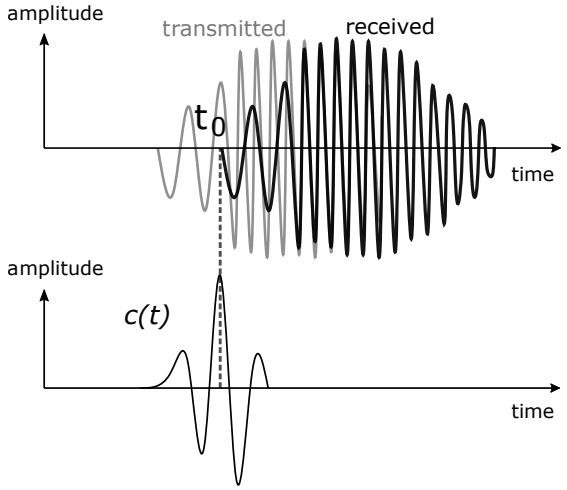

Figure 3.2: Cross-correlation method. Adapted from [8].

3.2.3 Envelope Detection

Envelope detection is an alternative to the other methods previously mentioned, which can be assumed as an intermediary version between threshold detection and CCR. In [55] a comparison made from the most usual procedures of ToF estimation demonstrated that envelope detection obtained satisfactory results, only losing to the CCR. However, in terms of computational processing this technique is most convenient.

In systems involving amplitude modulated (AM) signals, to recover the original signal, a reverse process, also known as demodulation, must be applied. The typical strategy to solve this task is the envelope detection (Figure 3.3), and its accomplishment can be achieved in the analog or digital domains. In the former, a common circuit is shown in Figure 3.4 and its operating principle is similar to a half-wave rectification. Another techniques such as full wave rectification and synchronous demodulation also are commonly used [56], [57].

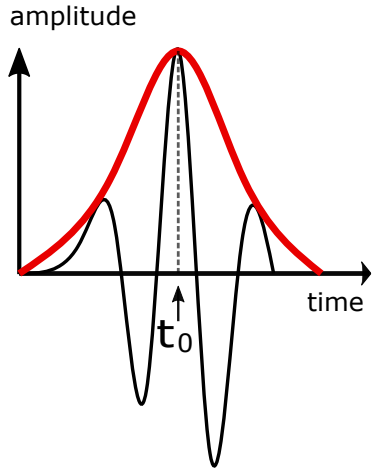

Figure 3.3: Envelope extracion of an echo signal.

Created many years ago, this scheme has an important role in engineering applications, especially in the field of communication. It is a simple circuit, which might be used as an example to illustrate many complex circuit analysis techniques on a circuit containing only three elements. As shown in Figure 3.4, the input signal is passed through a diode, where the negative part is removed. After that, the diode can be followed by a low-pass

filter, eliminating the high-frequency spikes and restoring the low-frequency signal, i.e., the original information [57].

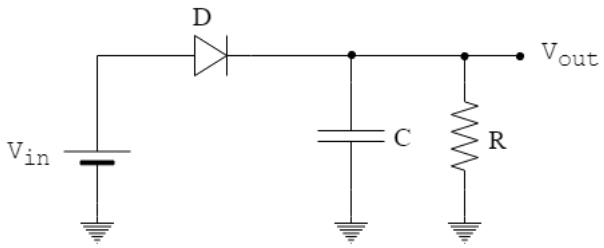

Figure 3.4: Circuit diagram of an analog envelope detector. Adapted from [56].

In digital domains, approaches that extract the analytic signal magnitude are explored. For this purpose, the Hilbert transform is commonly used to generate an analytic signal from a real signal, whose absolute value represents the envelope of the echo signal received [55]. The analytical signal $y(t)$ of a real signal $x(t)$ is defined by:

$$y(t) = x(t) + jh(t) \tag{3.6}$$

where $h(t)$ is the Hilbert Transform of $x(t)$ and $j = \sqrt{-1}$. The magnitude of the analytic signal, which is identical to the real signal, is called envelope as seen in Figure 3.3. Thus, from the envelope extraction it is possible to locate the peaks and determine the time between sending and receiving the echo signal. Hence, the problem of setting the threshold level is eliminated. This technique offers great precision, however it has a high computational consumption, involves complex calculus and in certain cases this method may be unstable [58]. For this reason, alternative approaches have been studied.

In [59] a novel method using interpolation to extract the envelope from a signal is introduced. Interpolation is one of the most important methods of numerical approximation, which allows to establish new data points from a set of known data points and is discussed in the following section.

3.3 Interpolation Concept

All analysis presented in this section is extracted from Ruggiero and Lopes [60]. Interpolate a set of data or a function $f(x)$ consists of approximating this function by another function $g(x)$. Therefore, the function $g(x)$ is used instead of the function $f(x)$.

The need for this replacement arises in various situations, for example:

i. When only the numerical values of the function are known for a set of points and it is necessary to calculate the value of the function at an unknown point;

ii. When the function under study has such expression that operations such as differentiation and integration are difficult to perform.

Considering $(n+1)$ distinct points: $x_0, x_1, ..., x_n$ called nodes of interpolation, and the values of $f(x)$ at this points: $f(x_0), f(x_1), ..., f(x_n)$. The interpolation form of $f(x)$ consists in obtaining a given function $g(x)$ such that:

$$\begin{cases} g(x_0) = f(x_0) \\ g(x_1) = f(x_2) \\ \quad . \qquad . \\ \quad . \qquad . \\ \quad . \qquad . \\ g(x_n) = f(x_n) \end{cases}$$

In this study it is adopted that $g(x)$ belongs to the category of polynomial functions. Thus, given the points $(x_0, f(x_0)), (x_1, f(x_1)), ..., (x_n, f(x_n))$, so $(n+1)$ points, it is desired to approach $f(x)$ by a polynomial $p_n(x)$ of degree less than or equal to n, as follows:

$$f(x_k) \;=\; p_n(x_k) \qquad k = 0, 1, 2, ..., \; n \tag{3.7}$$

where $p_n(x)$ is represented by:

$$p_n(x) = a_0 + a_1x + a_2x^2 + ... + a_nx^n \tag{3.8}$$

Therefore, getting $p_n(x)$ means getting the coefficients $a_0, a_1, ..., \ a_n$. Although there are several ways to obtain $p_n(x)$, an efficient and simple manner is using the Lagrange Polynomial, which is introduced in the subsection 3.3.1.

3.3.1 Lagrange Polynomial

Assuming $x_0, x_1, ..., \ x_n, (n+1)$ be distinct points; $y_i = f(x_i), \ i = 0, ..., \ n$ and $p_n(x)$ the polynomial with degree $\leq \ n$ that interpolates f in $x_0, ..., \ x_n$; so $p_n(x)$ can be described as $p_n(x) = y_0L_0(x) + y_1L_1(x) + ... + y_nL_n(x)$, where the polynomials $L_k(x)$ are of n degree. For each i, the condition $p_n(x_i) = y_i$ must be met, i.e.:

$$p_n(x_i) = y_0L_0(x_i) + y_1L_1(x_i) + ... + y_nL_n(x_i) = y_i \tag{3.9}$$

The simplest way to satisfy this condition implies in:

$$L_k(x_i) = \begin{cases} 0 \ if \ k \neq i \\ \\ 1 \ if \ k = i \end{cases}$$

and for that, $L_k(x)$ is defined by:

$$L_k(x) = \frac{(x - x_0)(x - x_1) \ ... \ (x - x_{k-1})(x - x_{k+1}) \ ... \ (x - x_n)}{(x_k - x_0)(x_k - x_1) \ ... \ (x_k - x_{k-1})(x_k - x_{k+1}) \ ... \ (x_k - x_n)} \tag{3.10}$$

In conclusion, the Lagrange form for the interpolation polynomial is:

$$p_n(x) = \sum_{k=0}^{n} y_kL_k(x) \tag{3.11}$$

where

$$L_k(x) = \frac{\prod_{\substack{j=0 \\ j \neq k}}^{n} (x - x_j)}{\prod_{\substack{j=0 \\ j \neq k}}^{n} (x_k - x_j)}$$

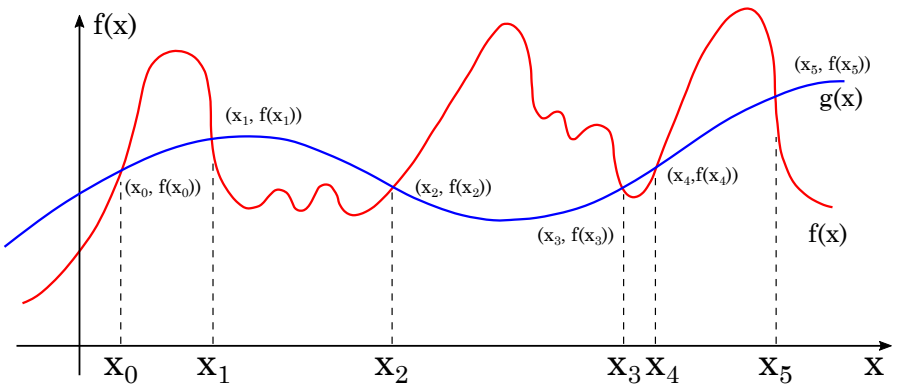

Figure 3.5: Interpolation of a function $f(x)$ with $n = 5$, as an example. Adapted from [60].

3.4 Ultrasonic Sensor Arrangements

Conventional ultrasonic range-finders mostly are composed of a single transmitter and a single receiver or a transducer that acts as both. The main disadvantage of this system is the wide beam of the emitted signal, causing a very poor resolution. Furthermore, other phenomena like the multi-reflection effect may arise and cause ambiguity [6]. In this sense, increasingly, approaches based on ultrasonic sensors have required improvements and greater reliability in their applications. Thus, systems adopting different schemes from traditional ones, including the use of multiple sensors, are proposed in several researches [1], [2], [61], [62].

Although the monaural, triaural and systems containing array of sensors does not apply in the proposal of the present work, a short overview is performed in this section.

3.4.1 Monaural Sensor System

The monaural scheme is basically a conventional ultrasonic ranging system, composed of a single transducer. The standard mode of operation is to transmit an acoustic signal in the air and measure the duration until it is reflected by some object through a receiver. The distance d can be obtained from Equation 3.1.

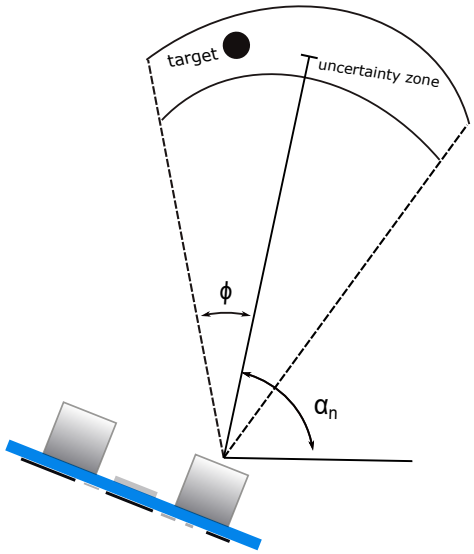

Figure 3.6: The beam width of a single sensor. Adapted from [63].

As previously mentioned, the beam width of these sensors is large (Figure 3.6), becoming unfeasible to locate the target using just one sensor. Furthermore, only the first reflection is measured in this configuration, making the amount of information obtained extremely limited [63]. However, this arrangement can be suitable for applications that require simple information, such as the presence of a distinct object [64] or liquid level detection [65].

3.4.2 Binaural Sensor System

The binaural sensor arrangement, as seen in Figure 3.7, aims to combine the use of a few ultrasonic sensors to provide more detailed spatial information and/or map the environment. According to Kreczmer [6], the disadvantages of a single sensor are significantly

reduced when a multi-sonar system is employed. This scheme consists of two or three ultrasonic sensors, as long as there is a transmitter and two receivers. In the present work it is used three sensors, one of which acts as a transmitter (Sensor C) and the other two as a receiver (Sensors A and B); moreover, it is assumed that the propagation of sound waves occurs in a horizontal plane, equivalent to the two-dimensional (2D) space. Thus, the location of an object is defined by the region of intersection with the horizontal plane through the sensors A and B, called detection area, as shown in Figure 3.8.

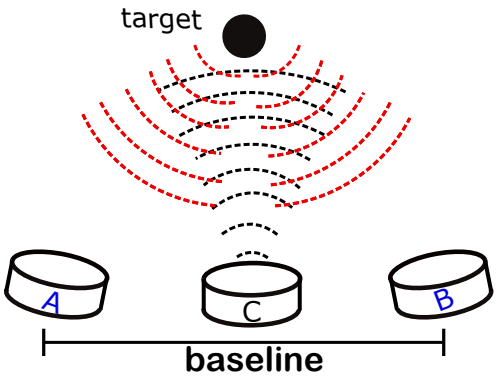

Figure 3.7: The proposed binaural sensor arrangement.

The receivers are separated by a known baseline (l) that allows locating the detected objects in a planar environment, estimating the ToF between the object and each sensor. Then, the distance calculation can be solved applying trigonometric techniques which are covered later. Also, fixing the angle and baseline it is possible to change the detection field when the two ultrasonic beam patterns overlap.

The ideal positioning of the system is defined by the baseline and the α angle, as can be seen in Figure 3.8. The maximum width of the detection area occurs when the beam patterns overlap completely, that is, with a close distance and the sensor is perpendicular to the x axis. When the width is small, as in Figure 3.10(b), the behavior is similar to a monaural system. When the width is larger, as shown in Figure 3.10(a), it is possible to expand the coverage area. By adjusting the angle of rotation the points of intersection can increase or decrease, and the mapping of all valid positions for the detection can be made by tracing arcs with fixed distances in the locating cone.

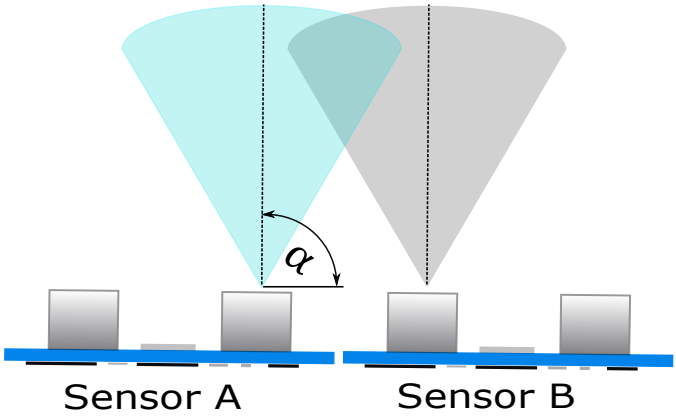

Figure 3.8: Detection area formed by the beam patterns. Adapted from [66].

3.4.3 Triaural Sensor System

The triaural design consists of a transmitter and three receivers. This configuration, and configurations with array of sensors can be considered an effective approach to detect targets in three-dimensional (3D) space. In addition, it is also possible to recognize the shape of the detected objects. However, accomplishing these tasks requires complex procedures and heavy computational consumption, resulting in a higher cost. Below, a brief outline about object classification using these systems is introduced.

Conforming to Kreczmer [6], information acquired from a single measurement are not enough to classify the targets. Reinforcing this statement, Kleeman and Kuc [67] proved that at least two measurements are required using ultrasonic transmitters located at different places. Signal paths for the usual classifications (edge, wall or corner) are shown in Figure 3.9. The first measurement is achieved by T_1 as an emitter and the second is performed by T_2; it is supposed that during both measurements the sensors are switched into receiving mode after the ultrasonic burst.

In all drawings the virtual image approach is applied. The edge case does not follow exactly this technique, but this sketch makes easier to notice some relations. Taking into account geometrical figures created through signal paths and their virtual images, is possible to establish a single condition for each case, as follows:

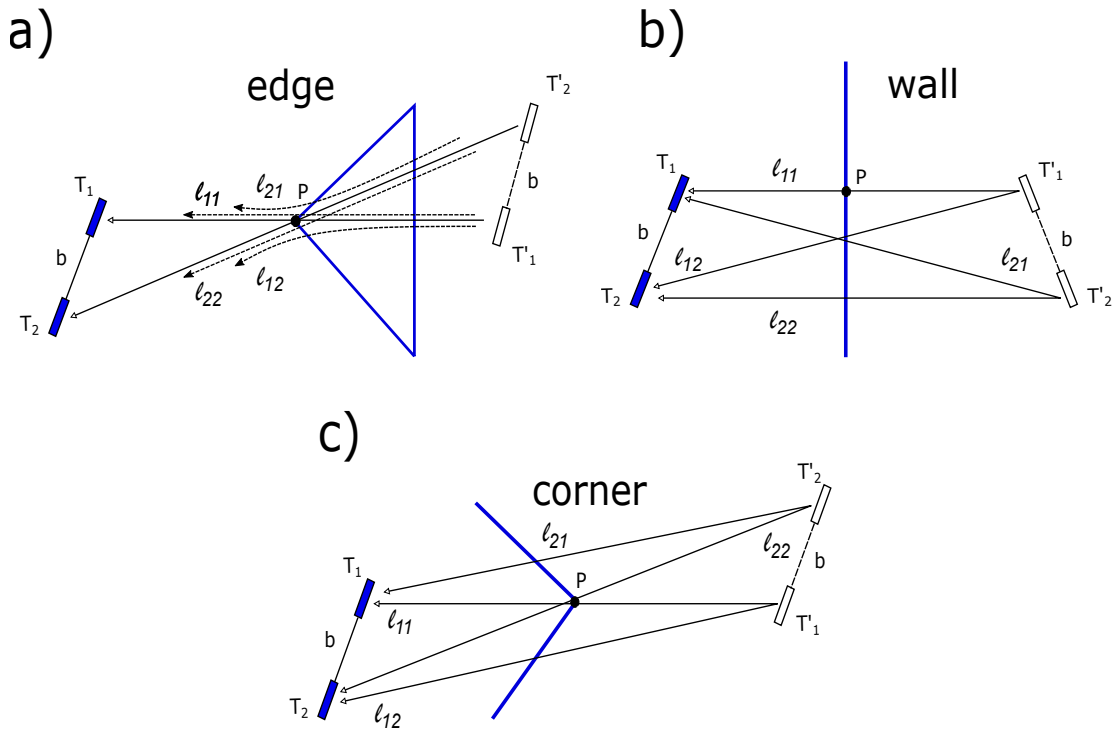

Figure 3.9: The virtual images of the ultrasonic system and signal paths for all cases. Adapted from [6].

$$\begin{aligned} edge \;\rightarrow\; & l_{12} + l_{21} - l_{11} - l_{22} = 0, \\ wall \;\rightarrow\; & (l_{12} + l_{21})^2 - 4b^2 - 4l_{11}l_{22} = 0, \\ corner \;\rightarrow\; & (l_{12} + l_{21})^2 + 4b^2 - 2l_{11}^2 - 2l_{22}^2 = 0, \end{aligned} \tag{3.12}$$

In Peremans and Chen [68], the Maximum Likelihood Estimation and Neural Network are exploited to solve this issue, based on similar conditions to those given above. In order to get a sense of the complexity of the problem, the introduced overview about object classification is just one of the simplest ways to accomplish it and is poorly accurate. There are more details to be studied, but the analysis will not be deepened, as it is out of focus of this work.

3.5 Signal Processing Techniques

Signal processing involves techniques that aims to improve strongly the understanding of information contained in several means. It is defined as an electrical engineering segment that models and analyzes data representations of physical events, responsible for all the technology used in our daily lives such as computers, mobile phones, radios and videos, i.e., is the science behind our digital lives and its investigation enables the enhancement of the ability to communicate and share information [69].

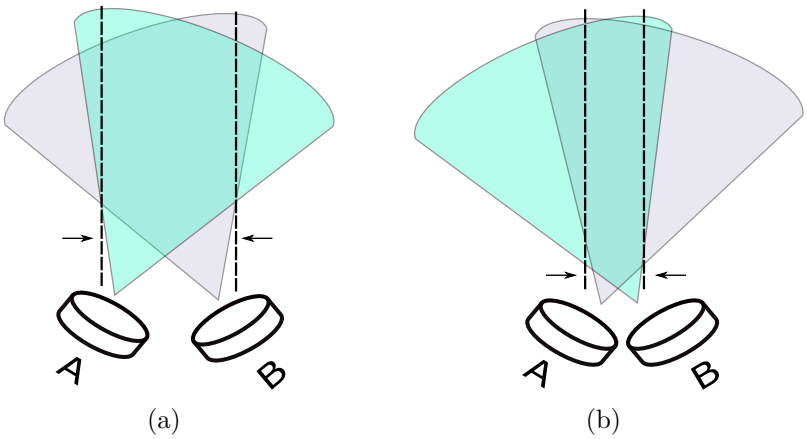

(a) (b)

Figure 3.10: (a) Wide overlap region and (b) Thin overlap region. Adapted from [66].

3.5.1 Sampling

In general, sampling is the technique which consists in collect a continuous time or frequency signal and represent it by a series of discrete data points. Basically, the sampling process establishes the value of a signal over a predefined frame of time [70].

According to Pelgrom [71], the sampling frequency f_s defines this frame and determines the sampling times, as follows:

$$t = \frac{n}{f_s} = nT_s, \qquad n = -\infty, ..., -3, -2, -1, 0, 1, 2, 3, ..., \ \infty \tag{3.13}$$

Between the sampling moments, there is a time period T_s, which in mathematical terms no value is defined. In practice, this time period is applied to perform operations

on the sample sequence; the set of operations, i.e. summation, multiplication or delay, constitute the class of time-discrete signal processing. In this analysis T_s is considered as a constant value, resulting in an uniform sampling model. Generalized non-uniform sampling requests extensive mathematical tools, becoming a complex study.

Sampling theory makes our life easier by efficiently transforming a signal from the analog domain to the digital, and vice versa, provided some requirements are met. An Analog-to-Digital Converter (ADC) samples the signal and addresses a sequence of values in which the operations previously quoted can be performed. The mathematical definition of this strategy uses a function called Dirac. Such function, $\delta(t)$, is a particular mathematical construct as it is only defined within the context of an integral, as described in Equation 3.14.

$$\int_{-\infty}^{\infty} f(t)\delta(t-t_0)dt = f(t_0) \tag{3.14}$$

A well-known, but not veridical, description states that the integral over a Dirac function is equal to 1, as can be seen in Equation 3.15.

$$\delta(t) = \begin{cases} 0, & -\infty < t < 0 \\ \frac{1}{\epsilon}, & 0 < t < \epsilon \\ 0, & \epsilon < t < \infty \end{cases} \quad \Rightarrow \quad \int_{-\infty}^{\infty} \delta(t)dt = 1 \tag{3.15}$$

with $\epsilon \to 0$.

A sequence of Dirac pulses mutually separated by a time period T_s defines the necessary time frame for sampling:

$$\sum_{n=-\infty}^{\infty} \delta(t - nT_s) \tag{3.16}$$

This sequence of pulses with a mutual time spacing of T_s can be associated to a Fourier series, which will have frequency components with $f_s = 1/T_s$ and all integer multiples of f_s. The factor of multiplication for each frequency component kf_s is C_k. Equating both

series, is obtained:

$$\sum_{n=-\infty}^{\infty} \delta(t - nT_s) = \sum_{k=-\infty}^{\infty} C_k e^{jk2\pi f_s t} \tag{3.17}$$

The coefficients C_k in Fourier series can be determined by integrating over a period.

$$C_k = \frac{1}{T_s} \int_{t=-T_s/2}^{T_s/2} \sum_{n=-\infty}^{\infty} \delta(t - nT_s) e^{-jk2\pi f_s t} dt \tag{3.18}$$

Within the integration range, there is only one valid Dirac pulse at $t = 0$, so the expanded formula comes down to:

$$C_k = \frac{1}{T_s} \int_{t=-T_s/2}^{T_s/2} \delta(t) e^{-jk2\pi f_s t} dt = \frac{1}{T_s} e^{-jk2\pi f_s \times 0} = \frac{1}{T_s} \tag{3.19}$$

The replacement of C_k outcomes in the mathematical description of the Fourier transform from the sequence of Dirac pulses in the time domain. Equation 3.17 can be rewritten as:

$$C_k = \frac{1}{T_s} \int_{f=-\infty}^{\infty} \sum_{k=-\infty}^{\infty} \delta(f - kf_s) e^{jk2\pi f_s t} df \tag{3.20}$$

where the final parcel is the standard inverse Fourier transform.

$$\sum_{n=-\infty}^{\infty} \delta(t - nT_s) \quad \Leftrightarrow \quad \frac{1}{T_s} \sum_{k=-\infty}^{\infty} \delta(f - kf_s) \tag{3.21}$$

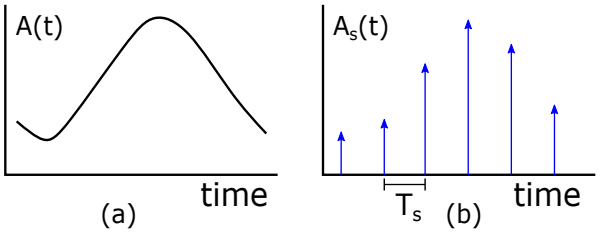

Figure 3.11: Sampling an analog signal **(a)** in the time domain results in a series of signal samples **(b)**. Adapted from [71].

The infinite sequence of short time pulses corresponds to an infinite sequence of frequency components at multiples of the sampling rate. Figure 3.11 displays an example

of the sampling of a signal $A(t)$ equivalent to $\mathbf{A}(\omega) = \mathbf{A}(2\pi f)$ with a bandwidth from $f = 0$ Hz to $f = BW$.

$$\mathbf{A}(\omega) = \int_{t=-\infty}^{\infty} A(t) e^{-j2\pi ft} dt \tag{3.22}$$

In mathematical concepts, the sampling is achieved by multiplying the time-continuous function $A(t)$, as seen in Figure 3.11 (a), with the sequence of Dirac-pulses, yielding a time discrete signal shown in Figure 3.11 (b). The result of the time-continuous function and the Dirac sequence is characterized for those time moments according to the multiples of the sampling period T_s:

$$A_s(t) = \sum_{n=-\infty}^{\infty} A(t) \times \delta(t - nT_s) \Rightarrow \sum_{n=-\infty}^{\infty} A(nT_s) \tag{3.23}$$

As stated in Putman [70], rebuilding a continuous time signal requires some conditions, such as a certain number of samples. A typical problem arises when the samples are too spaced, leading to the interruption of the process. This phenomenon is known as Aliasing, which an alias is a spurious signal when sampling over an analog signal happens at a slow rate.

Guidelines about signal processing suggests that the lowest frequency signal — red dotted trace as indicated in Figure 3.12 — fitted to the sampled data points will have the same frequency integrated into the reconstructed analog signal. Figure 3.12 shows that the sampled points are too scarce for proper restoration of the high frequency – black solid trace – signal. Thus, aliasing will contribute to corrupt the low end of the frequency spectrum, making it appear that there is more low frequency activity than can actually occurs.

The frequency at which a signal $f(a)$ suffers aliasing is corresponding to the difference between the sampling frequency $f(s)$ and the maximum frequency $f(m)$ in the bandwidth that is being measured, i.e., $f(a) = f(s) - f(m)$. So, to be unambiguous, the value of $f(s)$ must be at least twice that of $f(m)$.

Suppose that $f(s) < 2f(m)$, in this case $f(s) - f(m) < f(m)$ which implies that

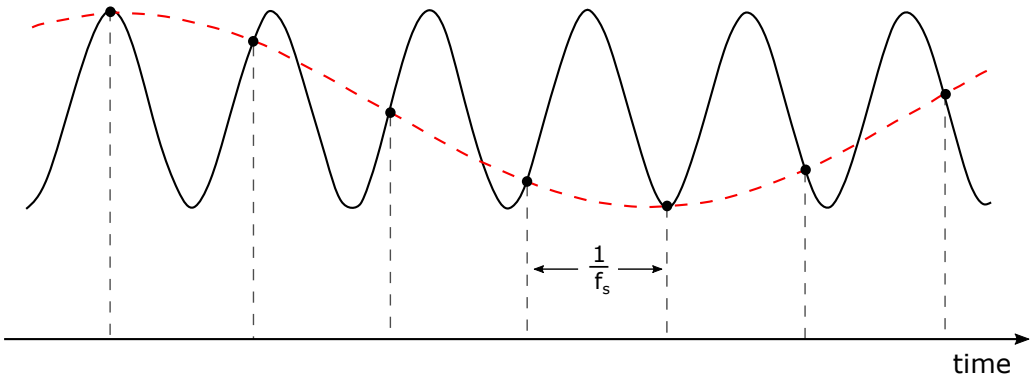

Figure 3.12: Example of an aliasing occurrence. Adapted from [70].

$f(a) - f(m)$, this situation indicates that the frequency at which was performed aliasing is less than the maximum frequency of the signal in the band. Clarifying, an example involving arbitrary numbers is demonstrated. Assuming that $f(s) = 30$ Hz and $f(m) = 18$ Hz; then, $f(a) = 30 - 18 = 12$ Hz.

Such condition means that signal corruption will begin at 12 Hz, i.e., within the range of interest. Therefore, it is essential to set the sampling rate greater than twice the maximum frequency. This rule is also known as the Nyquist–Shannon sampling theorem.

One way to avoid aliasing in the sampling process is to pass the signal through a low pass filter to enforce appropriate bandwidth limitations, which is commonly called anti-aliasing filter. Alternatively, another method of ensuring the integrity of signal reconstruction is called oversampling, consisting in a sampling with higher rates than the established by Nyquist-Shannon theorem.

3.5.2 Filtering

Filters are instruments that supposedly everyone had contact at some point in their life. Maybe it was a water filter used to remove impurities from water, or perhaps a coffee filter to trap the grounds from the liquid. Basically, the idea of filtering is the imposition of separating the desired parts from the unwanted ones, and of course, in this filtering description no water or coffee will be used, but rather digital signals. Electronic filters enables some signals to pass, but stop others. Moreover, there are a wide variety of

electronic filters and several ways that it can be classified. The selectivity in frequency is doubtless the most common approach of filters' classification, and a filter can have a lowpass, highpass, bandpass, or bandstop response, where each one indicates how a band of frequencies is influenced [72], [73].

In order to simplify the understanding of filter design and operating principles, some concepts are discussed in the following topics.

Transfer Function

As stated in [72], both analog and digital filters can be considered as a black box, where signals are inserted on one side of the box and output on the other side. Also, the analysis of the filter properties can be performed in the time or frequency domain. From a systems perspective, the impulse response $h(t)$ is valid to describe the system behavior in the time domain. An impulse response is the output of a system that has had an impulse introduced to input, i.e. when a brief input signal is applied.

The possibility to characterize the filter system in the frequency domain is feasible through the Transfer Function (TF) $H(s)$. For this, the transfer function is determined by the Laplace transform of $h(t)$.

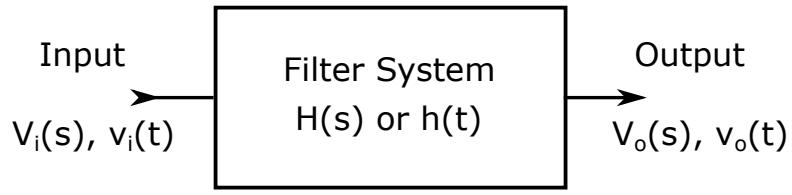

Figure 3.13: Typical representation of Transfer Function. Adapted from [72].

As seen in Equation 3.24, $H(s)$ is usually depicted as the ratio of two polynomials in s where in this case the numerator polynomial is order m and the denominator is a polynomial of order n, and G represents a general gain constant that can assume any value.

$$H(s) = \frac{G \cdot [s^m + a_{m-1} \cdot s^{m-1} + a_{m-2} \cdot s^{m-2} + ... + a_1 \cdot s + a_0]}{[s^n + b_{n-1} \cdot s^{n-1} + b_{n-2} \cdot s^{n-2} + ... + b_1 \cdot s + b_0]} \tag{3.24}$$

Alternately, the polynomials can be factored as shown in Equation 3.25. In this setting, the numerator and denominator polynomials have been separated into first-order factors. The z represent the roots of the numerator and are referred to as the zeros of the TF. Similarly, the p represent the roots of the denominator and are referred to as the poles of the TF.

$$H(s) = \frac{G \cdot [(s + z_0) \cdot (s + z_1) \cdots (s + z_{m-2}) \cdot (s + z_{m-1})]}{[(s + p_0) \cdot (s + p_1) \cdots (s + p_{n-2}) \cdot (s + p_{n-1})]} \tag{3.25}$$

Filter Selectivity

As previously mentioned, the central aim of the filters is to discriminate different frequency bands. Nomenclatures such as lowpass, highpass and so on are used to classify filters, however it takes more than a name to effectively define a filter. In general, an accurate set of specifications is needed in order to allow the proper design of a filter.

Lowpass Filter

Lowpass filters are enforced whenever it is crucial to restrict the high frequency content of a signal. Figure 3.14 displays a classic response of lowpass filters using frequency and gain specifications required for a precision filter construction. The passband extends from zero frequency to the passband edge frequency f_{pass}, and the stopband goes on from the stopband edge frequency f_{stop} to infinity.

Bandpass Filter

A convenient example for the application of bandpass filters is the processing of voice signals. Typically, the human voice has a frequency range of 300 Hz to 3 kHz. In this case, f_{pass1} would be 300 Hz and f_{pass2} would be 3 kHz. The stopband edge frequencies would be selected by how fast we would want the signal response to roll-off above and below the passband.

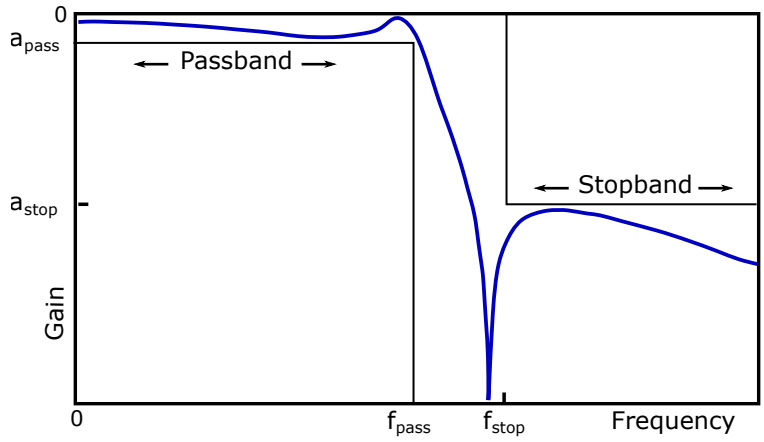

Figure 3.14: Lowpass filter specification. Adapted from [73].

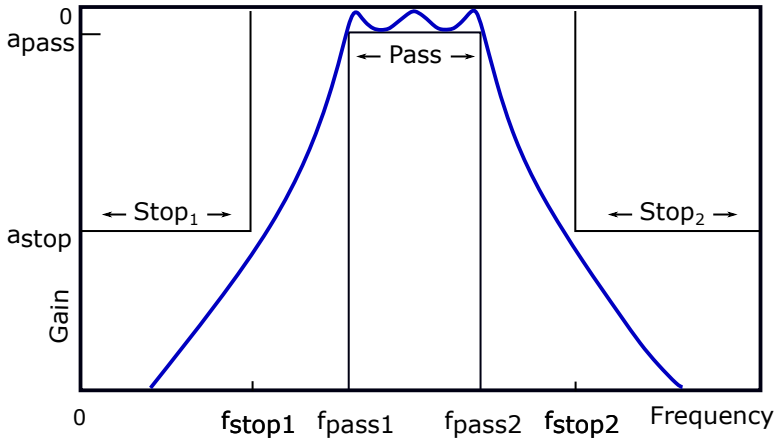

Figure 3.15: Bandpass filter specification. Adapted from [73].

Figure 3.15 shows the requirements for a bandpass filter. This filter will pass a band of frequencies while attenuating frequencies above or below that band. The passband is present between the lower passband edge frequency f_{pass1} and the upper passband edge frequency f_{pass2}. In addtion, a bandpass filter has two stopbands, which the lower stopband extends from zero to f_{stop1}, while the upper stopband extends from f_{stop2}.

Filters design is available in the analog and digital sphere. For the reason that digital filters perform optimally compared to analog filters and do not require physical implementation, only this segment is explored in the proposed work. This type of filter is categorized into two groups: Finite Impulse Response (FIR), which are also defined as non-recursive filters; and Infinite Impulse Response (IIR), which are recursive because

part of the output signal is fed back to the input [74].

Recursion in digital filtering processes employs negative feedback in order to get an abrupt roll-off using the minimum of operations, such as delay, sum and multiplication of elements. The feedback consists of a small portion of the output signal and, by virtue of the delays, any unexpected change in the input signal causes an output disturbance for a time or all the time in the event of system instability. Sensitivity to the filter coefficients adopted as multiplier factors and their truncation, limiting the number of decimal places, can lead to a positive feedback and, consequently, to the system oscillation [72].

FIR filters are often considered inefficient, because it requires a high-order of transfer function to satisfy the system requirements when compared with the order required by the IIR filters [75]. Hence, IIR filters have lower computational consumption, making it a suitable option for high-speed applications. Nevertheless, if this type of filter is not designed properly, it may be unstable [76].

An important technique in digital applications to filter sampled signals is the Z-transform, which overall, is represented by the following transfer function:

$$H(z) = \frac{b_0 + b_1 z^{-1} + b_2 z^{-2} + ... + b_N z^{-N}}{1 + a_1 z^{-1} + a_2 z^{-2} + ... + a_N z^{-N}} = \frac{Y(z)}{X(z)} \tag{3.26}$$

where the a and b coefficients determine the system characteristics of order N. Equation 3.26 can be rewritten, resulting in:

$$Y(z) \cdot [1 + a_1 z^{-1} + a_2 z^{-2} + ... + a_N z^{-N}] = X(z) \cdot [b_0 + b_1 z^{-1} + b_2 z^{-2} + ... + b_N z^{-N}] \tag{3.27}$$

In this case, z^{-i} is a delay of i sampling intervals, so it is possible to write the resulting function at any time k as follows:

$$y_k + a_1 y_{k-1} + a_2 y_{k-2} + ... + a_N y_{k-N} = b_0 x_k + b_1 x_{k-1} + b_2 x_{k-2} + ... + b_N x_{k-N} \tag{3.28}$$

that is, there is the possibility to use the following recurring relation to write the

output at time k:

$$y_k = \sum_{n=0}^{N} b_n x_{k-n} - \sum_{n=1}^{N} a_n y_{k-n} \tag{3.29}$$

In general, the design of IIR filters is performed through a mapping from the analog s-domain to the digital z-domain. The mapping can be performed by various approaches, but the most common is the Bilinear transform, also known as Tustin's method. In this technique, the relationship between the s and z complex variables is described by Equation 3.30, where T_s is the sampling period.

$$s = \frac{2}{T_s} \frac{1 - z^{-1}}{1 + z^{-1}} \tag{3.30}$$

IIR filters are classified according to classical continuous-time transfer function approximations, among them the Butterworth, Chebyshev and Elliptic, as demonstrated in Figure 3.16, that can generate discrete-time transfer function by using appropriate transformations. Each approach has its pros and cons, but for this project the Butterworth is selected.

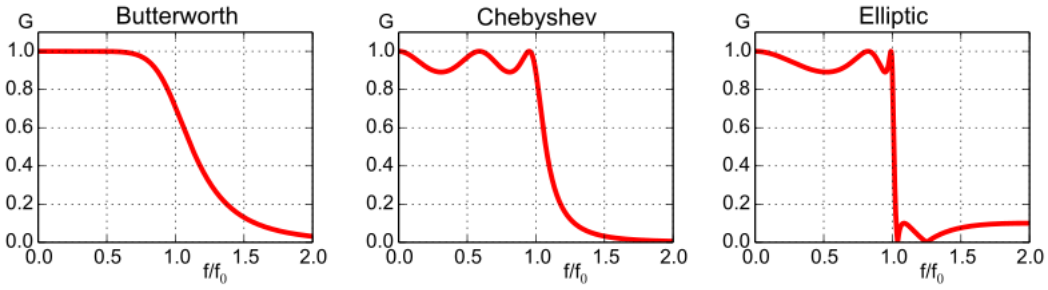

Figure 3.16: Phase response of the major types of IIR filters. Adapted from [77].

A meaningful feature of the Butterworth approximation is that its attenuation increases monotonically with frequency. Also, it increases very slowly in the passband and quickly in the stopband. If is desired to increase the attenuation, is necessary to increase the filter order. However, if the attenuation monotonicity is extinguished, a higher attenuation in the stopband may be obtained for the same filter order [75].

3.6 Triangulation

Triangulation is the process of determining the location of an object or a target from known points using trigonometric techniques. In general, the number of dimensions of the estimated position of an object is directly related to the number of sensors, for instance, two sensors can indicate a location in 2D, while three sensors can indicate a 3D location and so on [66].

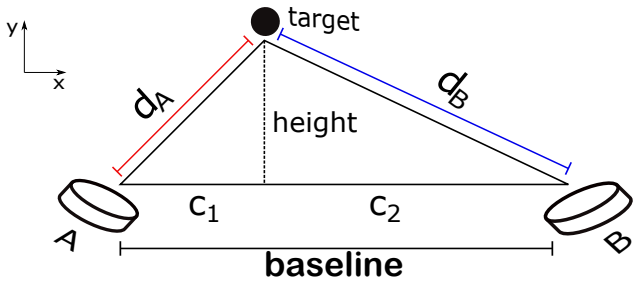

Figure 3.17: Triangulation created by the sensors.

In geometry, when the length of the sides of any triangle is known a theorem to calculate its area can be applied. This approach was created by the mathematician Heron of Alexandria and has been used in many mathematical applications [78]. With the distance of the baseline and the distance calculated by each sensor known, there is the possibility to estimate the area of the triangle formed (Figure 3.17) using Heron's formula, as shown in Equation 3.31.

$$\Delta(abc) = \sqrt{p(p-a)(p-b)(p-c)}, \tag{3.31}$$

$$where\ p = \frac{a+b+c}{2} \tag{3.32}$$

whose a, b, c are the known sides. Alternatively, the area of a triangle can be computed using the Equation 3.33.

$$\Delta(abc) = \frac{b \cdot\ h}{2} \tag{3.33}$$

where b is the base and h is the height of the triangle. Reorganizing Equation 3.33 is

possible obtain Equation 3.34.

$$h = \frac{\Delta(abc) \cdot \ 2}{b} \tag{3.34}$$

If the area provided by Equation 3.31 is placed in Equation 3.34 the y-coordinate of the target can be determined. By separating the original triangle into two right triangles and after that applying the Pythagorean Theorem it is possible to calculate the x-coordinate, according to Equations 3.35 and 3.36.

$$C_1 = \sqrt{d_A^2 - h^2}, \tag{3.35}$$

$$C_2 = \sqrt{d_B^2 - h^2} \tag{3.36}$$

where h, C_1, C_2, d_A and d_B are shown in Figure 3.17. If the Equation 3.35 is used, the system reference for the coordinates on the x-axis will originate from sensor A, otherwise, from sensor B.

Valid calculations but nonsense physical can arise using the equations described above. Thus, in order to avoid incoherent measurements some restrictions are established. A typical error is shown in Figure 3.18, to avoid it, it is observed that θ_1 and θ_2 angles are outside of the detection area.

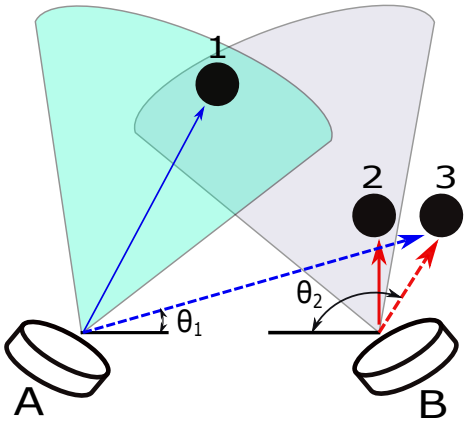

Figure 3.18: Typical triangulation error. Adapted from [66].

Figure 3.18 shows that sensor A detects the target 1 and sensor B detects the target 2. Nonetheless, θ_1 and θ_2 are not valid, which causes an error resulting in a false positioning,

represented by the target 3.

For a valid detection area Figure 3.19 displays how θ_1 and θ_2 should be, indicating that θ_1 has to be equal $\alpha_1 \pm \phi$, where α_n is the angular position of the sensor n corresponding to the x-axis and ϕ is half the angle of the detection beam, which this value is particular to each sensor model. Then, the angular interval can be given by $\cos(\alpha_1 - \phi) \leq \cos\theta_1 \leq \cos(\alpha_1 + \phi)$.

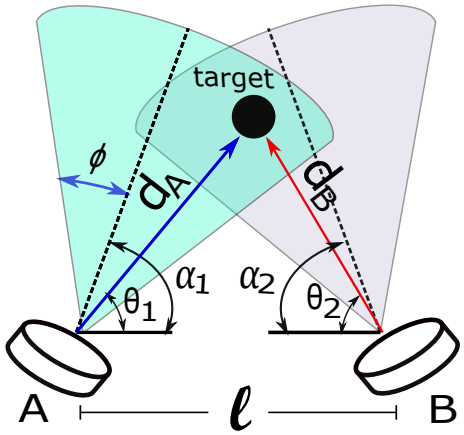

Figure 3.19: Example of a valid detection. Adapted from [66].

Similarly, to sensor B the angular limiting range is $\cos(\alpha_2 - \phi) \leq \cos\theta_2 \leq \cos(\alpha_2 + \phi)$, where:

$$\cos\theta_1 = \frac{l^2 + d_A^2 - d_B^2}{2ld_A}, \tag{3.37}$$

and

$$\cos\theta_2 = \frac{l^2 + d_B^2 - d_A^2}{2ld_B} \tag{3.38}$$

α_1, α_2 and ϕ are constant, then, it is necessary to calculate only $\cos\theta_1$ and $\cos\theta_2$. Measurements outside this range should be discarded.

Chapter 4

Implementation

This chapter will present the applied tools and implementation approach for improving and obtaining accurate measurements by combining conventional ultrasonic sensors with sophisticated signal processing techniques. Thus, essential points will be aborted, being: hardware design, data acquisition, data processing and system settings.

4.1 Hardware Design

In order to ensure a proper execution and testing of the proposed system, a set of components is required. For that, the sonar has an electronic scheme composed by three ultrasonic modules and two MCU, as well as an external power supply (Appendix C). In this section, these elements will be presented, briefly covering the most relevant specifications for its application. The accomplishment of this work is divided into three parts, where in each the technique and approach to processing the data are distinct. The block diagram, as shown in Figure 4.7, represents the structure for the first and second stage, and Figure 4.1 illustrates the final system architecture.

The following subsections are devoted to describe the components that compose the hardware structure of the system.

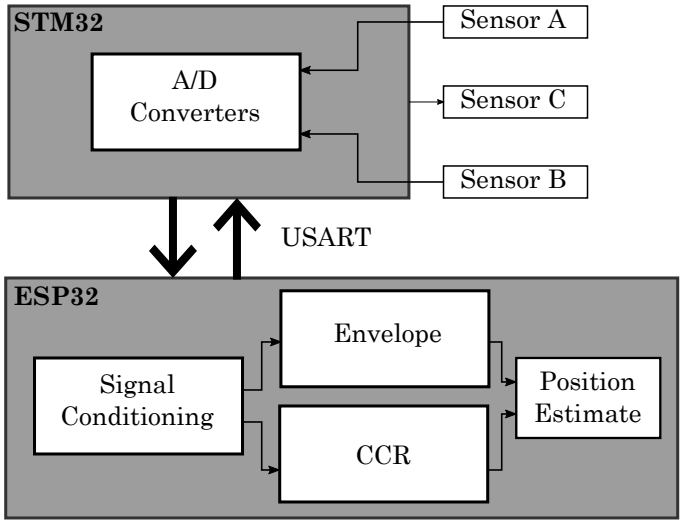

Figure 4.1: Final system architecture.

4.1.1 Ultrasonic Module HY-SRF05

Conventionally, the low cost ultrasonic ranging module HY-SRF05 provide a detection range of 2 to 450 cm, which the accuracy can reach up to 0.3 cm. The module is powered with a Direct Current (DC) voltage of 5V and has a low current consumption, typically less than 2 mA.

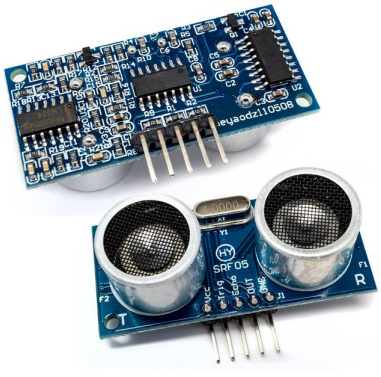

(a) HY-SRF05.

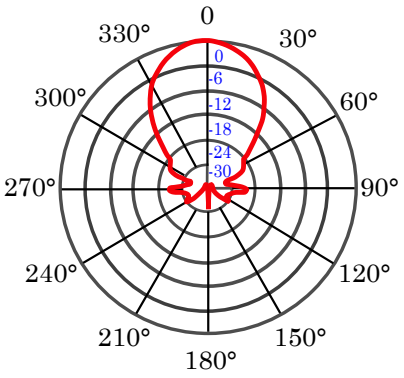

(b) HY-SRF05 beam pattern.

The emitted signal from the module is generated by eight cycle burst of ultrasound at 40 kHz, and for this, a trigger pulse with a minimum duration of 10 μs is required. When the signal is reflected back to the receiver, the echo pin yields an digital output with a proportional duration of the round trip of the signal (Figure 4.2), i.e., it acts as

a timer computing the time between the transmission and reception of the ultrasonic signal [79]. However, such technique is not exploited, because its operating principle is based on threshold detection level.

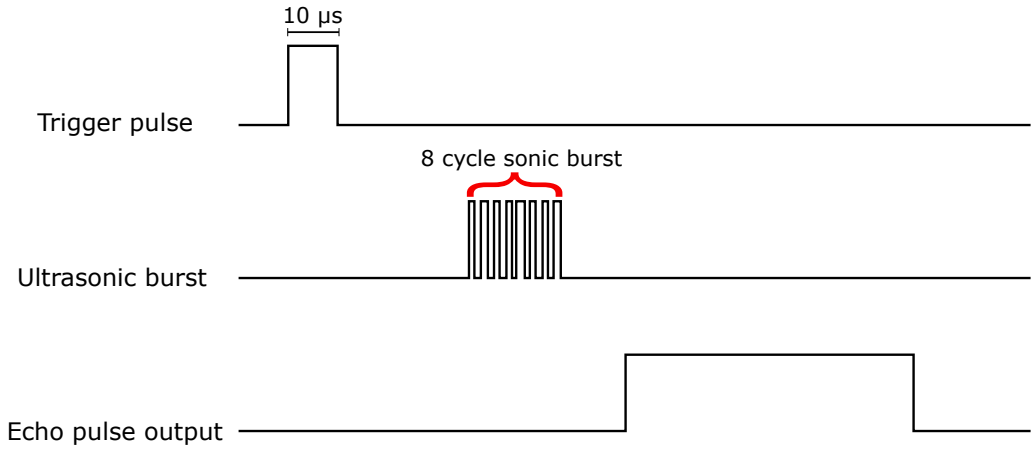

Figure 4.2: Timing diagram of the ultrasonic ranging module HY-SRF05. Adapted from [80].

4.1.2 STM32

The STM32 family of MCUs, supplies a foundation for building a wide range of embedded systems from simple to complex real-time applications. The employed model STM32F103C8T has 20 kB of SRAM and an ARM 32-bit Cortex-M3 core with clock of 72 MHz. It offers up to nine communication interfaces, such as Inter-Integrated Circuit (I2C), Serial Peripheral Interface (SPI) and Universal Asynchrounous Receiver/Transmiter (UART); besides that, it comes with two 12-bit built-in ADC, which the 12 MHz ADC clock can perform a sample in slightly more than 1 μs [81], [82].

This MCU is responsible for performing the dual sampling of the ultrasonic signals acquired from the HY-SRF05 modules and sending the data to other platforms.

4.1.3 ESP32

ESP32 is a low cost chip developed by Espressif Systems, containing integrated Wi-Fi (2.4 GHz) and Bluetooth. It is capable of functioning reliably in assorted environments,

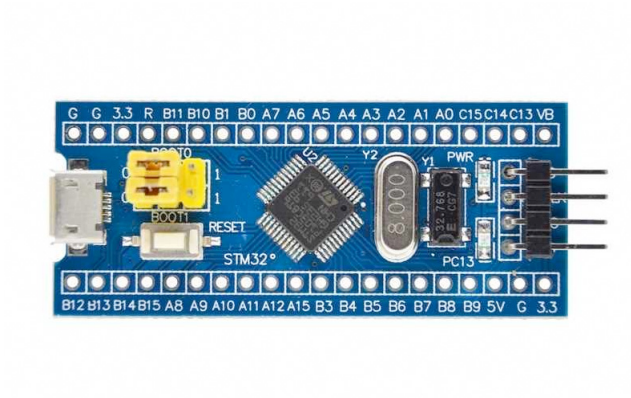

Figure 4.3: STM32F103C8T.

with an operating temperature ranging from −40 °C to +125 °C. Engineered for mobile devices, wearable electronics and Internet of Things (IoT) applications, the chip achieves ultra-low power consumption with a combination of several types of proprietary software. ESP32 can be found in two forms: chip or module form [83]. In this project, it is used the second option, ESP32-WROOM-32, which is a complete development board, as depicted in Figure 4.4.

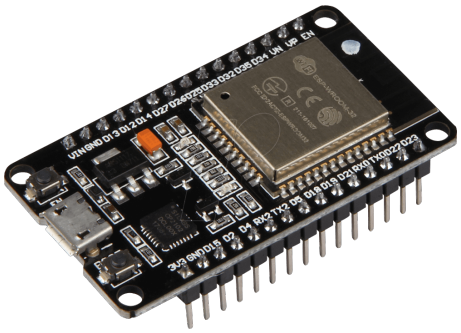

Figure 4.4: ESP32-WROOM-32

ESP32 has 520 kB of SRAM and two Xtensa 32-bit LX6 microprocessors with an adjustable clock between 80 to 240 MHz. The board presents 32 General Purpose Input/Output (GPIO) pins, including communication interfaces for I2C, I2S, SPI and UART. Also, it has two 12-bit built-in ADC with sampling rate up to 200 kHz [84].

4.2 Data Acquisition

Analyzing the traditional echo pulse response, but from an electronic point of view, it is possible to notice that, before the echo pin generates the digital output the received signal passes through a conditioning, such as filtering and gain stages; and finally, it is submitted to a variable threshold hysteresis comparator, as can be seen in Figure D.1 (Appendix D). The last step is unattractive, due to some constraints that affect the accuracy and ability to investigate the received signal in detail. Thus, the output signal of the third operational amplifier (Pin 7), before it is inserted into the comparator is extracted.

Appendix D displays the wiring diagram of the HC-SR04 ultrasonic range module, which is considered a version prior to HY-SRF05. Unfortunately, some specific information is not provided in the data sheet of this device, so a few data is collected from similar versions. In this sense, to verify that the schematic diagram is valid, a connection is made in Pin 7 which its output is forward to STM32 ADC. As result, the conventional waveform of an ultrasonic signal (blue trace) is shown in Figure 4.5, proving that is correct.

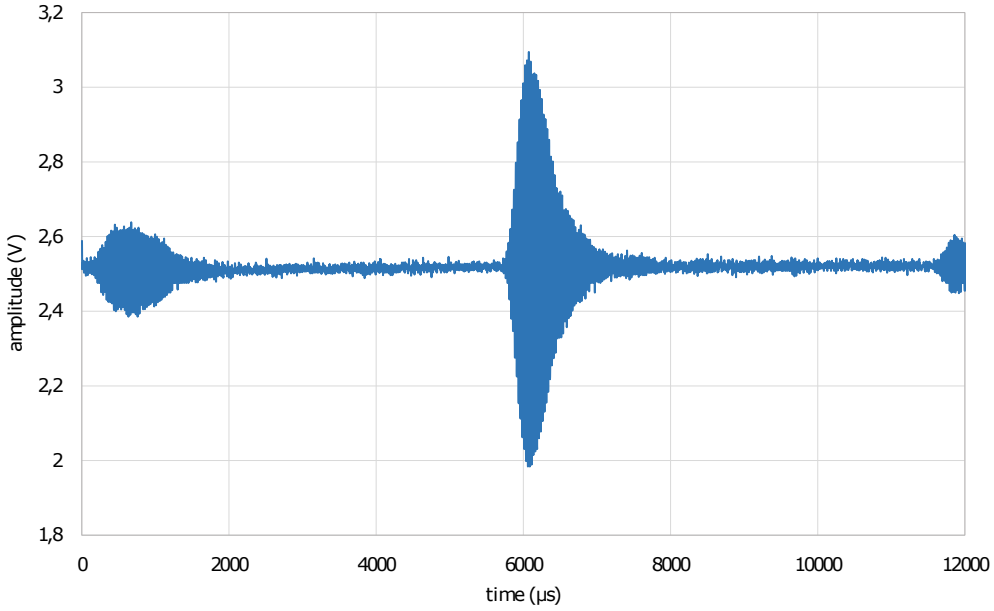

Figure 4.5: Typical ultrasonic waveform.

Among the available MCUs, the specifications of the STM32 ADC were more attractive

and, according to the data sheet, by selecting the prescaler equal to 2, the ADC clock can be estimated, as follows:

$$f_{ADC} = \frac{f_{CLK}}{prescaler} \rightarrow \frac{72 \times 10^6}{2} = 36 \text{ MHz} \tag{4.1}$$

Also, knowing that the STM32 ADC consumes 71.5 clock cycles it is possible establish the sampling period T_s:

$$T_s = 71.5 \cdot \frac{1}{f_{ADC}} \rightarrow 71.5 \cdot \frac{1}{36 \times 10^6} \approx 1.99 \ \mu s/sample \tag{4.2}$$

which this value is corresponding to a sampling rate approximately of 500 kHz against 200 kHz from the ESP32. However, tests using a signal generator have been performed on the ADC of ESP32 and STM32, to make clear our choice. A 2 Vpp sine wave configured with a frequency equal to the ultrasonic (40 kHz) is applied in both MCUs, thus, the sampled data is plotted on the graphics in Figure 4.6.

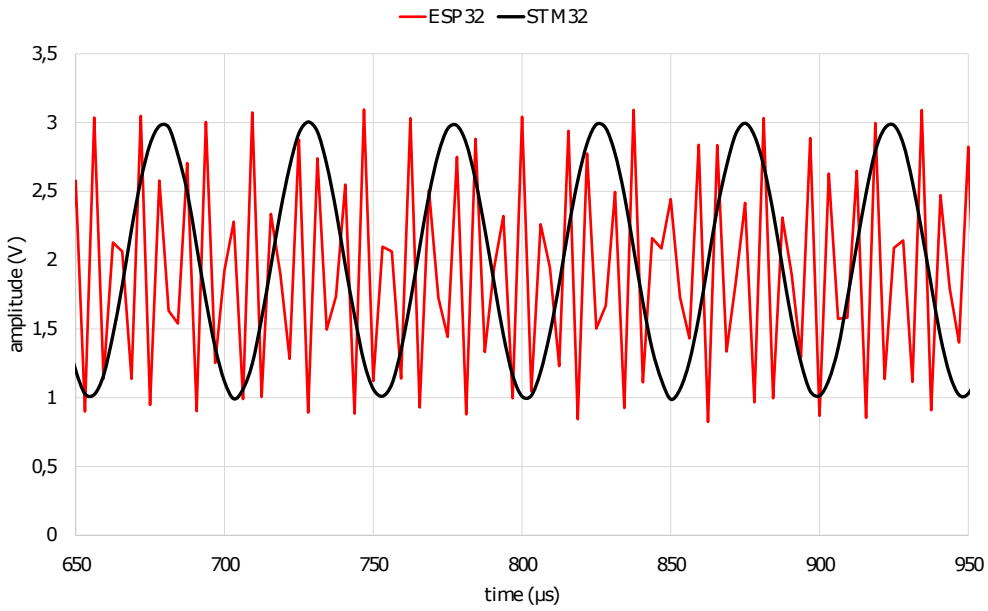

Figure 4.6: ESP32 and STM32 sampling performance.

As can be seen in Figure 4.6, it is explicit that STM32 ADC outperforms ESP32 ADC. For this reason, the STM32 is selected to accomplish the signal sampling. In addition, it

is responsible for triggering the sensors.

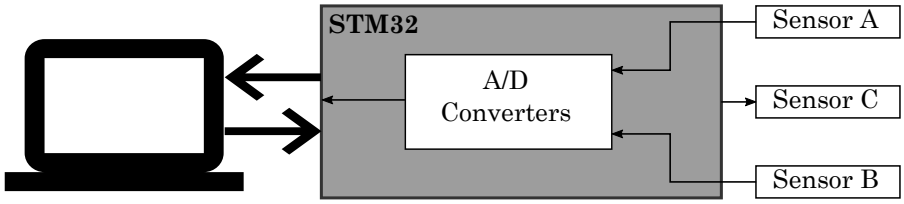

Figure 4.7: Initial system architecture.

4.3 Data Management

This section will introduce the stages of the implementation and how data is handled. Initially, the characteristics of received ultrasonic signal were analyzed with the intention of checking significant aspects as amplitude, noise and frequency. Later, signal conditioning and data processing are performed.

4.3.1 System Sketching

Firstly, signal sampling has been carefully designed to prevent data corruption, such as aliasing occurrence. The ADC is configured with a sampling frequency of 500 kHz, having a frequency 12 times higher than the ultrasonic signal, thus, meeting the Nyquist-Shannon criterion. Next, the sampled data from STM32 is transmitted over UART to MATLAB (Figure 4.7). For triggering the sensors, before MCU starts the sampling, a delay of 450 μs is required, because it is the time between the falling edge of the trigger pulse and the falling edge of the last cycle sonic burst, as can be seen in Figure 4.2. Otherwise, the system will start the sampling process without the sonic burst having been completed. The extracted signal from the modules presented a variable noise, sometimes distorting the signal completely. Thus, a second order Butterworth bandpass filter is designed in MATLAB to be applied to the raw data. Conforming to the HY-SRF05 manufacturer, the modules operate at a frequency of 40 kHz, but this measurement is subject to error. For this reason, the upper and lower cutoff frequencies of the filter are established as 38 kHz

and 41 kHz, respectively. However, before finding out the transfer function of the filter and its coefficients is necessary to establish the sampling period executed by the MCU. For that, two analyzes were performed: in the first, a square wave was generated by setting a GPIO in high logical level when sampling starts and in low logical level when sampling ends; in the second, a timer was used as a counter. The sampling period obtained from both approaches was equal to 3.125 μs. Figure 3.15 shows the raw and filtered signal.

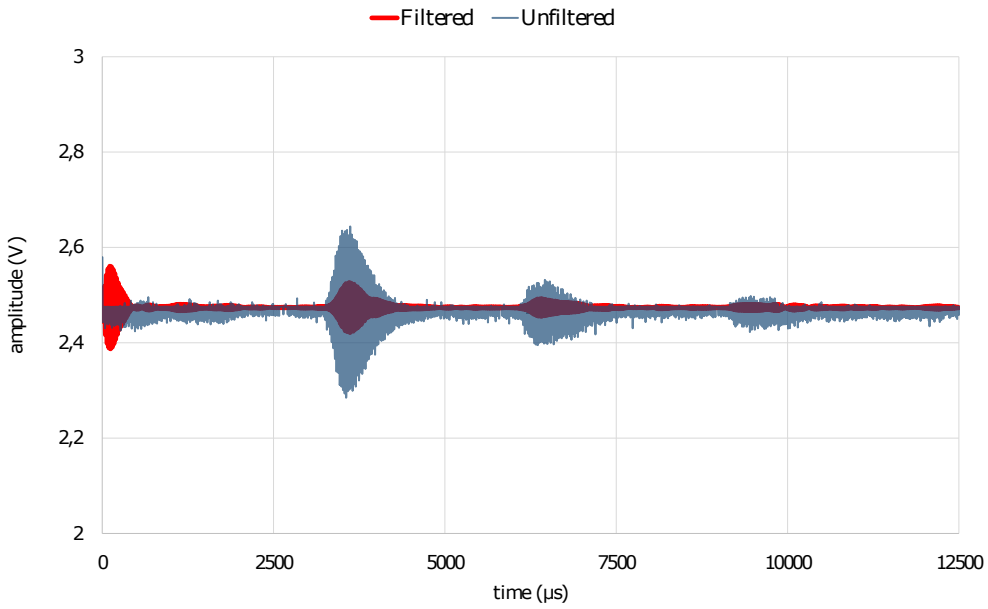

Figure 4.8: Comparison between unfiltered and filtered ultrasonic signal.

After filtering, it was noted that the signal was attenuated, reducing its amplitude. So, to deal with this issue an variable gain amplifier is recommended. Currently, there are IC that perform this task, also known as Programmable-Gain Amplifier (PGA), but due to unavailability in the local market and the time factor, the problem was solved with the design of a similar device, which scheme is displayed in Figure 4.9. According to the signal attenuation, a specific gain is selected automatically by the MCU through an electronic switch (SN74HC4066). For instance, if S_1 is enabled and the the rest are disabled, the operation gain coefficient will be:

$$G_1 = 1 + (R_f)/(R_1 + R_2 + R_3 + R_4) \tag{4.3}$$

For S_2 closed and the rest open:

$$G_2 = 1 + (R_f + R_1)/(R_2 + R_3 + R_4) \tag{4.4}$$

And so on:

$$G_3 = 1 + (R_f + R_1 + R_2)/(R_3 + R_4) \tag{4.5}$$

$$G_4 = 1 + (R_f + R_1 + R_2 + R_3)/(R_4) \tag{4.6}$$

The maximum range of stored data is limited to eight thousand readings, four thousand from each receiver sensor, due to the fact of the ADC provides 12-bit resolution, the data type to save each set of samples is an integer of 16-bit or 2 bytes, i.e. each reading consumes 2 bytes that multiplied by 8000 result in 16 kB, almost reaching the total SRAM of the MCU. The remaining memory is left free to perform other tasks and mainly to prevent memory crash.

The average temperature at the room where the tests and implementation is realized was about 20 °C, that corresponds to 293.15 K. Through the Equation (3.3) the speed of sound is defined as approximately 343 m/s; from this point, it can be stated that the distance is covered 0.034 $cm/\mu s$. The reciprocal is equal to 29.412 $\mu s/cm$, which considering a round trip corresponds to 58.824 $\mu s/cm$. Using this constant it is possible to simplify the determination of the distance and rewritten the Equation (3.1):

$$d = \frac{T_f}{K}, \tag{4.7}$$

where $K \approx 59$.

Knowing that the sampling period is $Ts = 3.125\ \mu s$, it implies in a sampling space of 12500 μs. Applying the Equation (4.7), we can estimate that the proposed system has a maximum range of about 212 cm depth, that is, along the y-axis, and the x-axis is bounded by the established baseline.

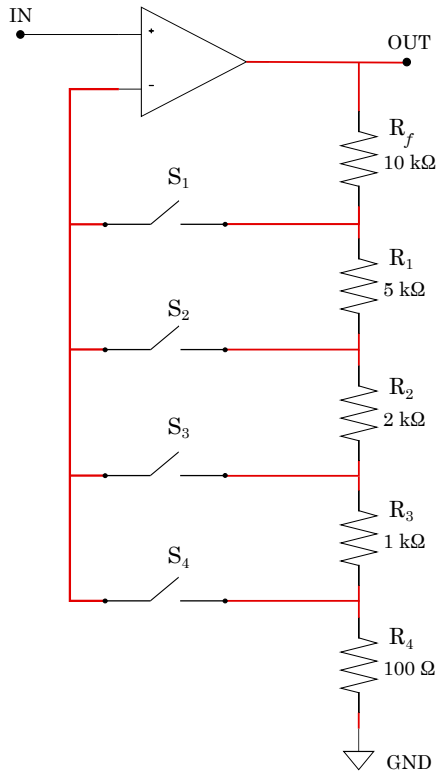

Figure 4.9: Designed variable gain amplifier.

After receiving and storing data from each sensor, the envelope detection is accomplished by a built-in function in MATLAB using Hilbert transform approach. Thereupon, the ToF is calculated to determine if the detected object is in a valid detection area. Lastly, the coordinates estimate of the object is computed.

Basically, the STM32 acts an an external ADC and MATLAB as the brain, processing all data and estimating the coordinates of a target or object present in the detection field. This stage is of fundamental importance for the work development, allowing to evaluate the obtained measurements, as well as built a sketch for the proposed system. Therefore, time consumption is not accounted in this stage.

4.3.2 Proposed Technique

The main purpose of the second stage is to improve the performance of the binaural system by matching the most efficient ToF techniques, such as envelope detection and

CCR, to define with high accuracy the x and y axis coordinates of one or more targets existing in the detection area using triangulation.

As mentioned in 3.2.2, the CCR is achieved only with the received signals. From the known time delay between the sensors A and B is possible to determine which of the sensors receives the echo first and consequently if it is closer or not to the object. In spite of obtaining this information, it is not enough to estimate the ToF, because it is necessary to have some reference of the origin, i.e. when the signal is transmitted.

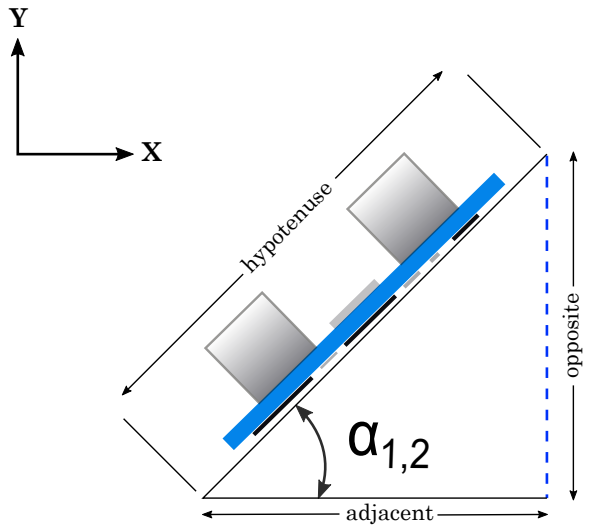

Figure 4.10: Application of trigonometry for angle adjustment.

In an effort to solve the aforementioned problem, the technique described in 3.2.3 is employed to find out the ToF of one of the received echoes. So, the envelope detection is applied to the sensor closest to the target, believing that accuracy may be better. Following, the ToF of the other sensor is defined based on the time delay provided by the CCR. For example, suppose the sensor A is the closest sensor to the target and the delay time given by CCR is 2 ms advanced from sensor B. Then, the ToF of the sensor B will be the ToF of the sensor A subtracted 2 ms. If sensor B were the closest sensor, the opposite analogy would be used.

The same procedures of the first stage, from sampling to data reception, are performed, except for the proposed technique to achieve the position estimation of the targets. Also, time consumption is not accounted in this stage.

4.3.3 Embedded System Application

The third and last stage is described by the construction of the proposed scheme as an embedded system. Nonetheless, the performance of previous stages is evaluated, intending to select the most appropriate before starting implementation. From the results, it can be seen that envelope detection is good, but the combined technique showed better efficiency. Moreover, this is a new approach that can become a powerful tool in obstacle detection. Thus, this method is selected to be incorporated to the system.

At first, the elaboration of an algorithm in the MCUs programming language (C++), is carried out. The approach developed in MATLAB environment has made this step simpler, requiring only to transcribe from one language to another. However, the built-in functions used in MATLAB needed to be fully redesigned in C++. As criteria, priority was given to less complex methods, implying less computational processing and, consequently, low cost.

The accomplishment of CCR is achieved through the implementation of Equation (3.5) on ESP32, which some auxiliary strategies including logical shift and data normalization are enforced. In order to perform the envelope extraction, a windowing is applied to the signal to locate the peaks every ten samples, and after that, the unknown points between each peak are interpolated using the Lagrange Polynomial. Then, a second order Butterworth lowpass filter is designed to soften the envelope, which phase delay caused by the filter is negligible. Unlike the approach using Hilbert transform, the procedures to execute this technique does not require complex operations.

As previously mentioned, STM32 has a restricted memory, therefore, a larger memory MCU is required. For this reason, ESP32 is included in the hardware design. Aiming to integrate both MCUs, an analysis about the available communication protocols is enacted. From the best known protocols, such as SPI and I2C, it is possible to notice that both are based on master/slave model which one device or process, known as master, controls one or more devices or processes, known as slaves. In general, once the connection is established, the direction of the control is always from the master to the slave. I2C protocol consists

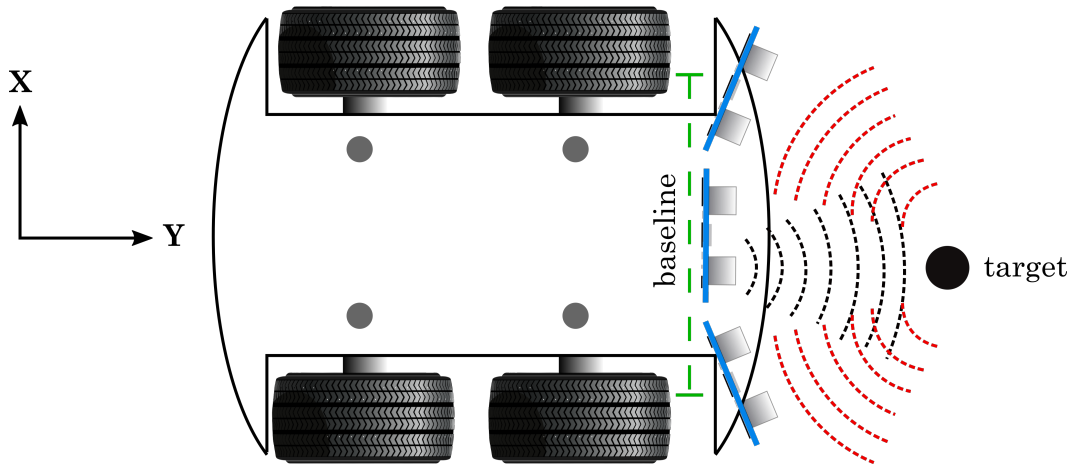

Figure 4.11: Top view of the proposed system on a mobile robot.

of two wires for data transmission and is limited up to 400 kbps [85], in contrast, SPI has a maximum rate in the order of Mbps, but requires two more buses to establish a communication [86]. Thus, due to the lack of flexibility and simplicity, another interface that requires only two buses supporting transmission rate up to 4.5 Mbps is applied.

The Universal Synchronous Asynchronous Receiver/Transmitter (USART), sometimes called Serial Communications Interface (SCI) works with no fixed protocol which can be synchronous or asynchronous, and both the transmission/reception may occurs at the same time, also known as full duplex operation [87]. In our system, the transmission ensues with 8 bits of data plus a start and stop bit in asynchronous mode, configured at the highest transmission rate supplied by both MCUs — 4 Mbps. As an example, the send of data 0x25 or 00100101b is shown in Figure 4.12.

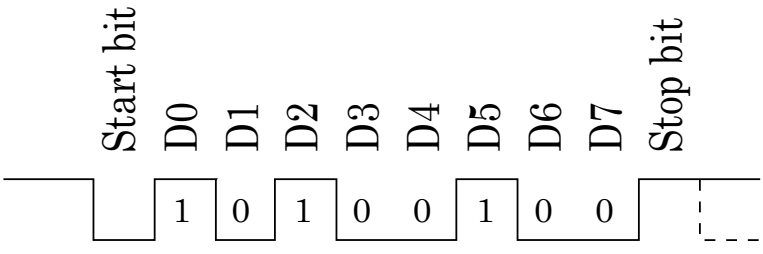

Figure 4.12: Asynchronous 8-bit waveform example. Adapted from [87].

STM32 performs signal sampling continuously, and after all eight thousand samples

are collected, each sample is break into two 8-bit packets to be transmitted to ESP32 over USART. Since ESP32 has two cores, it is feasible to allocate one core to perform data processing and the other to receive. However, because data size is not trivial, the reception buffer can store only a few sets of measurements. In addition, if ESP32 is still processing the data and cannot store the new readings into the reception buffer, a command to clear older data and make room for newer data is executed. In order to make easier, the use of dynamic memory allocation is performed.

4.4 System Settings

The framework is configured with particular features, such as distinct angles and baselines for experimental tests. Intending to make the system viable for mobile robots applications, the baseline is limited in up to 51 cm, which is already a considerable value. Contrarily, if a very large baseline were used, the construction of the robot would be impractical. Figure 4.11 demonstrates how baseline size can influence devices architecture.

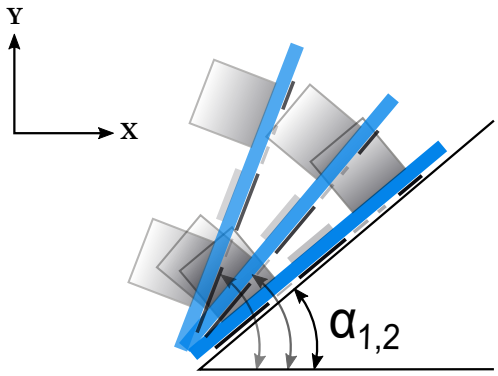

Figure 4.13: Sensor angular orientation.

Measurements are obtained by setting $\alpha_{1,2}$ angle between 0° to 45° with respect to the x axis; higher angles bring the detection field closer to the sensors, which is not ideal as the system will be more prone to failure, as indicated in Figure 4.13. Angle setting is done using the basic principles of trigonometry, as outlined in Figure 4.10, which α is defined as:

$$\alpha_{1,2} = \arctan\left(\frac{opposite}{adjacent}\right) \tag{4.8}$$

Targets used in the experimental tests include one transparent object (plastic bottle), three flat-shaped objects (cardboard boxes) and one cylindrical object. The dimension of these objects are presented in Appendix E.

4.5 Ground Truth and Binaural System

The experimental tests were performed in an indoor environment, with a clean and flat surface, being allowed in this area only the objects previously mentioned. Figure 4.14 illustrates the constructed layout using masking tapes to delimit the space, which the dimensions of the area vary according to the defined baselines (l). Furthermore, aiming to validate the system estimates, a centimeter-scale measuring tape is used.

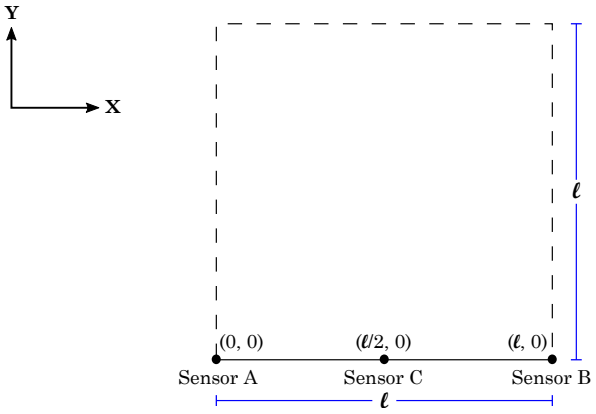

Figure 4.14: Layout established for testing.

The selection of a proper method to establish the system accuracy is one of the difficulties faced in this work. Due to the wide beam of the sensor (Figure 4.2(b)), which is approximately 55°, the point at which the ultrasonic wave reflects on the object is unknown, thus, making the system analysis complex. Figure 4.15 exemplifies this situation, where the black and green dots means valid localization inserted in a credible detection perimeter (red trace). In order to perform an evaluation, the center of the object is

adopted as real coordinate (black dot) and correlated with the coordinates calculated by the system (green dots). All investigation and report obtained, which will be introduced in the following chapter, is based on this assumption.

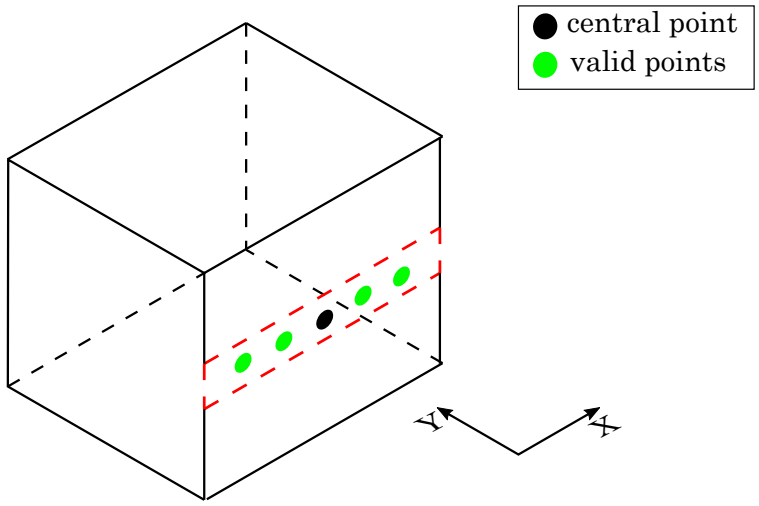

Figure 4.15: Propagation of valid points around the conventional true value.

Chapter 5

System Integration, Testing and Results

This chapter will be dedicated to the presentation of results regarding the data acquisition, data management and signal processing techniques using the methodologies proposed and discussed in the previous chapters.

5.1 Evaluation of Methods

This section introduces the performance of the discussed techniques developed in MATLAB through the data acquisition from STM32. The main purpose of this stage is verify the accuracy of the measurements, as well as analyze the general performance of the developed system using envelope detection and the merged technique, envelope plus CCR. An important aspect of the x and y coordinates is that they can be represented as a 2D spatial vector (Figure 5.1). In order to simplify the evaluation of both methods the length of the vector is calculated to estimate the relative (R_E) and systematic error (S_E) for all measurements (Equation 5.1 and 5.2) [88].

$$S_E = \left|\overline{M} - CTV\right| \tag{5.1}$$

$$R_E = \frac{S_E}{CTV} \tag{5.2}$$

where $\overline{M}$ is the average of n measurements and CTV is the conventional true value.

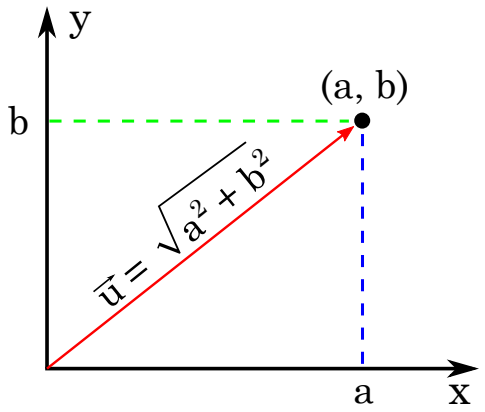

Figure 5.1: The length of vector $\vec{u}$ in Cartesian coordinates.

Moreover, the standard deviation ($\sigma_{x,y}$) is obtained from:

$$\sigma_{x,y} = \sqrt{\frac{\sum_{i=0}^{n}(a_i - \overline{a})^2}{(n-1)}} \tag{5.3}$$

where a_i is the sample in the i position of the data set, $\overline{a}$ is the arithmetic mean of all samples and n is the number of samples.

The analysis is divided into two stages: the first with only one object, and the second with two objects present in the detection area. In the former, the object number two (Appendix E) is used and the receiver sensors are placed with $\alpha_{1,2} = 45°$ and $l = 51\,cm$. The experiments are performed with the object positioned to the left, right and center of the detection area. About sixty samples of each possibility are obtained and the mean, standard deviation, systematic error and relative error of each one are calculated, as can be seen in Table 5.1.

Since the raw echo signal is used, there is the possibility to make a wide investigation about the analyzed environment. If a second object is present in the detection area, this information can be discovered through the existence of more than one crest in the

Table 5.1: Analysis of the first tests adopting envelope detection technique.

Location	$(x, y)\, real$ (cm)	$\overline{(x, y)}$ (cm)	σ_x (cm)	σ_y (cm)	S_E (cm)	R_E (%)
Left	(11.5, 91.8)	(13.3, 92.8)	1.66	0.71	1.23	1.33
Center	(25.6, 84.5)	(26.6, 80.9)	0.48	0.15	3.13	3.56
Right	(35.0, 86.4)	(35.3, 86.1)	0.75	0.25	0.16	0.13

Table 5.2: Analysis of the first tests adopting the proposed technique.

Location	$(x, y)\, real$ (cm)	$\overline{(x, y)}$ (cm)	σ_x (cm)	σ_y (cm)	S_E (cm)	R_E (%)
Left	(11.50, 91.8)	(10.74, 94.38)	1.43	1.18	2.47	2.68
Center	(25.6, 84.5)	(24.35, 85.9)	0.10	0.41	0.99	1.11
Right	(35.0, 86.4)	(36.22, 86.72)	1.01	0.93	0.76	0.82

waveform of the echo signal. In the second stage, the object described before is used together with the object number one (Appendix E), and the same procedures are applied. The positioning of both objects is arbitrary, the object number two is closer to the sensors and the object number one further away. The mean, standard deviation, systematic error and relative error of each situation are presented in Table 5.3.

Table 5.3: Analysis of further tests adopting envelope detection technique.

Object No.	$(x, y)\, real$ (cm)	$\overline{(x, y)}$ (cm)	σ_x (cm)	σ_y (cm)	S_E (cm)	R_E (%)
2	(35.50, 54.0)	(32.90, 53.90)	0.27	0.26	1.48	2.27
1	(19.0, 111.20)	(20.60, 110.80)	2.47	0.65	0.11	0.10

Table 5.4: Analysis of further tests adopting the proposed technique.

Object No.	$(x, y)\, real$ (cm)	$\overline{(x, y)}$ (cm)	σ_x (cm)	σ_y (cm)	S_E (cm)	R_E (%)
2	(35.50, 54.0)	(33.1, 54.0)	0.40	0.27	1.28	1.99
1	(19.0, 111.20)	(19.56, 110.72)	1.10	0.21	0.37	0.33

Figure 5.2 shows a frequent error in the receivers. The target was more than $1\,cm$ apart, however the system indicated that the object was at a smaller distance. The problem seems to occur because the echo signal interferes with a signal that travels directly from the transmitter to the receiver, without reflecting on the object. In an attempt to

reduce the direct signal, paper tubes were added at the receivers and at the transmitter. Also, Murata [89] states that the sonic burst is driven by the dimensions of the ultrasonic radiation surface and the frequency, but it is possible to make the emission more intense and measuring distance longer by attaching a horn to the outside of the ultrasonic module, similar to the proposed solution.

When the CCR is applied to the received echoes a signal with triangular shape is produced, resulting in an improper time delay. Probably this situation occurs because both signals has a significant DC offset, thus, to solve this problem, the offset removal is performed through the normalization of the data, subtracting each sample by the arithmetic mean of all samples.

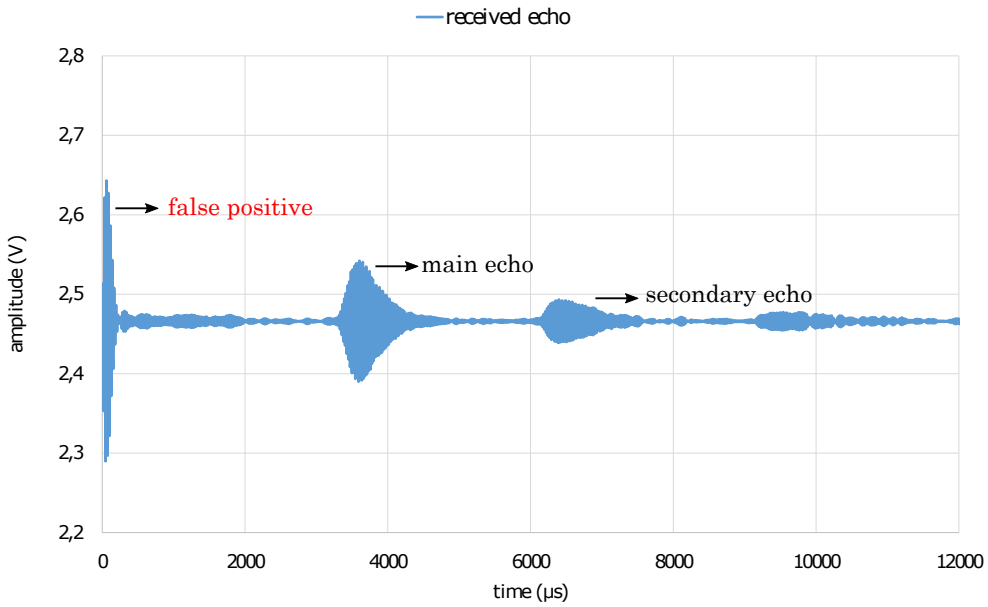

Figure 5.2: Received echo signal with two objects in the detection area.

The transmitted signal by the sensor generates eight cycle sonic burst at 40 kHz, i.e. it provides eight square pulses with period of 25 μs. In this case, applying CCR between the transmitted and received signal would not be appropriate, to implement this idea it would be necessary to detect the transmitted signal in a waveform similar to that of the received signal, as set out in Figure 4.5. Therefore, the CCR is applied only to the received signals from sensor A and B (Figure 3.7). From this point, knowing the time lag

there is the possibility to establish which of the receiving sensors is closest to the target and then proceed with the ToF estimation.

Particularly in this stage, to use CCR when more than one object is in the scene, it is necessary to separate the echo signals received by the sensors according to the crests of the waveform and apply it to each of them with its corresponding crest, as evidenced in Figure 5.3; i.e. the CCR would have to be applied to the first part of the sensor A with the first part of the sensor B and so on. Otherwise, if the entire signal is used, a single time delay is provided and consequently is not possible to distinguish which target that delay is referring to.

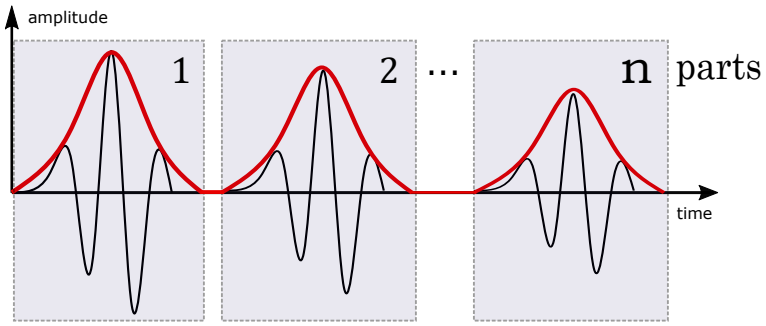

Figure 5.3: Fragmentation of the received echo signal.

The identical process employed in the envelope detection is enforced to achieve the location of the objects using the matched approach. Table 5.2 and 5.4 presents the standard deviation, mean and systematic error of each case.

Both techniques were successful, showing errors within an acceptable range, but the combined method showed slightly higher efficiency. From the beginning, the main purpose of this study is to develop a novel approach to achieve obstacle detection with high accuracy. For this reason, the method involving envelope detection and CCR is chosen to be integrated to the final arrangement of the system.

5.2 System Integration

This section will present the efficiency of the algorithm designed for ESP32, focusing on filtering and digital envelope detection as well as the time performance of the system. Also, it is described the accomplishment and results of a new set of measurements in multiple configurations, with assorted α angle and baseline, applying CCR combined with envelope detection.

As mentioned earlier, MATLAB built-in functions needed to be redesigned to fit on ESP32. From this perspective, the MCU performance is compared to the version based on MATLAB. Figure 5.2 displays the achievement of envelope detection using linear interpolation (red line) against Hilbert transform (black line), highlighting the difference between the raw and filtered signal.

Aiming to determine the total time which the system takes to complete each measurement, some elements such as information exchange between devices and data processing are considered. In this sense, the duration of the communication between STM32 and ESP32 can be easily estimated: four thousand samples of each sensor, totaling eight thousand, are stored in 16-bit variables resulting in 128 kbits, with the transmission rate known — 4 Mbits per second — it can be stated that the transfer is completed in approximately 32 milliseconds. The period to carry out all data computation is a bit more complicated, requiring the use of a MCU timer. In addition, the time counting was performed several times and the obtained value was not constant, ranging from 4 to 5 seconds. Thus, an average value of 4.5 seconds was assigned as the total data processing time. By summing these values, it is possible to establish the approximate system execution as 4.53 seconds per measurement.

5.2.1 Case A: First Scenario

In this case, the analysis was realized with $\alpha_{1,2} = 0^\circ$ and $l = 35.5$ cm using the objects number three, four and five, as shown in Appendix E. One hundred and fifty measurements were collected, excluding invalid detection outside the condition imposed in section 3.6.

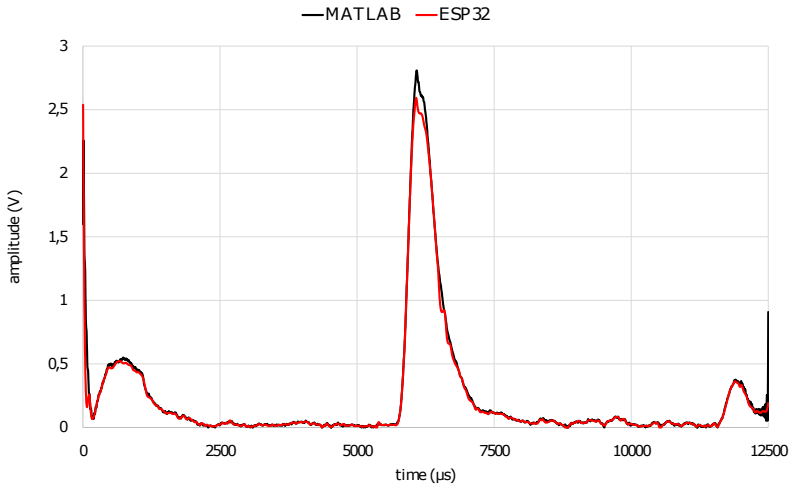

(a) Raw envelope.

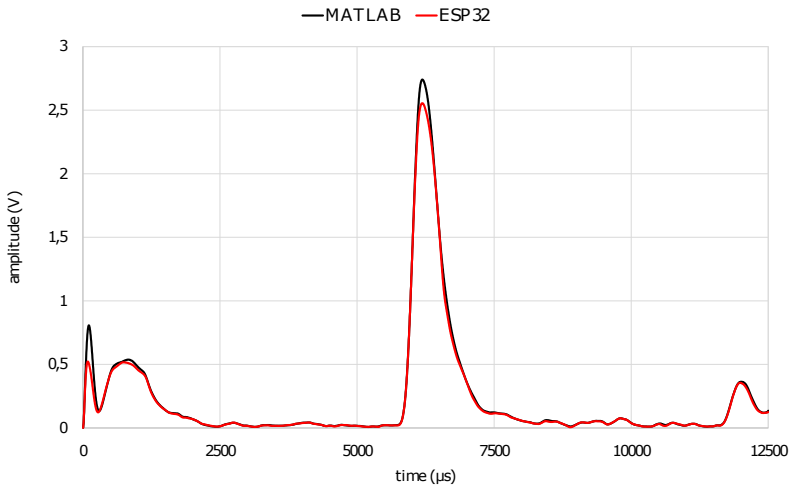

(b) Filtered envelope.

Figure 5.4: Upper envelope extracted from an echo signal.

The targets were positioned to the left, right and center of the detection area. Table 5.5 to 5.7 shows the mean, standard deviation, systematic error and relative error of each situation.

It was possible to distinguish the left, center and right movements of all objects, but due to the fact that the item number four has a favorable shape and occupies a large part of the detection area, in Table 5.6 the classification of its location is not displayed.

Table 5.5: Analysis of the first scenario using object number three as target.

Location	$(x, y)\,real$ (cm)	$\overline{(x, y)}$ (cm)	σ_x (cm)	σ_y (cm)	S_E (cm)	R_E (%)
Left	(14.35, 96.20)	(14.21, 96.09)	2.29	0.47	0.13	0.13
Center	(17.75, 35.20)	(17.85, 35.53)	0.30	1.03	0.76	0.86
Right	(19.0, 65.50)	(20.10, 66.68)	1.35	0.69	1.44	2.11

Table 5.6: Analysis of the first scenario using object number four as target.

Location	$(x, y)\,real$ (cm)	$\overline{(x, y)}$ (cm)	σ_x (cm)	σ_y (cm)	S_E (cm)	R_E (%)
—	(18.50, 43.55)	(19.08, 45.07)	1.00	0.52	1.67	3.54
—	(18.65, 44.50)	(18.99, 44.97)	0.91	0.51	0.57	1.18
—	(22.25, 72.80)	(21.98, 72.72)	2.51	0.78	0.15	0.20

Table 5.7: Analysis of the first scenario using object number five as target.

Location	$(x, y)\,real$ (cm)	$\overline{(x, y)}$ (cm)	σ_x (cm)	σ_y (cm)	S_E (cm)	R_E (%)
Left	(13.90, 85.60)	(14.20, 85.11)	3.22	0.61	0.43	0.50
Center	(17.95, 40.20)	(17.89, 40.93)	1.02	0.63	0.64	1.45
Right	(22.50, 57.60)	(21.82, 57.69)	0.71	0.45	0.16	0.26

5.2.2 Case B: Second Scenario

The second scheme was configured with $\alpha_{1,2} = 40°$ and $l = 50$ cm adopting the objects number four and five as target. Once more, one hundred and fifty samples of valid detection are stored and the procedure of first scenario is reproduced. Table 5.8 and 5.9 indicates the mean, standard deviation, systematic error and relative error of each object.

Table 5.8: Evaluation of the second scenario using the object number four object as target.

Location	$(x, y)\,real$ (cm)	$\overline{(x, y)}$ (cm)	σ_x (cm)	σ_y (cm)	S_E (cm)	R_E (%)
Left	(17.10, 39.40)	(22.68, 40.17)	0.42	0.46	3.18	7.40
Center	(27.8, 15.20)	(26.37, 14.31)	0.21	0.77	1.68	5.30
Right	(37.10, 43.50)	(30.08, 44.69)	0.43	0.44	3.30	5.77

In this case, because the baseline is larger than first, it is possible to discriminate location of the object number four.

Table 5.9: Evaluation of the second scenario using object number five as target.

Location	$(x, y)\,real$ (cm)	$\overline{(x, y)}$ (cm)	σ_x (cm)	σ_y (cm)	S_E (cm)	R_E (%)
Left	(18.10, 29.50)	(24.75, 30.37)	0.38	0.78	4.57	13.20
Center	(27.02, 17.20)	(27.06, 16.9)	0.29	0.71	0.13	0.41
Right	(32.20, 33.80)	(25.36, 34.83)	0.48	0.99	3.62	7.75

5.2.3 Case C: Third Scenario

The last scenario presents a configuration with $\alpha_{1,2} = 45°$ and $l = 19$ cm employing the object number three and five. As the value of the baseline is smaller and closer to the object dimensions, the classification of positioning is not taken into account in this report, only the error analysis. Also, the procedure used in the previous scenarios is reproduced. Table 5.10 provides the mean, standard deviation, systematic error and relative error of each measurement.

Table 5.10: Report of the third scenario detecting object number three and five.

Object No.	$(x, y)\,real$ (cm)	$\overline{(x, y)}$ (cm)	σ_x (cm)	σ_y (cm)	S_E (cm)	R_E (%)
3	(15.25, 38.50)	(12.71, 40.07)	0.68	0.45	0.63	1.52
5	(11.40, 56.80)	(11.70, 57.61)	0.96	0.43	0.87	1.50

In order to verify how the system behaves with very close objects, the object no. three was positioned a short distance from the sensors. This item was selected because it has the smallest dimension along the y axis among the available objects. Table 5.11 shows the mean, standard deviation, systematic error and relative error of this situation.

Table 5.11: Target analysis near the sensors.

Object No.	$(x, y)\,real$ (cm)	$\overline{(x, y)}$ (cm)	σ_x (cm)	σ_y (cm)	S_E (cm)	R_E (%)
3	(9.75, 8.50)	(11.78, 10.22)	0.36	0.39	2.67	20.65

5.2.4 Case Analysis

The graph in Figure 5.5 presents the average of relative error according to α angle. Furthermore, all objects and positioning are included in this evaluation and the baseline value is unconsidered. So, analyzing the system behavior from this point of view, it is possible to conclude that when α is equal to 0° the system demonstrates the smallest relative error.

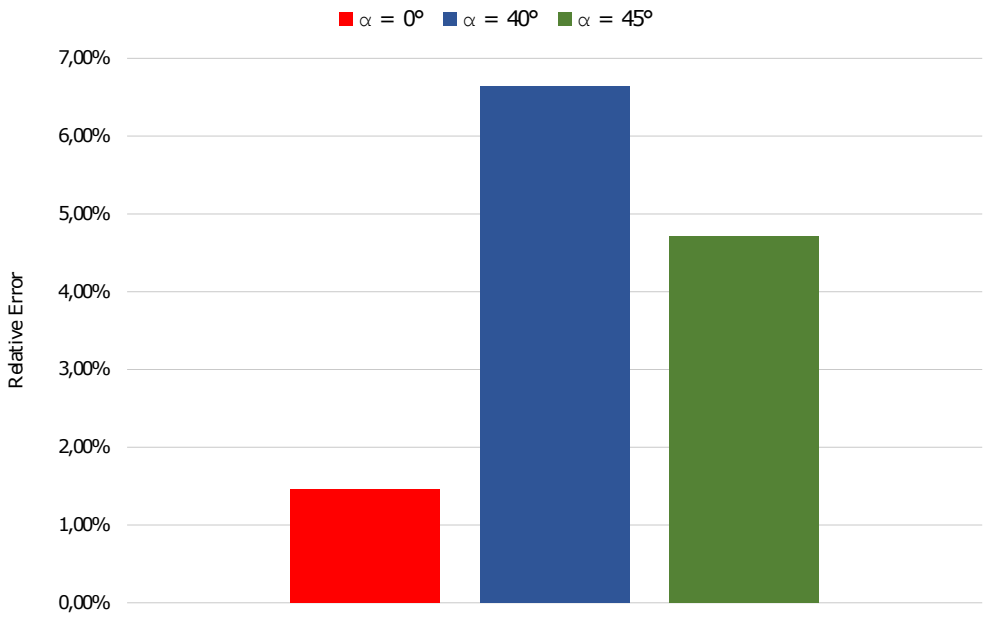

Figure 5.5: Average of relative error according to α angles.

As expected, the detection of the object no. three presented the best performance in the measurements, due to the fact that flat surfaces can be more easily reflected by ultrasonic signal. On the other hand, roughness surfaces and different shapes yields a wide dispersion of the reflected signal. In this investigation, the edge or corner of the object is not considered, attributed to increases in complexity and different strategy to be applied. Figure 5.6 shows the dispersion of the samples relative to the mean value of the measurements about object number three on the right (Case A). Similar graphics in respect to another cases are presented in Appendix F.

The motion of the objects to left, center and right with respect to the baseline was successful comprised. Of course some situations presenting improper characteristics, such

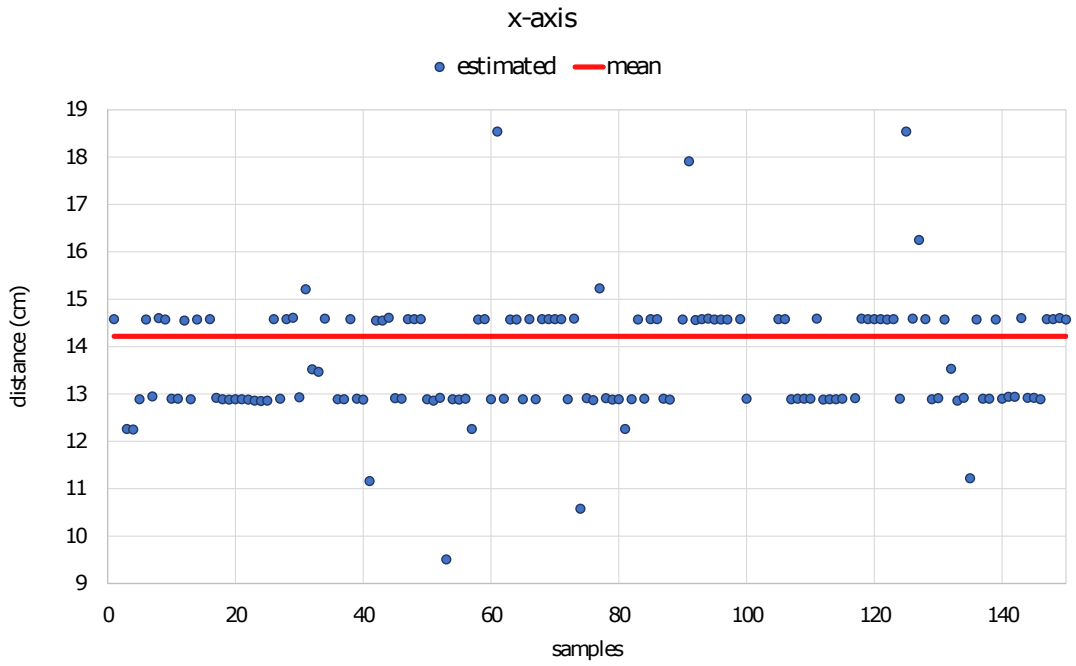

(a) Scatter of x-axis around the mean value.

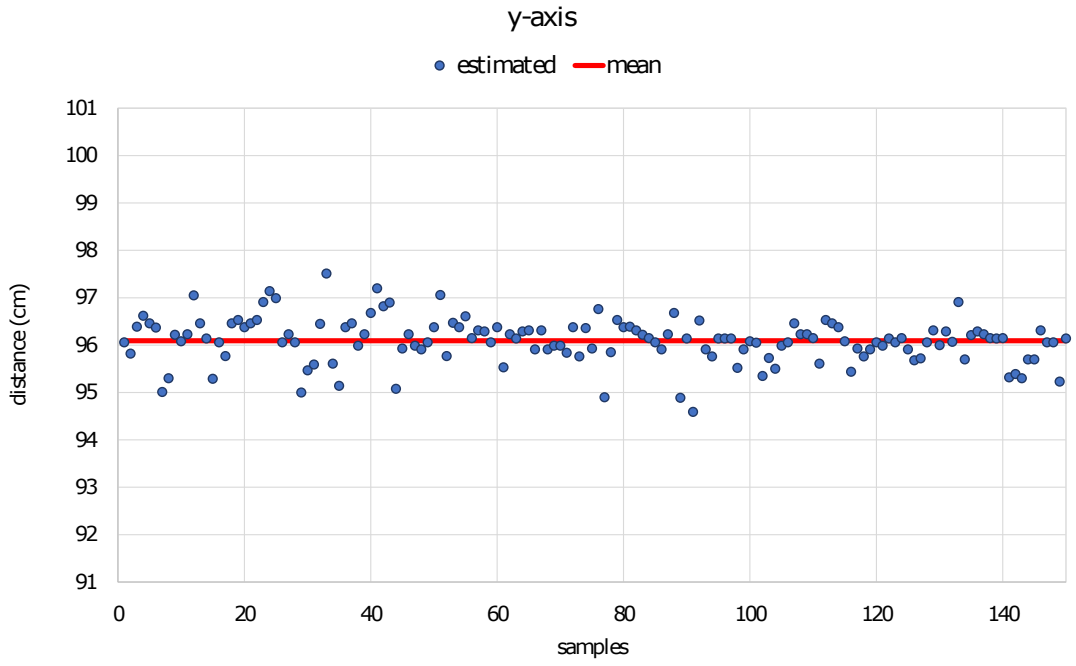

(b) Scatter of y-axis around the mean value.

Figure 5.6: Case A: Object number three positioned on left of the detection area.

as a large object and a small baseline or a not favorable orientation of α, makes the location classification a difficult task. For this reason, it is important to carefully design the settings to be used on the system.

Figure 5.7 represents graphically the Tables 5.5 to 5.7, denoting the difference between the real coordinates (adopted as the center of the object) and estimated by the system for the best case, i.e. the first scenario. Solid line (black) means the conventional true value and dotted line (red) means the calculated coordinate.

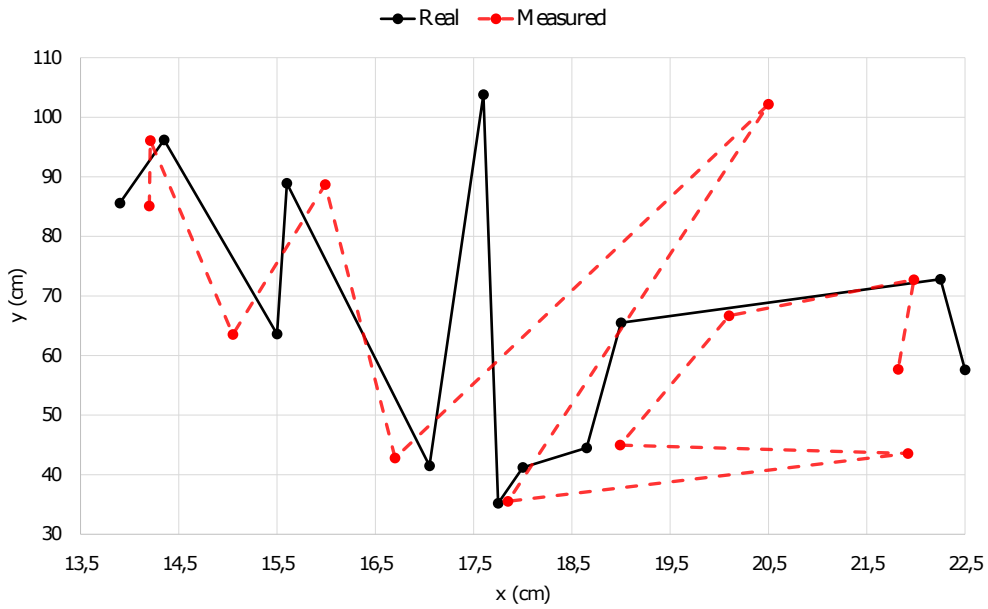

Figure 5.7: Comparison between the measured and real coordinate of the best case.

Bearing in mind the errors inherent in the measurement process, the Measurement Result (MR) of Case A is expressed according to Equation 5.4.

$$MR = \overline{M} - S_E \pm Re/n^{\frac{1}{2}} \tag{5.4}$$

where $\overline{M}$ is the arithmetic mean of n samples, S_E the systematic error and Re is the repeatability, which can be calculated as a product of multiplying the t-Student coefficient by the standard deviation (Equation 5.5).

$$Re = \pm\ t \cdot \sigma_{x,y} \tag{5.5}$$

Tables 5.5 to 5.7 are rewritten in Tables 5.12 to 5.14, presenting the MR of each positioning. Intending to apply the t-distribution with a confidence of 95%, a lower number of samples is required. For this reason, ten random samples of each set are selected with $(n-1)$ degrees of freedom, representing t equal to 2.26 [88].

Table 5.12: Measurement result of Case A employing object number three.

Location	$(x, y)\,real$ (cm)	MR_x (cm)	MR_y (cm)
Left	(14.35, 96.20)	14.35 ± 2.02	96.20 ± 0.37
Center	(17.75, 35.20)	17.75 ± 0.24	35.20 ± 0.62
Right	(19.0, 65.50)	19.0 ± 0.49	65.50 ± 0.58

Table 5.13: Measurement result of Case A employing object number four.

Location	$(x, y)\,real$ (cm)	MR_x (cm)	MR_y (cm)
—	(18.50, 43.55)	18.50 ± 0.68	43.55 ± 0.20
—	(18.65, 44.50)	18.65 ± 0.91	44.50 ± 0.52
—	(22.25, 72.80)	22.25 ± 1.29	72.80 ± 0.50

Table 5.14: Measurement result of Case A employing object number five.

Location	$(x, y)\,real$ (cm)	MR_x (cm)	MR_y (cm)
Left	(13.90, 85.60)	13.90 ± 2.19	85.6 ± 0.44
Center	(17.95, 40.20)	17.95 ± 0.95	40.20 ± 0.58
Right	(22.50, 57.60)	22.50 ± 0.59	57.60 ± 0.28

5.2.5 System Cost and Architecture Proposal

This section details the price of required components used to develop the sonar, taking into account the average price in the Portuguese and international market.

Unfortunately, a physical structure to incorporate the arrangement was not built, in this sense, costs related to the system housing are not estimated. However, a prototype

Table 5.15: Estimated budget for the projected system.

Quantity	Item	Portugal	International	Currency
1	STM32	3.90	1.80	EUR
1	ESP32	12.50	2.72	EUR
3	HY-SRF05	14.95	5.12	EUR
Total	—	31.40	9.64	EUR

(∗) Prices from Bot'n Roll, Electrofun, eBay and Aliexpress (2019).

is built in a computer aided design for future implementation, as shown in Figure 5.8.

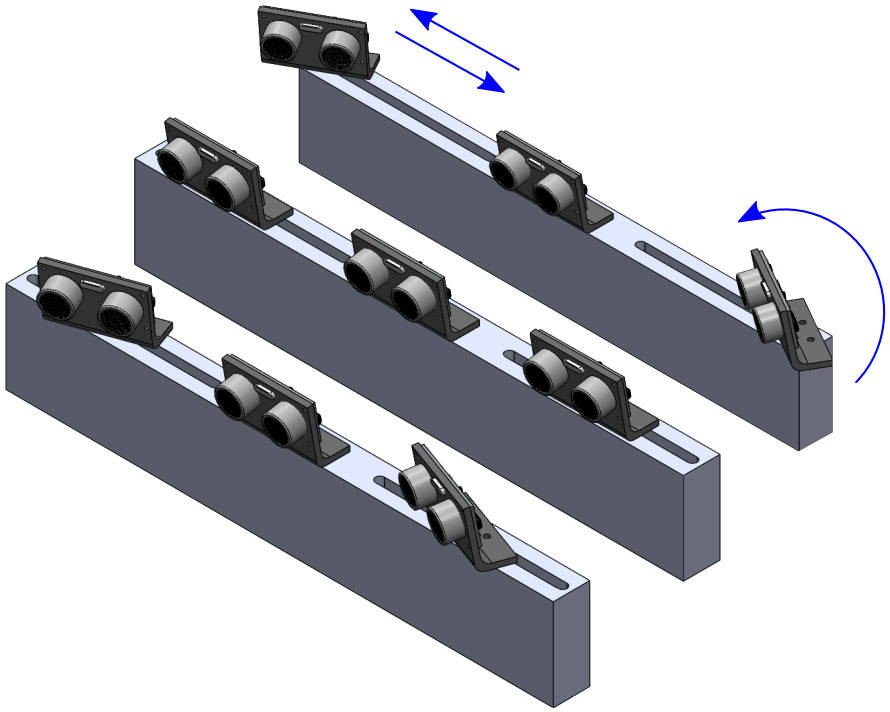

Figure 5.8: Proposed physical structure, presenting distinct configurations.

In order to achieve angular rotation, a servomotor is suggested to be coupled to the base of the ultrasonic sensors. In addition, movement along the rails to vary the baseline can be accomplished with a stepper motor. The technical drawing, with all dimensions is presented in Appendix G.

Chapter 6

Conclusion and Future Work

A system based on low cost elements, providing an accurate and reliable detection of objects in a two-dimensional space was accomplished. Different fields of study, involving robotics, mathematics and signal processing were employed, in order to achieve the settled objectives. Two optimal methods for performing the ToF estimation — envelope detection and CCR — were analyzed, where a novel approach matching them was proposed. Envelope detection is valuable, but the combined technique has been shown to be more efficient.

The selection of an appropriate method to evaluate the system was one of the difficulties encountered during the system validation. Due to the wide beam pattern of the sensor, the point at which the ultrasonic wave reflects on the object is unknown, making the comparison of estimated coordinates with the real ones complex. After the experimental tests were carried out, it was verified that all the coordinates calculated by the system were credible.

From the results, it is clear that the system performed properly with acceptable error levels. On the other hand, the system was not able to get fast processing, which is a significant constraint for real-time applications. Overall, the low cost sonar using the matched technique can be an attractive alternative to the traditional models of ultrasonic detection, presenting good accuracy and repeatability of the measurements. The use of sonar is a common approach in mobile robotics, which was the main focus of this work.

However, the application of the system can be extended to other areas, such as electronic aid systems for visually impaired and blind individuals.

6.1 Future Works

Based on the work introduced, it is possible to identify several aspects that may support further studies and improvements, as follows:

- Optimize the processing time with another MCU or even a DSP for real-time applications;
- Integrate the system with any mobile navigation device for testing and validation;
- Make a comparison between other ultrasonic sensor arrangements;
- Build a physical structure such as a module to be attached to devices;
- Perform the measurements with other set of configurations and objects.

Bibliography

[1] Z. S. Lim, S. T. Kwon, and M. G. Joo, "Multi-object identification for mobile robot using ultrasonic sensors", *International Journal of Control, Automation and Systems*, vol. 10, no. 3, pp. 589–593, 2012.

[2] C. Walter and H. Schweinzer, "Locating of objects with discontinuities, boundaries and intersections using a compact ultrasonic 3D sensor", in *2014 International Conference on Indoor Positioning and Indoor Navigation (IPIN)*, IEEE, 2014, pp. 591–600.

[3] D. Bank, "A novel ultrasonic sensing system for autonomous mobile systems", *IEEE Sensors Journal*, vol. 2, no. 6, pp. 597–606, 2002.

[4] H. Cong-Nguyen, S.-B. Oh, N.-G. Kim, D.-J. Park, and S.-H. Han, "Real-time robust control of mobile robot using ultrasonic sensor", in *2008 International Conference on Control, Automation and Systems*, IEEE, 2008, pp. 2585–2589.

[5] R. V. Jawale, M. V. Kadam, R. S. Gaikawad, and L. S. Kondaka, "Ultrasonic navigation based blind aid for the visually impaired", in *2017 IEEE International Conference on Power, Control, Signals and Instrumentation Engineering (ICPCSI)*, IEEE, 2017, pp. 923–928.

[6] B. Kreczmer, "Objects localization and differentiation using ultrasonic sensors", in *Robot Localization and Map Building*, IntechOpen, 2010.

[7] G. Kaniak and H. Schweinzer, "A 3D airborne ultrasound sensor for high-precision location data estimation and conjunction", in *2008 IEEE Instrumentation and Measurement Technology Conference*, IEEE, 2008, pp. 842–847.

[8] J. C. Jackson, R. Summan, G. I. Dobie, S. M. Whiteley, S. G. Pierce, and G. Hayward, "Time-of-flight measurement techniques for airborne ultrasonic ranging", *IEEE transactions on ultrasonics, ferroelectrics, and frequency control*, vol. 60, no. 2, pp. 343–355, 2013.

[9] M. O. Khyam, S. S. Ge, X. Li, and M. R. Pickering, "Highly accurate time-of-flight measurement technique based on phase-correlation for ultrasonic ranging", *IEEE sensors journal*, vol. 17, no. 2, pp. 434–443, 2016.

[10] J. D. N. Cheeke, *Fundamentals and applications of ultrasonic waves*. CRC press, 2016.

[11] R. Siegwart, I. R. Nourbakhsh, and D. Scaramuzza, *Introduction to autonomous mobile robots*. MIT press, 2011.

[12] M. Becker, C. M. Dantas, and W. P. Macedo, "Obstacle avoidance procedure for mobile robots", in *ABCM Symposium series in Mechatronics*, ABCM, vol. 2, 2006, pp. 250–257.

[13] H. Diwan, "Development of an obstacle detection and navigation system for autonomous powered wheelchairs", PhD thesis, University of Ontario Institute of Technology, 2019. [Online]. Available: `http://hdl.handle.net/10155/1051`.

[14] M. Aliff, M. Yusof, N. S. Sani, and A. Zainal, "Development of fire fighting robot (QRob)", *Development*, vol. 10, no. 1, 2019.

[15] J. Chen and Y. K. Cho, "Detection of damaged infrastructure on disaster sites using mobile robots", in *2019 16th International Conference on Ubiquitous Robots (UR)*, IEEE, 2019, pp. 648–653.

[16] J. Azeta, C. Bolu, D. Hinvi, A. Abioye, H. Boyo, P. Anakhu, and P. Onwordi, "An android based mobile robot for monitoring and surveillance", *Procedia Manufacturing*, vol. 35, pp. 1129–1134, 2019.

[17] M. U. Khan, "Mobile robot navigation using reinforcement learning in unknown environments", *Balkan Journal of Electrical and Computer Engineering*, vol. 7, no. 3, pp. 235–244, 2019.

[18] M. Cinietal, "Real-time obstacle avoidance by an autonomous mobile robot using an active vision sensor and a vertically emitted laser slit", in *Intelligent Autonomous Systems*, vol. 7, 2002, pp. 301–309.

[19] H. Yu and L. Kong, "Autonomous mobile robot based on differential Global Positioning System", in *2018 IEEE International Conference on Mechatronics and Automation (ICMA)*, IEEE, 2018, pp. 392–396.

[20] P. Rana, A. Kumar, and S. Roy, "Implementation of obstacle detection and avoidance methodology for low cost autonomous vehicle", *International Journal of Advanced Engineering and Management*, vol. 2, no. 6, pp. 135–140, 2017.

[21] J. Krejsa and S. Vechet, "Low cost laser rangefinder evaluation", in *Proceedings of the Engineering Mechanics 2018 24th International Conference, Svratka, Czech Republic*, 2018, pp. 433–436.

[22] A. R. Patkar and P. P. Tasgaonkar, "Object recognition using horizontal array of ultrasonic sensors", in *2016 International Conference on Communication and Signal Processing (ICCSP)*, IEEE, 2016, pp. 0983–0986.

[23] National Oceanic and Atmospheric Administration (NOAA), *An Introduction to LiDAR Technology, Data, and Applications*, `http://coast.noaa.gov/data/digitalcoast/pdf/lidar-101.pdf`, [Accessed: Aug 28, 2019], 2012.

[24] Y. Peng, D. Qu, Y. Zhong, S. Xie, J. Luo, and J. Gu, "The obstacle detection and obstacle avoidance algorithm based on 2D LiDAR", in *2015 IEEE International Conference on Information and Automation*, IEEE, 2015, pp. 1648–1653.

[25] G. Xu, *Gps: Theory, algorithms and aplications*. Springer, 2007.

[26] D. Maier and A. Kleiner, "Improved gps sensor model for mobile robots in urban terrain", in *2010 IEEE International Conference on Robotics and Automation*, IEEE, 2010, pp. 4385–4390.

[27] X. Ruan and W. Li, "Ultrasonic sensor based two-wheeled self-balancing robot obstacle avoidance control system", in *2014 IEEE International Conference on Mechatronics and Automation*, IEEE, 2014, pp. 896–900.

[28] R. Lewis and A. Johnston, "A scanning laser rangefinder for a robotic vehicle", 1977.

[29] C.-C. Tsai, "A localization system of a mobile robot by fusing dead-reckoning and ultrasonic measurements", *IEEE Transactions on Instrumentation and Measurement*, vol. 47, no. 5, pp. 1399–1404, 1998.

[30] N. Harper and P. McKerrow, "Recognising plants with ultrasonic sensing for mobile robot navigation", *Robotics and Autonomous Systems*, vol. 34, no. 2-3, pp. 71–82, 2001.

[31] J.-M. Lee, D. H. Lee, H. An, N. Huh, M. K. Kim, and M. H. Lee, "Ultrasonic satellite system for the positioning of mobile robots", in *30th Annual Conference of IEEE Industrial Electronics Society, 2004. IECON 2004*, IEEE, vol. 1, 2004, pp. 448–453.

[32] F. Rivard, J. Bisson, F. Michaud, and D. Létourneau, "Ultrasonic relative positioning for multi-robot systems", in *2008 IEEE International Conference on Robotics and Automation*, IEEE, 2008, pp. 323–328.

[33] W. Adiprawita, A. S. Ahmad, J. Sembiring, and B. R. Trilaksono, "New resampling algorithm for particle filter localization for mobile robot with 3 ultrasonic sonar sensor", in *Proceedings of the 2011 International Conference on Electrical Engineering and Informatics*, IEEE, 2011, pp. 1–6.

[34] L. Chassagne, O. Bruneau, A. Bialek, C. Falguière, E. Broussard, and O. Barrois, "Ultrasonic sensor triangulation for accurate 3D relative positioning of humanoid robot feet", *IEEE Sensors Journal*, vol. 15, no. 5, pp. 2856–2865, 2014.

[35] S. Vaseghi, *Advanced digital signal processing and noise reduction*. Wiley, 2008, ISBN: 9780470740163. [Online]. Available: `https://books.google.pt/books?id=vVgLv0ed3cgC`.

[36] T. Moore and D. Stouch, "A generalized extended kalman filter implementation for the robot operating system", in *Intelligent autonomous systems 13*, Springer, 2016, pp. 335–348.

[37] M. Grewal and A. Andrews, *Kalman filtering: Theory and practice using matlab*, Third edition. Wiley, 2011, ISBN: 9781118210468.

[38] L. C. Básaca, J. Rodríguez, O. Y. Sergiyenko, V. V. Tyrsa, W. Hernández, J. I. N. Hipólito, and O. Starostenko, "Resolution improvement of dynamic triangulation method for 3D vision system in robot navigation task", in *IECON 2010-36th Annual Conference on IEEE Industrial Electronics Society*, IEEE, 2010, pp. 2886–2891.

[39] R. Qi, T. L. Lam, H. Qian, and Y. Xu, "Arc tracking on an eight-axis robot system", in *2011 IEEE International Conference on Robotics and Biomimetics*, IEEE, 2011, pp. 678–683.

[40] F. Keyrouz, "Advanced binaural sound localization in 3D for humanoid robots", *IEEE Transactions on Instrumentation and Measurement*, vol. 63, no. 9, pp. 2098–2107, 2014.

[41] Y. Shen, "Efficient normalized cross correlation calculation method for stereo vision based robot navigation", *Frontiers of Computer Science in China*, vol. 5, no. 2, pp. 227–235, 2011.

[42] P. Marwedel, *Embedded system design*. Springer, 2006, vol. 1.

[43] R. Dubey, *Introduction to embedded system design using field programmable gate arrays*. Springer Science & Business Media, 2008.

[44] A. Malinowski and H. Yu, "Comparison of embedded system design for industrial applications", *IEEE transactions on industrial informatics*, vol. 7, no. 2, pp. 244–254, 2011.

[45] C.-H. Kuo, H.-W. Yeh, C.-E. Wu, and K.-M. Hsiao, "Development of autonomous robotic wheelchair controller using embedded systems", in *IECON 2007-33rd Annual Conference of the IEEE Industrial Electronics Society*, IEEE, 2007, pp. 3001–3006.

[46] S. S. Bhatlawande, J. Mukhopadhyay, and M. Mahadevappa, "Ultrasonic spectacles and waist-belt for visually impaired and blind person", in *2012 National Conference on Communications (NCC)*, IEEE, 2012, pp. 1–4.

[47] H.-S. Kim and J.-S. Choi, "Advanced indoor localization using ultrasonic sensor and digital compass", in *2008 International Conference on Control, Automation and Systems*, IEEE, 2008, pp. 223–226.

[48] G. Andria, F. Attivissimo, and N. Giaquinto, "Digital signal processing techniques for accurate ultrasonic sensor measurement", *Measurement*, vol. 30, no. 2, pp. 105–114, 2001.

[49] W. Li, Q. Chen, and J. Wu, "Double threshold ultrasonic distance measurement technique and its application", *Review of Scientific Instruments*, vol. 85, no. 4, p. 044 905, 2014.

[50] K.-N. Huang and Y.-P. Huang, "Multiple-frequency ultrasonic distance measurement using direct digital frequency synthesizers", *Sensors and Actuators A: Physical*, vol. 149, no. 1, pp. 42–50, 2009.

[51] R. Queirós, R. Martins, P. S. Girao, and A. C. Serra, "A new method for high resolution ultrasonic ranging in air", *Proc. international measurement confederation, Rio de Janeiro*, 2006.

[52] R. Kuc and M. W. Siegel, "Physically based simulation model for acoustic sensor robot navigation", *IEEE Transactions on Pattern Analysis and Machine Intelligence*, no. 6, pp. 766–778, 1987.

[53] I. Amidror, *The theory of the moiré phenomenon volume ii: Aperiodic layers*. Springer, 2007.

[54] D. Marioli, C. Narduzzi, C. Offelli, D. Petri, E. Sardini, and A. Taroni, "Digital time-of-flight measurement for ultrasonic sensors", *IEEE Transactions on Instrumentation and Measurement*, vol. 41, no. 1, pp. 93–97, 1992.

[55] B. Xu, L. Yu, and V. Giurgiutiu, "Advanced methods for time-of-flight estimation with application to lamb wave structural health monitoring", in *Proc. International Workshop on SHM*, 2009, pp. 1202–1209.

[56] P. Pejovic, *Peak Detector and/or Envelope Detector — A Detailed Analysis —*, Apr. 2018. DOI: 10.5281/zenodo.1310694. [Online]. Available: https://doi.org/10.5281/zenodo.1310694.

[57] K. W. Busch and M. A. Busch, "Light polarization and signal processing in chiroptical instrumentation", in *Chiral Analysis*, Elsevier, 2018, pp. 73–151.

[58] C. Fritsch, A. Ibanez, and M. Parrilla, "A digital envelope detection filter for real-time operation", *IEEE Transactions on Instrumentation and Measurement*, vol. 48, no. 6, pp. 1287–1293, 1999.

[59] X. F. Jia, H. Q. An, and S. G. Zhang, "Cubic spline interpolation method for the envelope tracking of middle and low frequency voltage flicker", in *Advanced materials research*, Trans Tech Publ, vol. 960, 2014, pp. 704–709.

[60] M. A. G. Ruggiero and V. L. d. R. Lopes, *Cálculo numérico: Aspectos teóricos e computacionais*. Makron Books do Brasil, 1997.

[61] B. Stanley and P. McKerrow, "Measuring range and bearing with a binaural ultrasonic sensor", in *Proceedings of the 1997 IEEE/RSJ International Conference on Intelligent Robot and Systems. Innovative Robotics for Real-World Applications. IROS'97*, IEEE, vol. 2, 1997, pp. 565–571.

[62] D. Caicedo and A. Pandharipande, "Ultrasonic arrays for localized presence sensing", *IEEE Sensors journal*, vol. 12, no. 5, pp. 849–858, 2011.

[63] H. Peremans, K. Audenaert, and J. M. Van Campenhout, "A high-resolution sensor based on tri-aural perception", *IEEE transactions on Robotics and Automation*, vol. 9, no. 1, pp. 36–48, 1993.

[64] A. Kianpisheh, N. Mustaffa, P. Limtrairut, and P. Keikhosrokiani, "Smart parking system (SPS) architecture using ultrasonic detector", *International Journal of Software Engineering and Its Applications*, vol. 6, no. 3, pp. 55–58, 2012.

[65] E. Vargas, R. Ceres, J. Marti, L. Caldero, *et al.*, "Ultrasonic sensor for liquid-level inspection in bottles", *Sensors and Actuators A: Physical*, vol. 61, no. 1-3, pp. 256–259, 1997.

[66] C. Gearhart, A. Herold, B. Self, C. Birdsong, and L. Slivovsky, "Use of ultrasonic sensors in the development of an electronic travel aid", in *2009 IEEE Sensors Applications Symposium*, IEEE, 2009, pp. 275–280.

[67] L. Kleeman and R. Kuc, "Mobile robot sonar for target localization and classification", *The International Journal of Robotics Research*, vol. 14, no. 4, pp. 295–318, 1995.

[68] H. Peremans and J. Chen, "Triaural perception: A comparison of neural network and maximum likelihood algorithms to solve the correspondence problem", in *Sensors and Control for Automation*, International Society for Optics and Photonics, vol. 2247, 1994, pp. 97–107.

[69] *What is signal processing?*, Apr. 2018. [Online]. Available: `https://signalprocessingsociety.org/our-story/signal-processing-101`.

[70] J. A. Putman, "Signal processing techniques", *EEG Info*, pp. 1–16, 1989.

[71] M. J. Pelgrom, "Analog-to-digital conversion", in *Analog-to-Digital Conversion*, Springer, 2013, pp. 133–137.

[72] S. Winder, *Analog and digital filter design*. Elsevier, 2002.

[73] L. D. Thede, *Practical analog and digital filter design*. Artech House Norwood, Mass, USA, 2005.

[74] B. A. Shenoi, *Introduction to digital signal processing and filter design*. John Wiley & Sons, 2005.

[75] P. S. Diniz, E. A. da Silva, and S. L. Netto, *Processamento digital de sinais-: Projeto e análise de sistemas*. Bookman Editora, 2014.

[76] L. Litwin, "FIR and IIR digital filters", *IEEE potentials*, vol. 19, no. 4, pp. 28–31, 2000.

[77] P. Podder, M. M. Hasan, M. R. Islam, and M. Sayeed, "Design and implementation of butterworth, chebyshev-i and elliptic filter for speech signal analysis", *International Journal of Computer Applications*, vol. 98, no. 7, 2014.

[78] Á. Bényi, "A Heron-type formula for the triangle", *The Mathematical Gazette*, vol. 87, no. 509, pp. 324–326, 2003.

[79] M. Liu, B. Liang, and J. Sun, "Automatic car tracing based on ultrasonic distance measurement", in *The Proceedings of the Second International Conference on Communications, Signal Processing, and Systems*, Springer, 2014, pp. 1221–1227.

[80] V. Zhmud, N. Kondratiev, K. Kuznetsov, V. Trubin, and L. Dimitrov, "Application of ultrasonic sensor for measuring distances in robotics", in *Journal of Physics: Conference Series*, IOP Publishing, vol. 1015, 2018, p. 032 189.

[81] ST Microelectronics. Datasheet, *STM32F103X8, STM32F103XB*, 2015.

[82] G. Brown, "Discovering the STM32 microcontroller", *Cortex*, vol. 3, 2012.

[83] A. Kurniawan, *Internet of things projects with ESP32: Build exciting and powerful IoT projects using the all-new espressif ESP32*. Packt Publishing, 2019.

[84] Espressif Systems. Datasheet, *ESP32 Series, Version 3.1*.

[85] V. Himpe, "I2C Bus FAQ. Version 1.6", 1996.

[86] N. Anand, G. Joseph, S. S. Oommen, and R. Dhanabal, "Design and implementation of a high speed serial peripheral interface", in *2014 International Conference on Advances in Electrical Engineering (ICAEE)*, IEEE, 2014, pp. 1–3.

[87] MICROCHIP, *Getting Started – USART*, 2001. [Online]. Available: `http://ww1.microchip.com/downloads/en/devicedoc/usart.pdf`.

[88] J. C. da Silva Neto, *Metrologia e controle dimensional*. Elsevier, 2012.

[89] Murata. Catalog, *Ultrasonic Sensor, S15E-5*, Application Manual, Oct. 2008.

Appendix A

Publications

Moreira, T.; Lima, J.; Costa, P. and Cunha, M. (2019). "Low-cost Sonar based on the Echolocation". In Proceedings of the 16th International Conference on Informatics in Control, Automation and Robotics - Volume 1: ICINCO, ISBN 978-989-758-380-3, pages 818-825. DOI: 10.5220/0008119108180825

Papers Submitted and Accepted

Moreira, T.; Lima, J.; Costa, P. and Cunha, M. (2019). "Low Cost Binaural System Based on the Echolocation". In 4th Iberian Robotics Conference (ROBOT2019).

Braun, J.; Fernandes, L.; Moya, T.; Oliveira, V.; Brito, T.; Lima, J. and Costa, P. (2019). "Robot@Factory Lite: An educational approach for the competition with simulated and real environment". In 4th Iberian Robotics Conference (ROBOT2019).

Appendix B

The System Flowchart

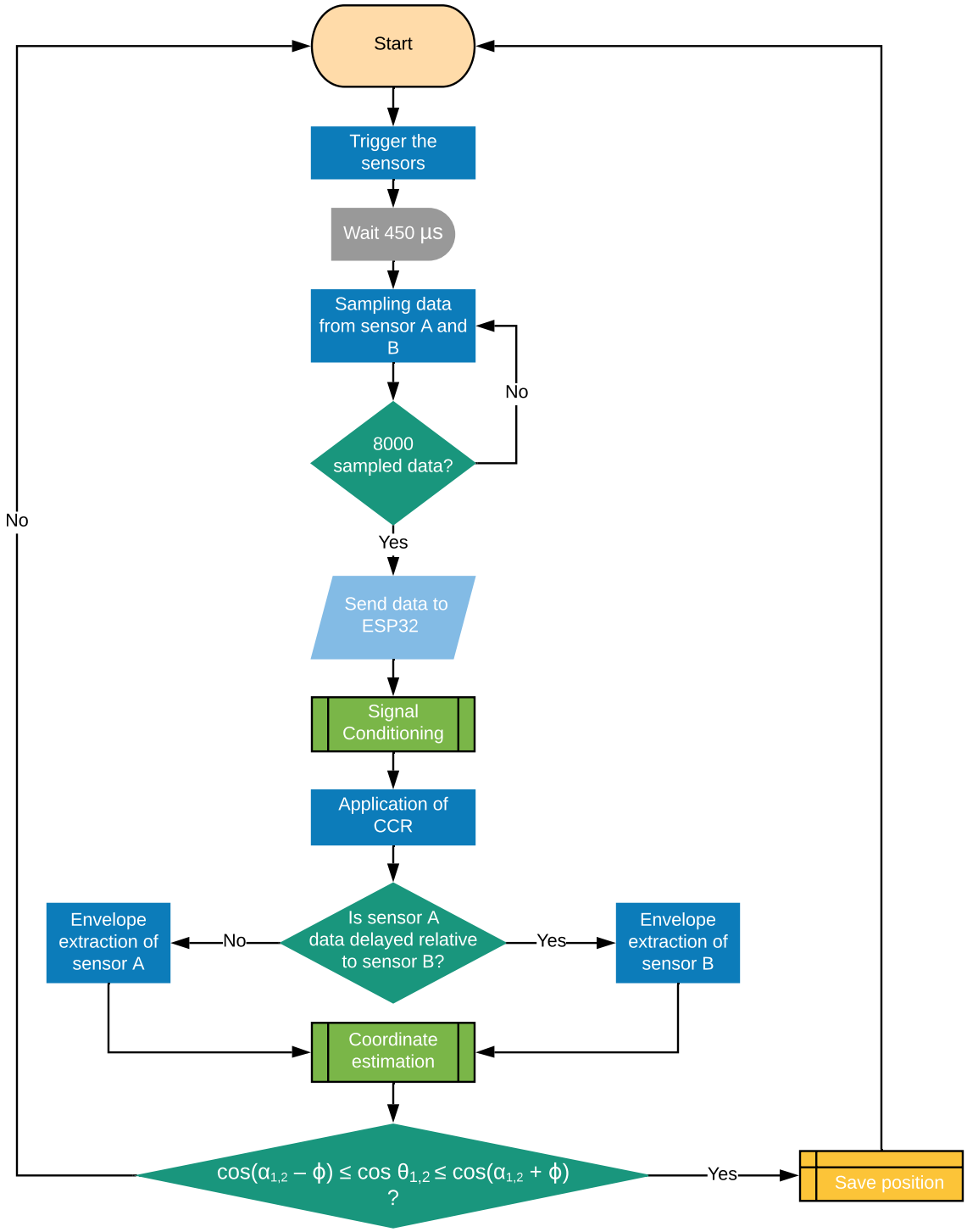

Figure B.1: Flowchart illustrating the achievement of the measurements.

Appendix C

Schematic Diagram of the System

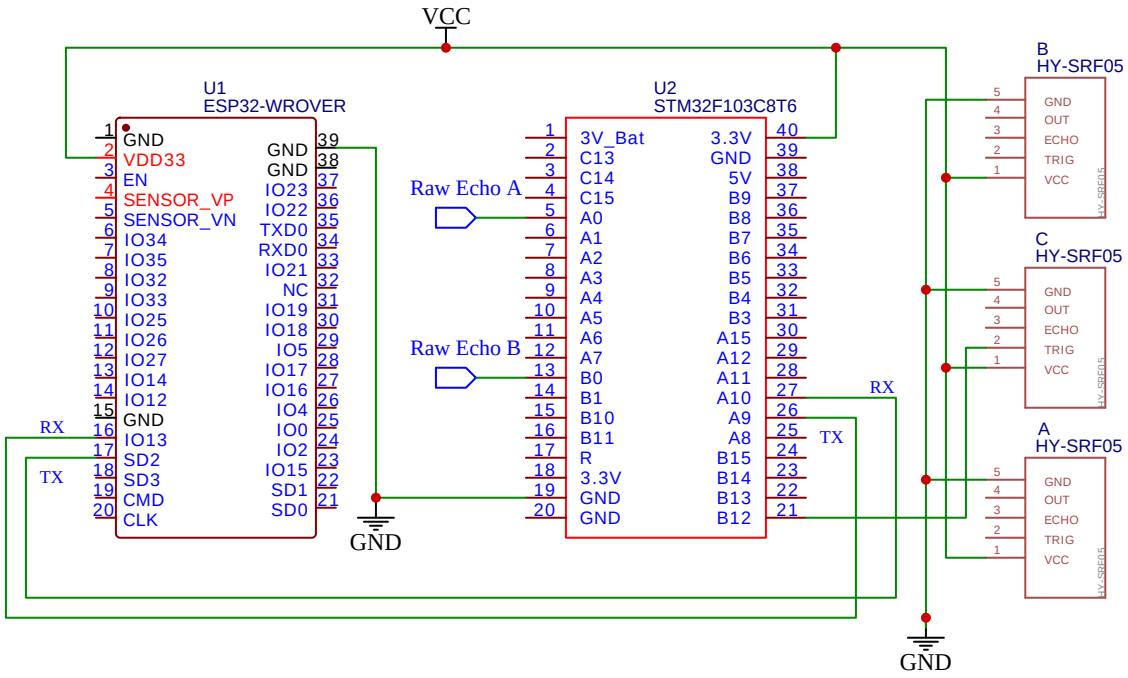

Figure C.1: Diagram of the physical connections.

Appendix D

HC-SR04 Circuit Diagram

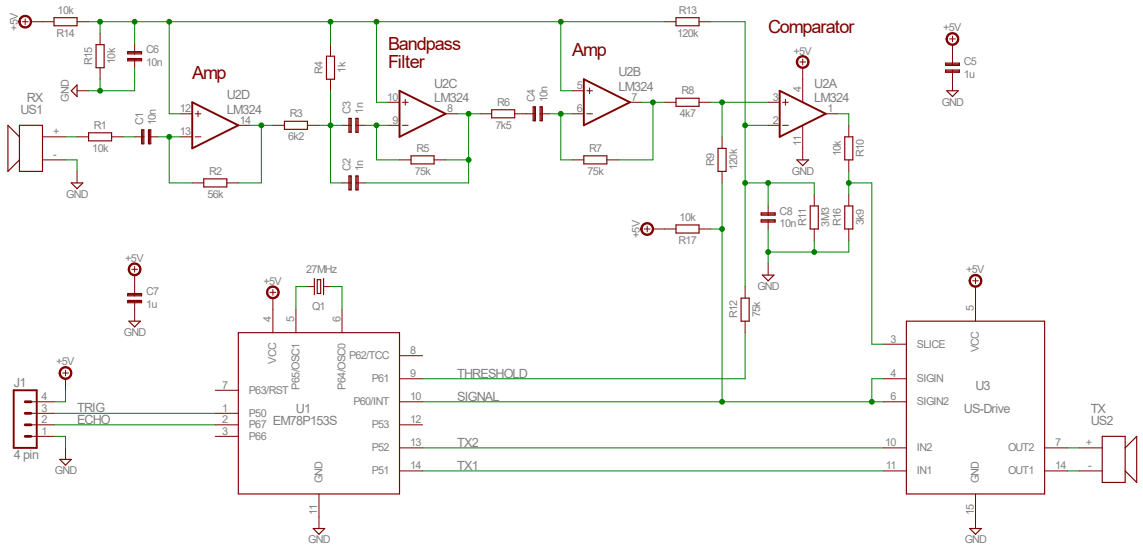

Figure D.1: HC-SR04 Schematic.

Appendix E

Objects Dimension

The set of items applied as target is composed of three cardboard boxes with different sizes, one cylindrical and a transparent object.

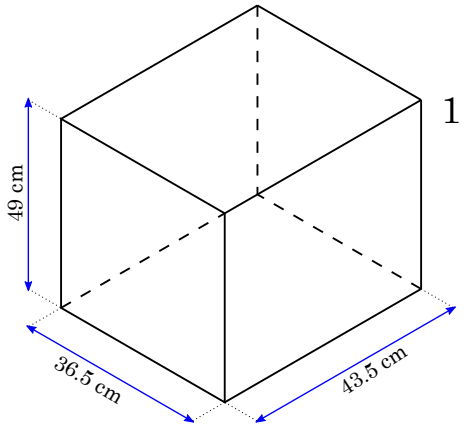

Figure E.1: Object number one.

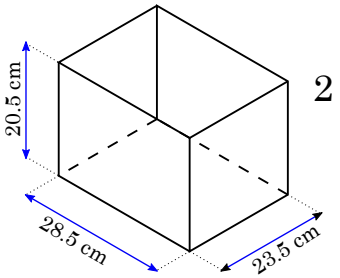

Figure E.2: Object number two.

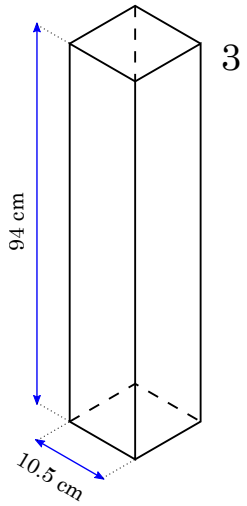

Figure E.3: Object number three.

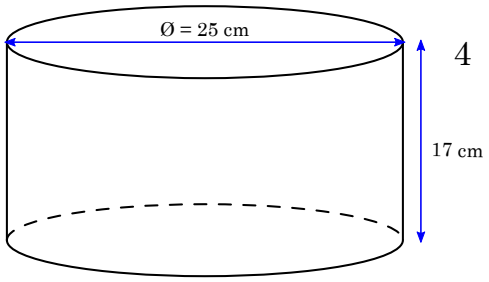

Figure E.4: Object number four.

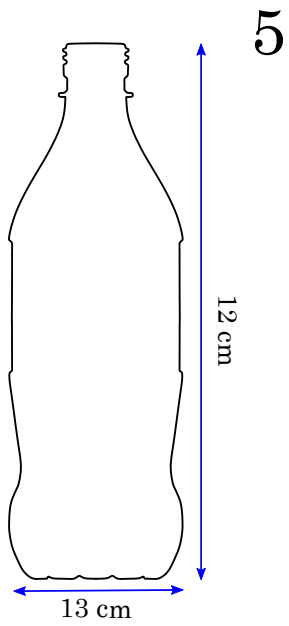

Figure E.5: Object number five.

Appendix F

Graphical Results

The following graphics displays the dispersion of x-axis and y-axis samples around the mean value of each measurement.

First Scenario

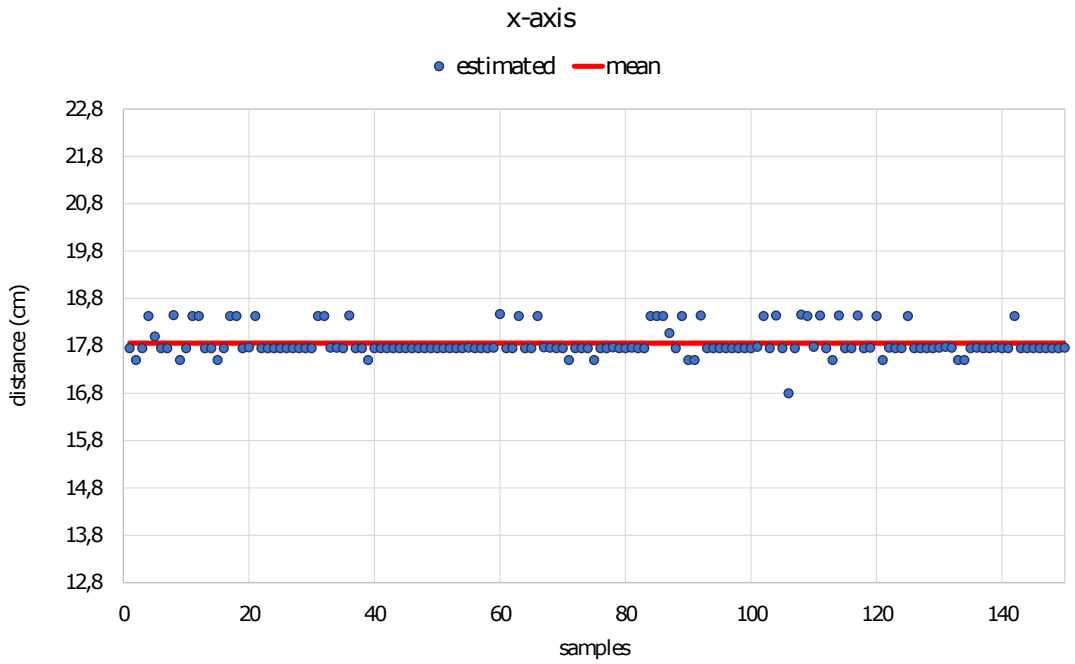

(a) x-axis scatter.

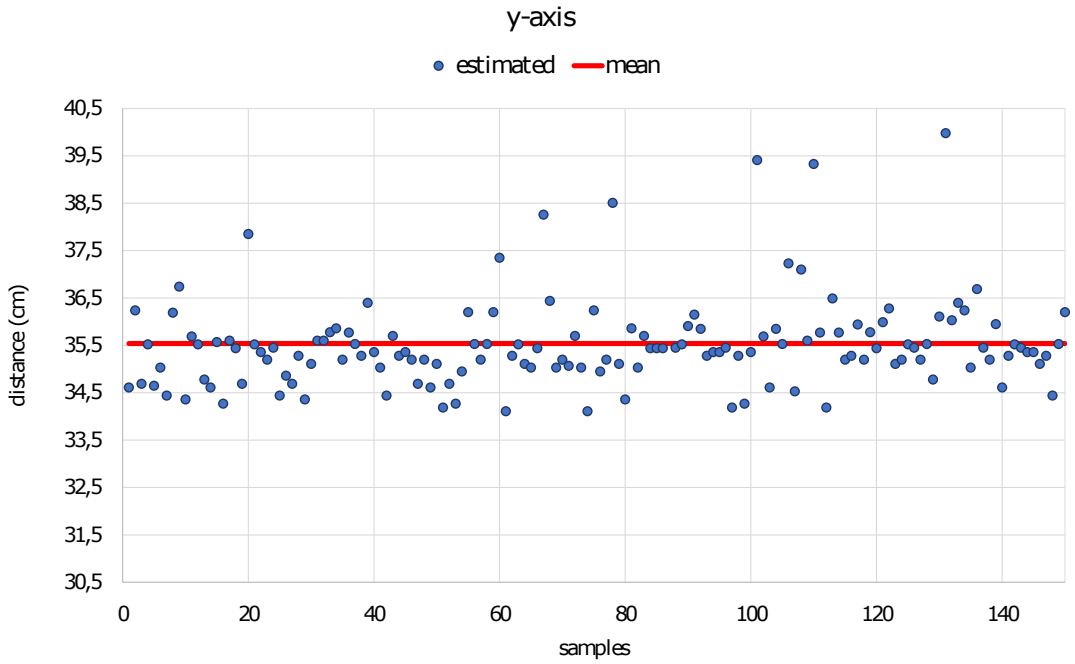

(b) y-axis scatter.

Figure F.1: Case A: Object number three positioned in center of the detection area.

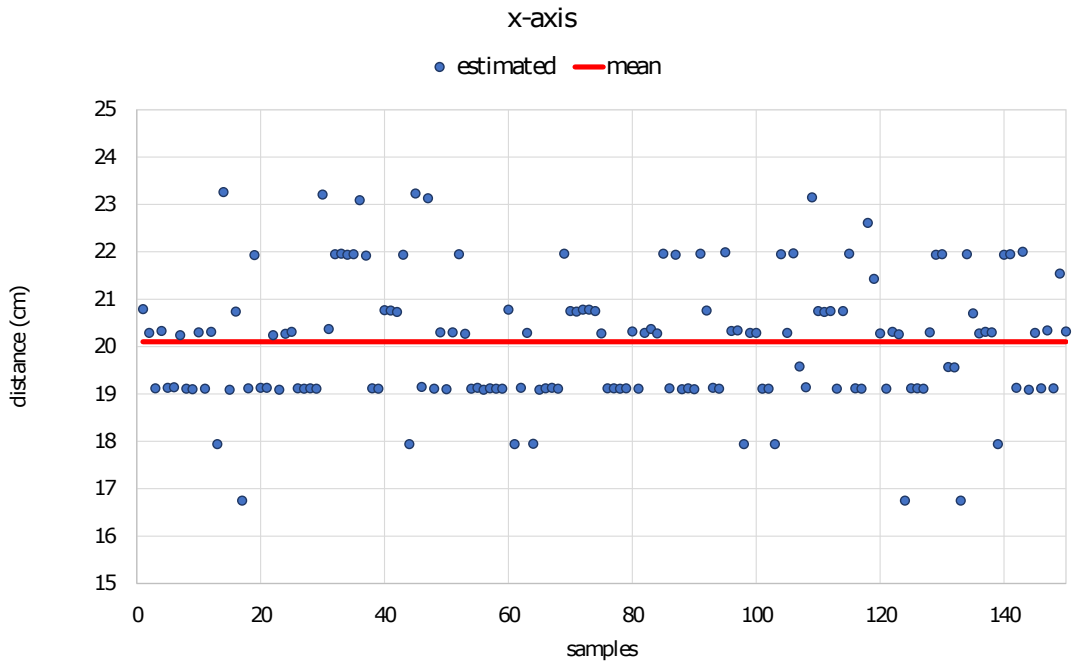

(a) x-axis scatter.

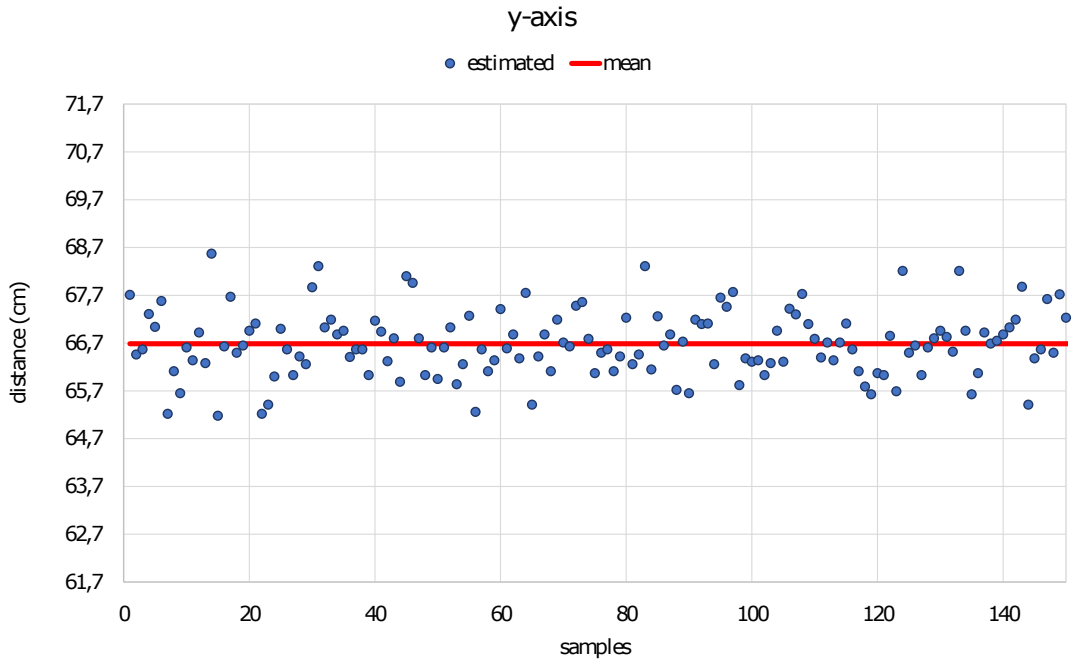

(b) y-axis scatter.

Figure F.2: Case A: Object number three positioned on right of the detection area.

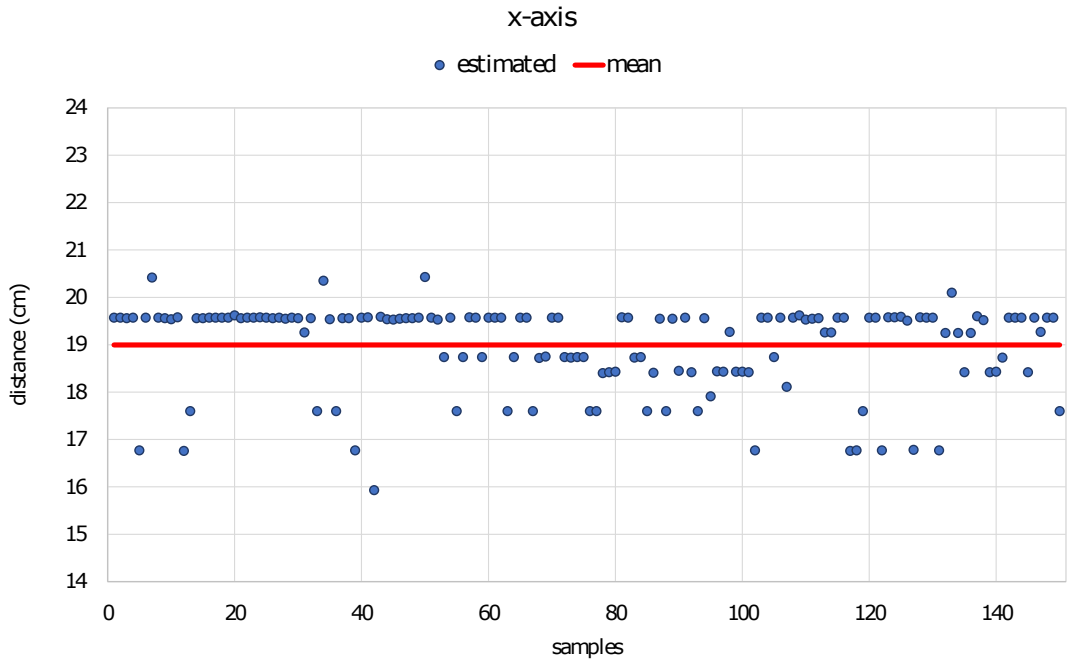

(a) x-axis scatter.

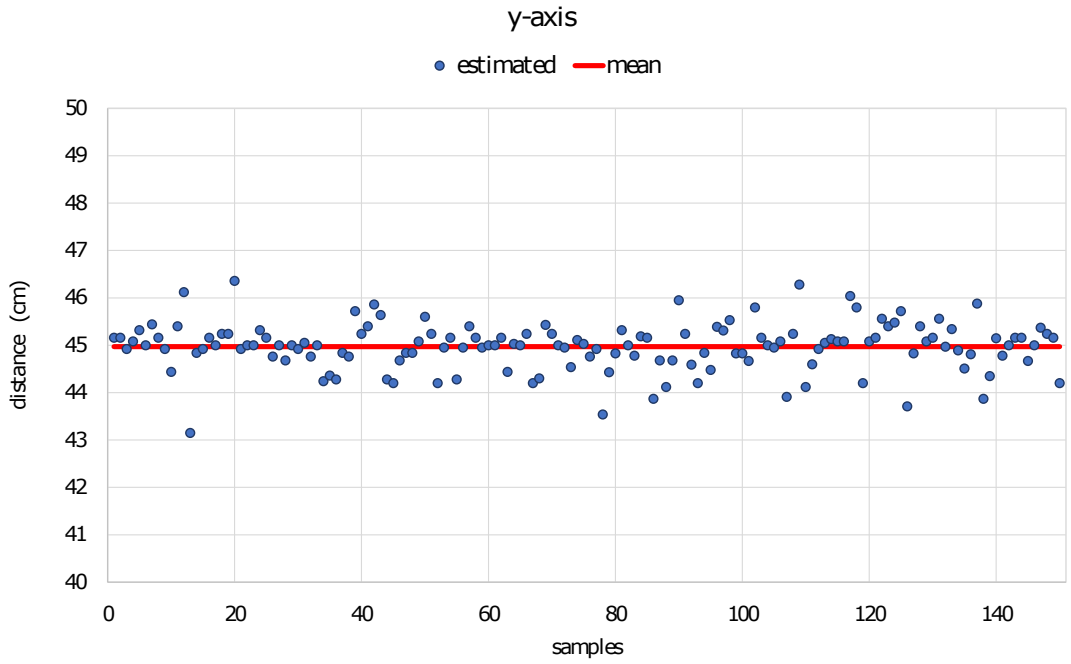

(b) y-axis scatter.

Figure F.3: Case A: First measurement of object number four (see Table 5.6).

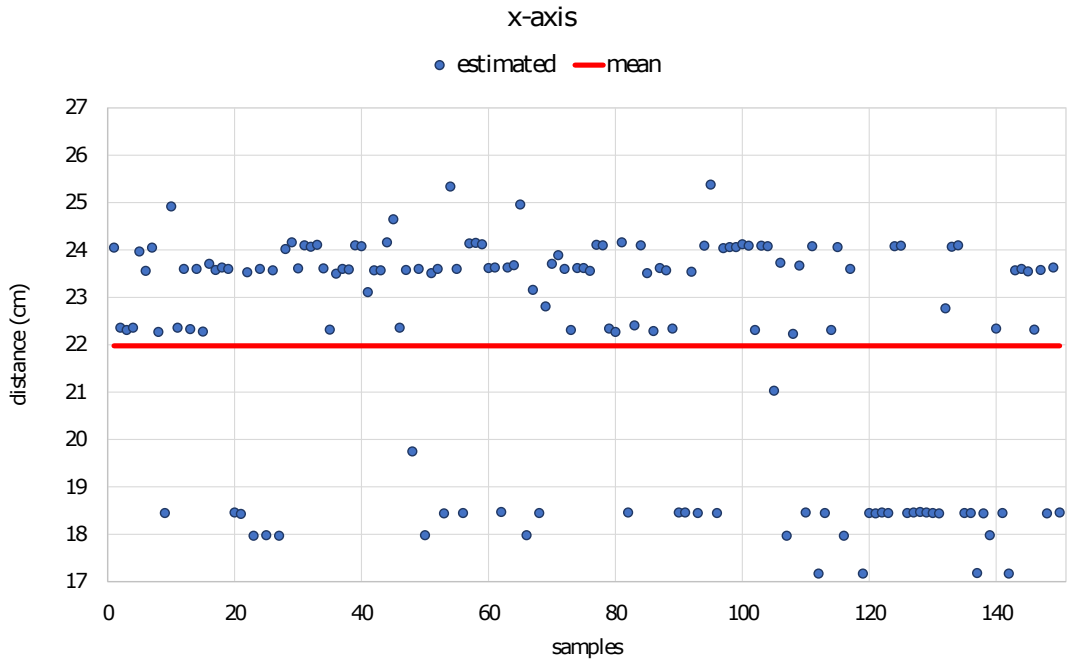

(a) x-axis scatter.

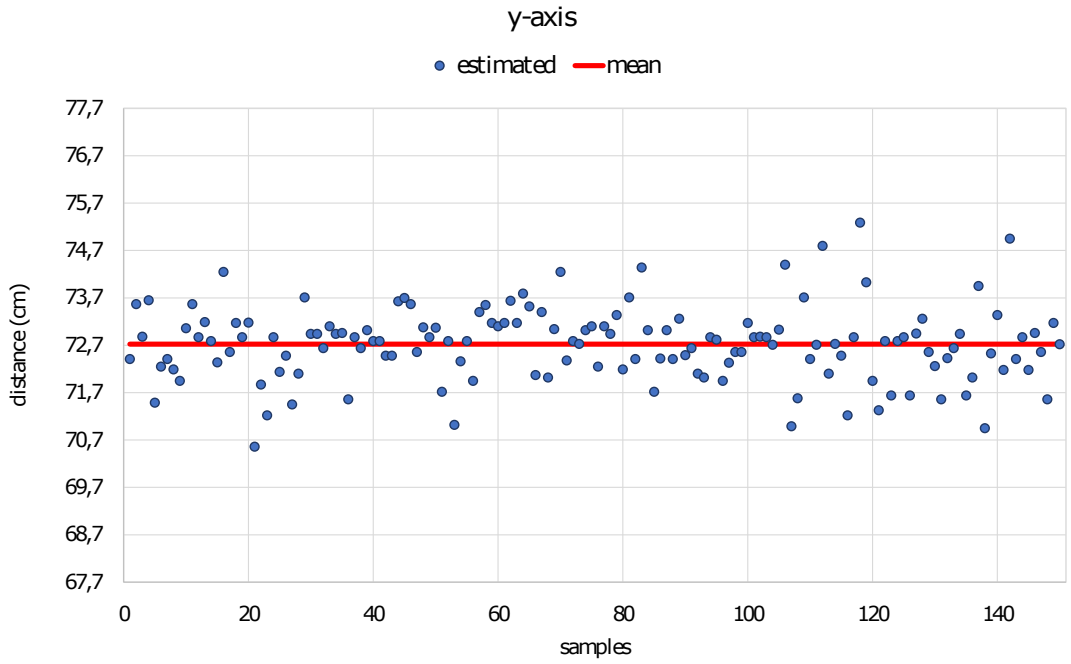

(b) y-axis scatter.

Figure F.4: Case A: Second measurement of object number four (see Table 5.6).

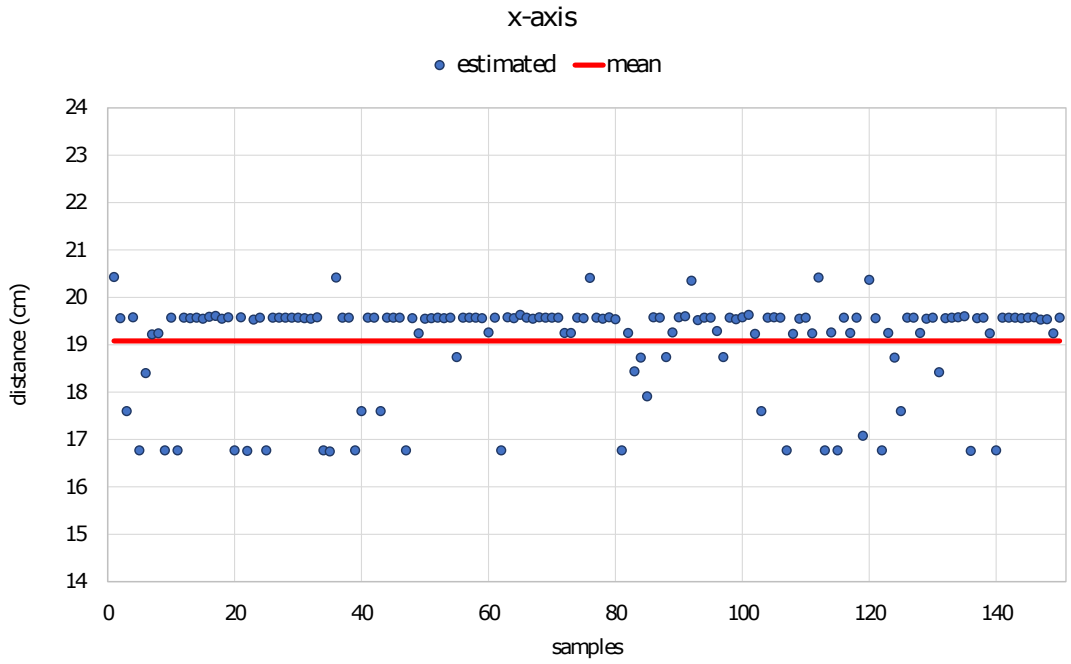

(a) x-axis scatter.

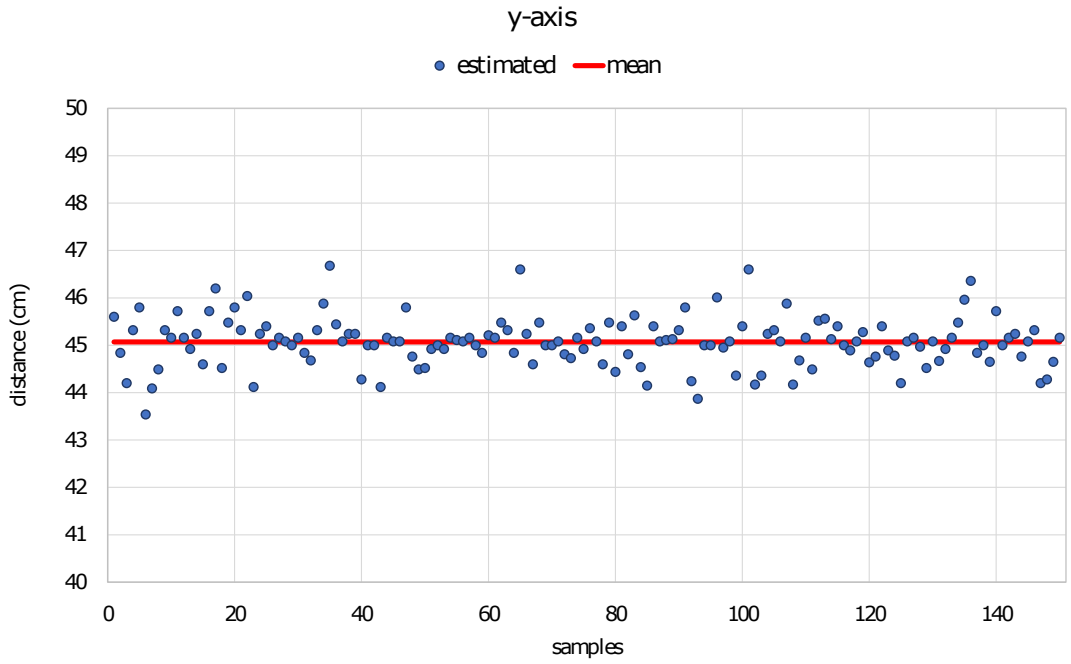

(b) y-axis scatter.

Figure F.5: Case A: Third measurement of object number four (see Table 5.6).

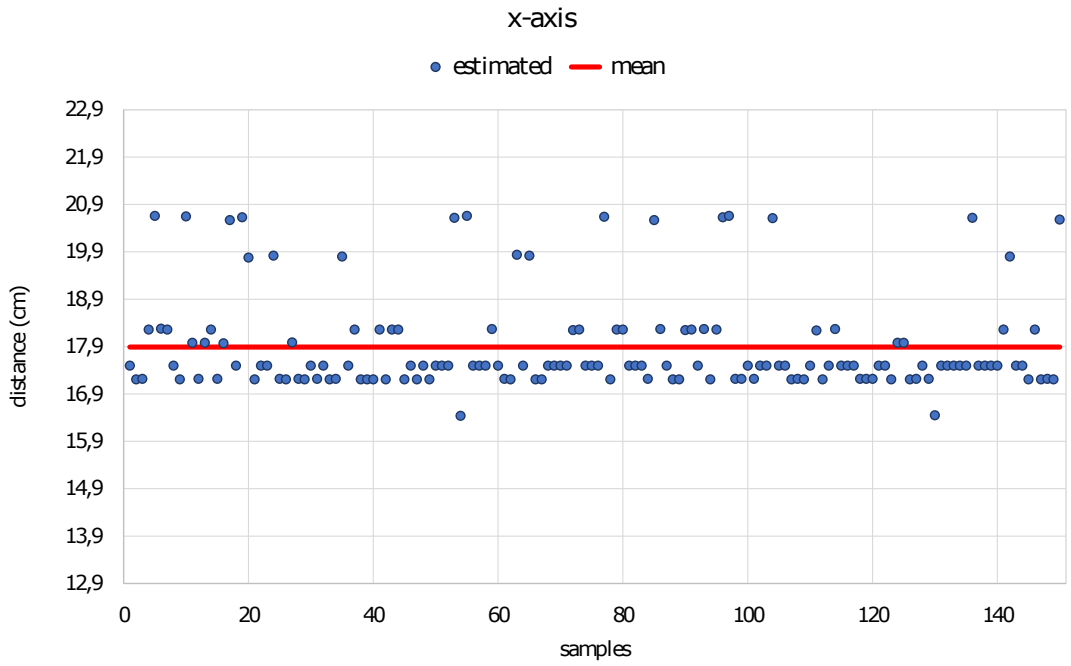

(a) x-axis scatter.

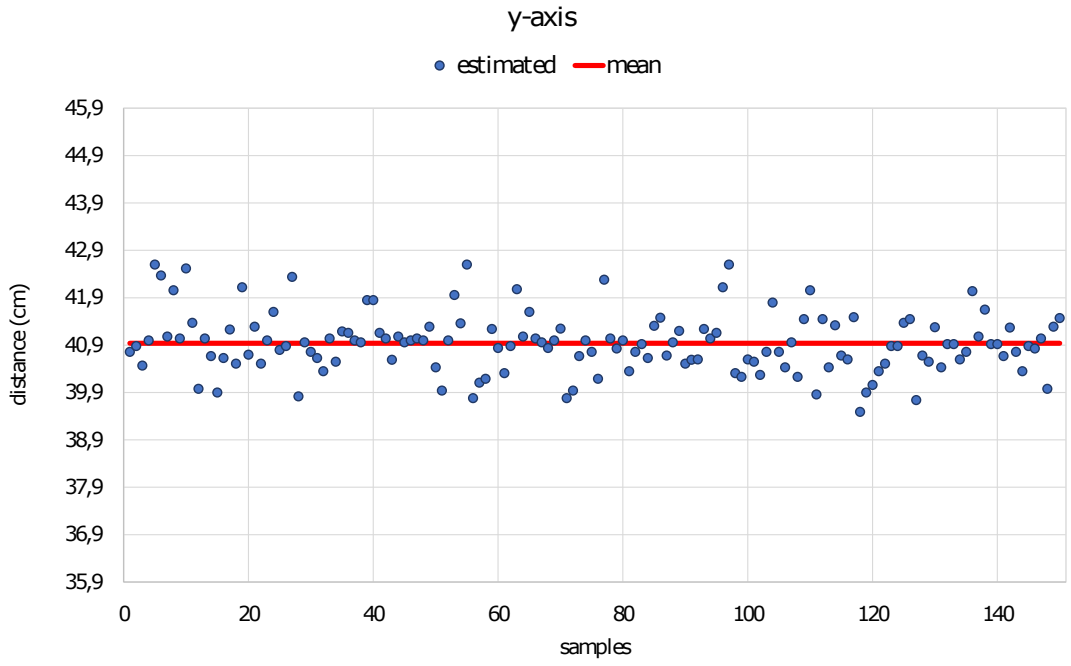

(b) y-axis scatter.

Figure F.6: Case A: Object number five positioned in center of the detection area.

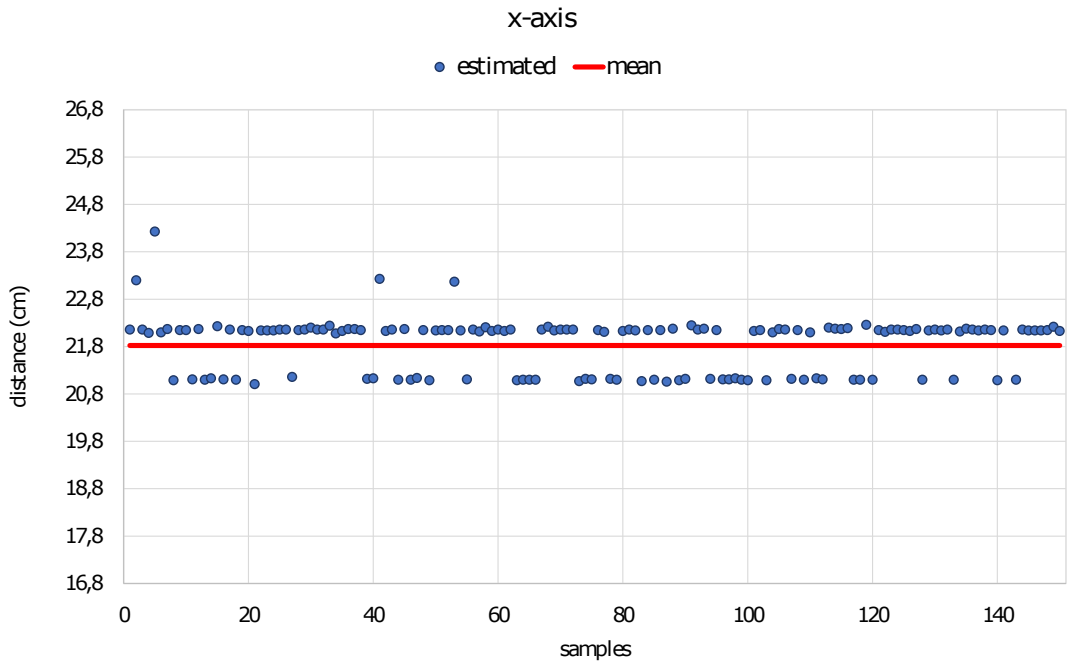

(a) x-axis scatter.

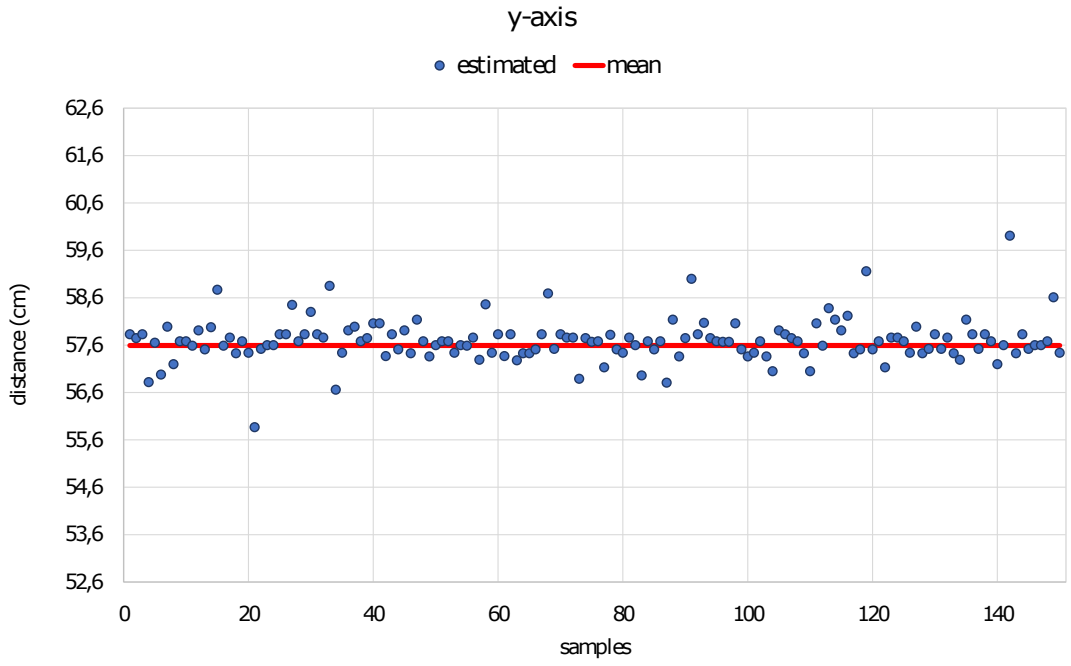

(b) y-axis scatter.

Figure F.7: Case A: Object number five positioned on right of the detection area.

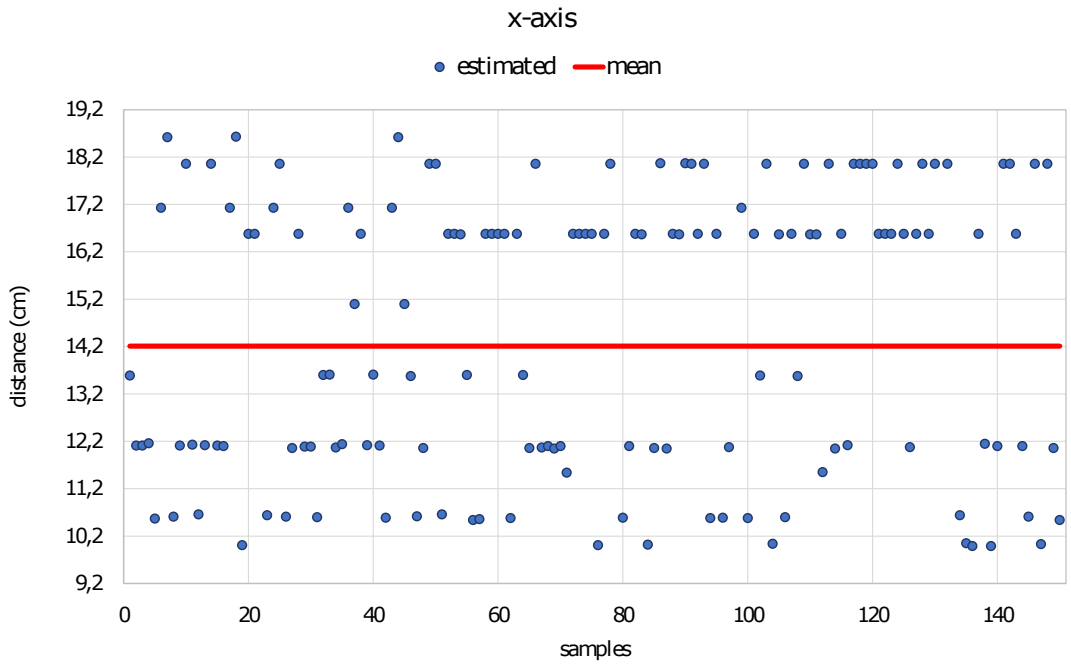

(a) x-axis scatter.

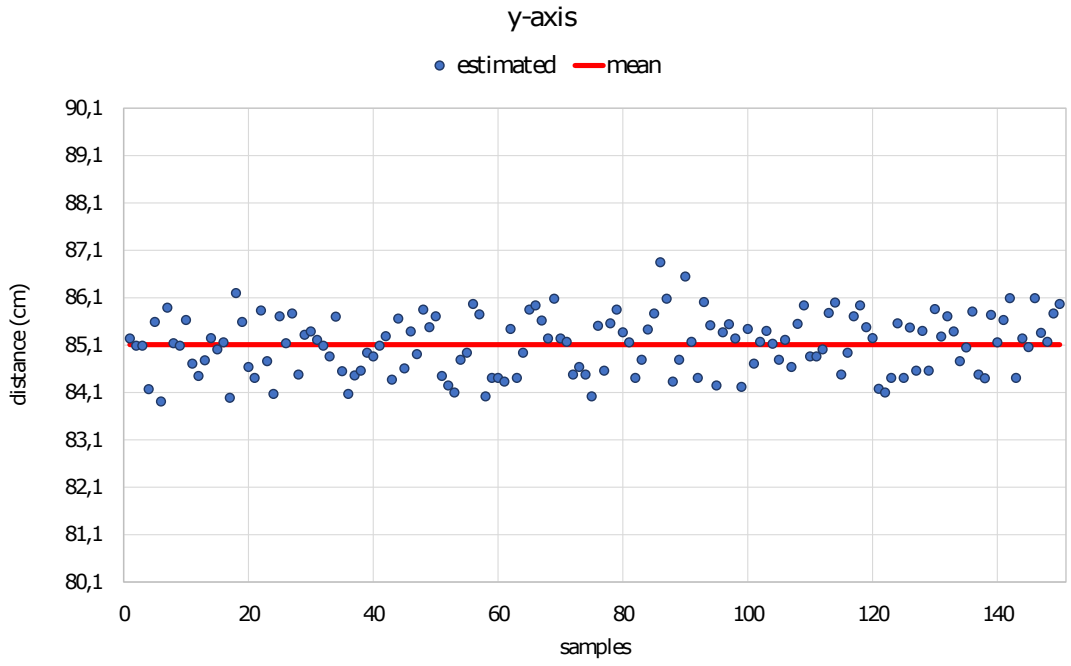

(b) y-axis scatter.

Figure F.8: Case A: Object number five positioned on left of the detection area.

Second Scenario

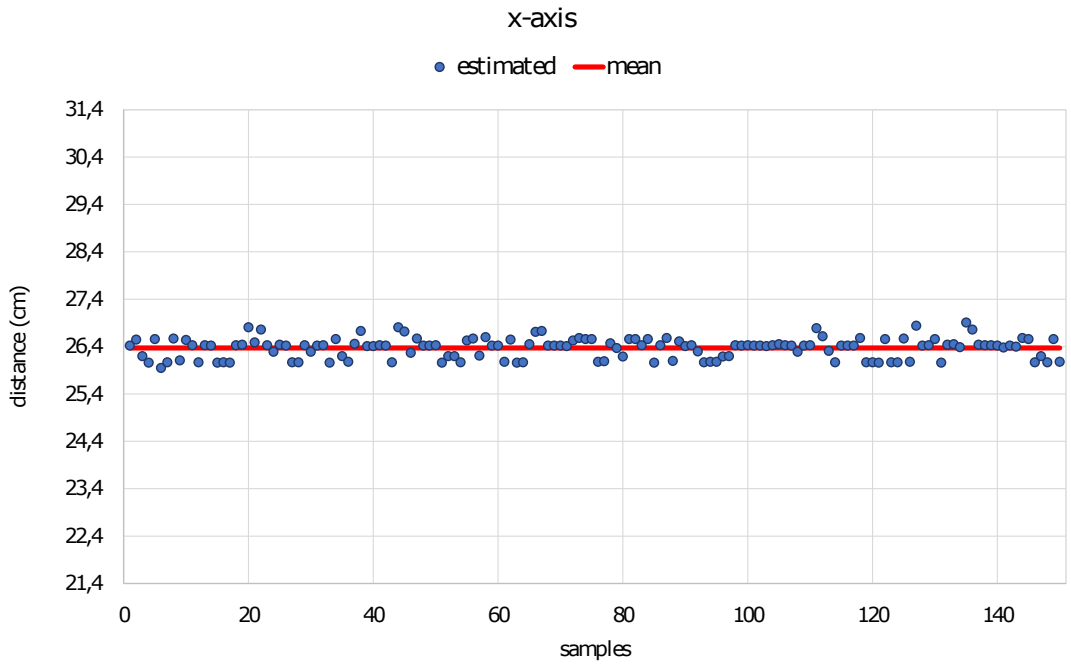

(a) x-axis scatter.

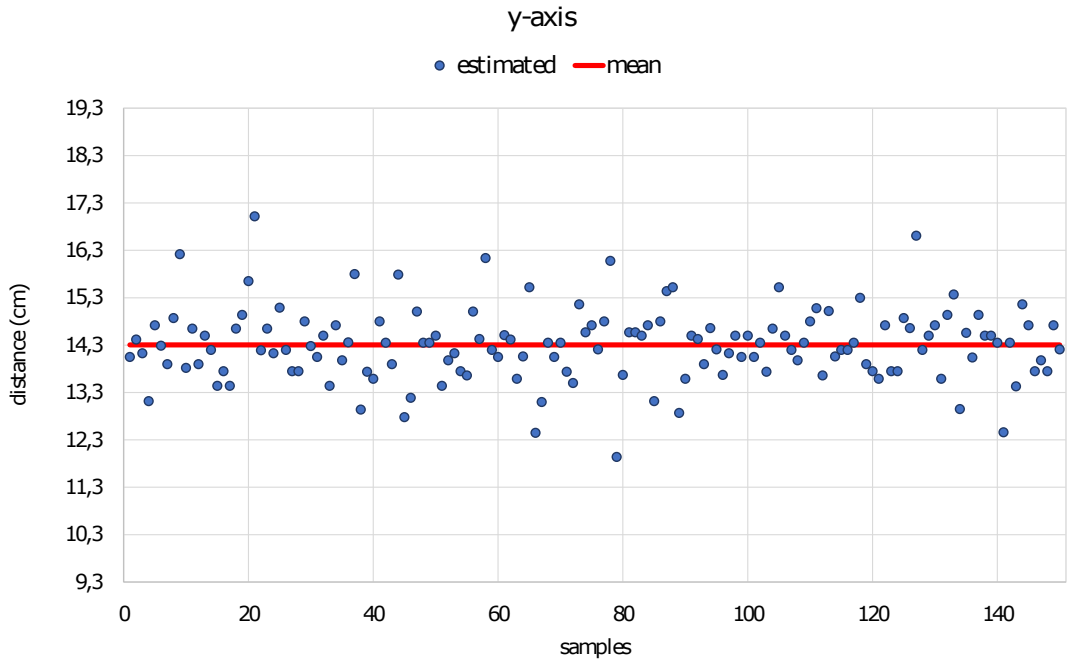

(b) y-axis scatter.

Figure F.9: Case B: Object number four positioned in center of the detection area.

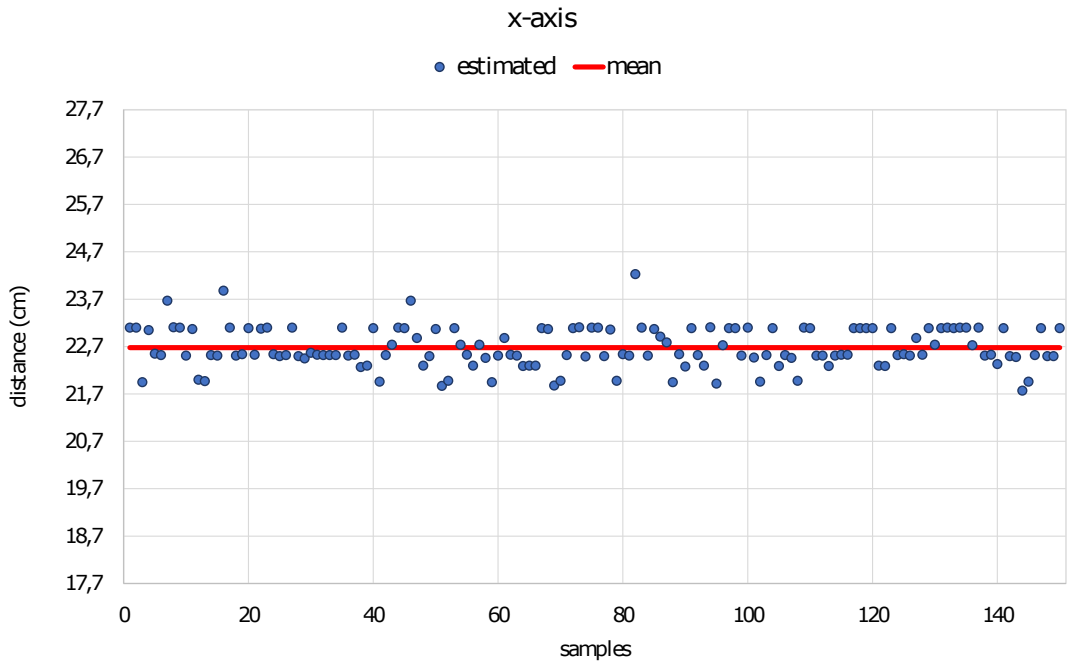

(a) x-axis scatter.

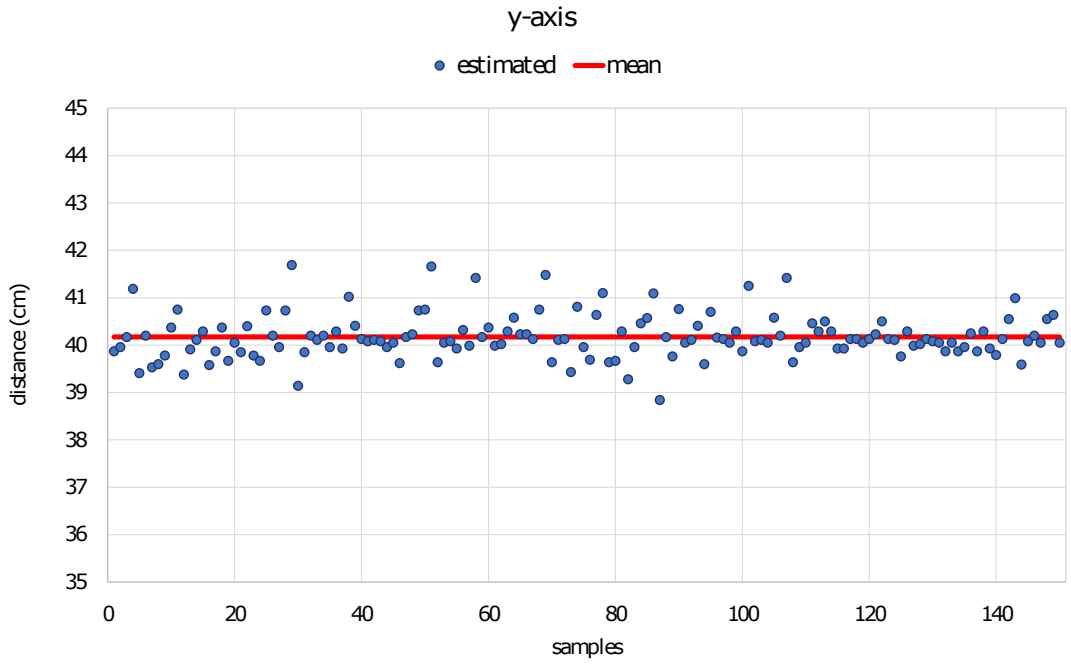

(b) y-axis scatter.

Figure F.10: Case B: Object number four positioned on left of the detection area.

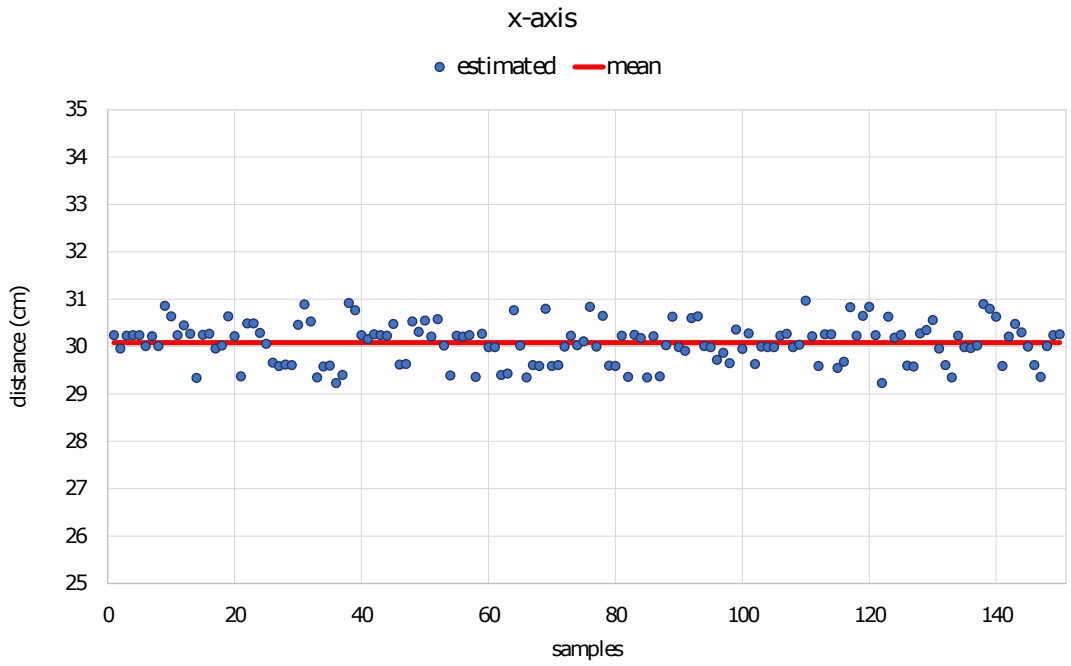

(a) x-axis scatter.

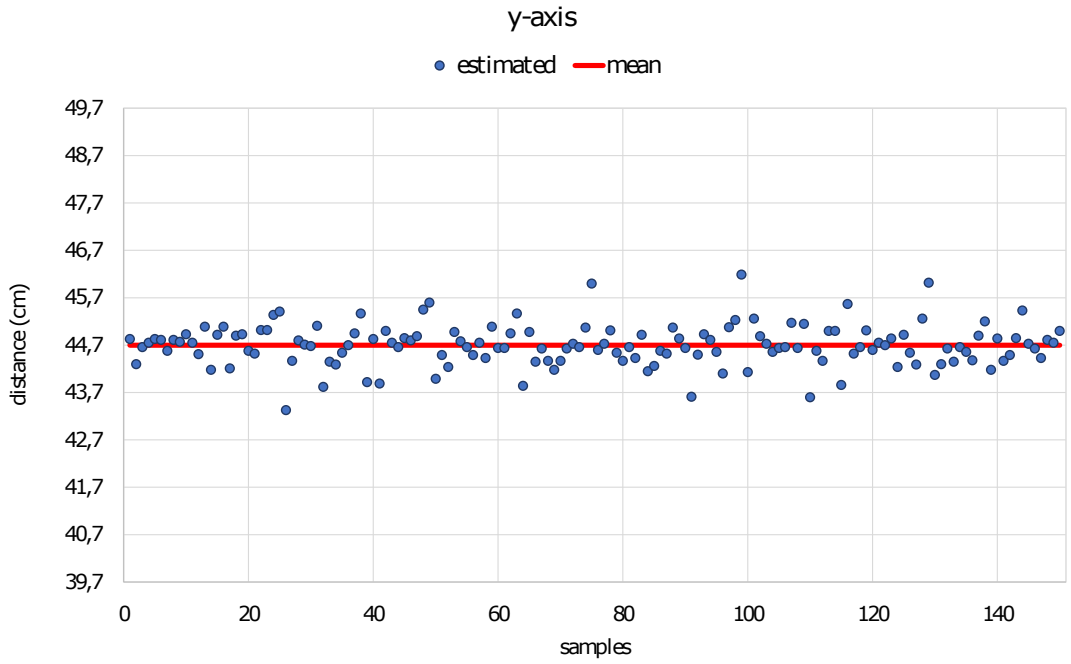

(b) y-axis scatter.

Figure F.11: Case B: Object number four positioned on right of the detection area.

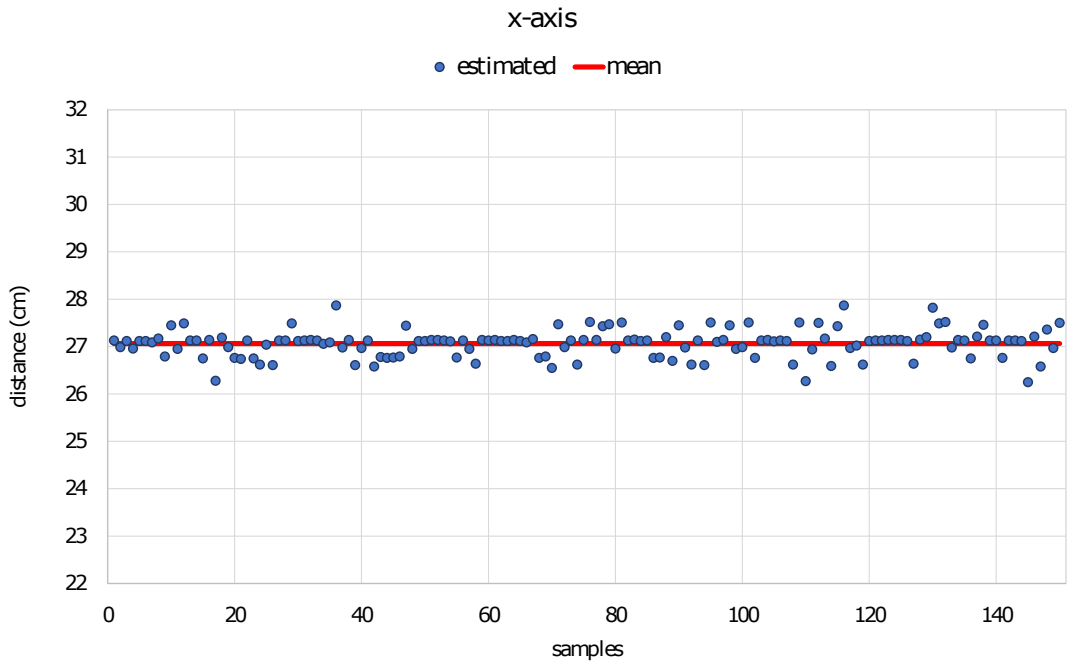

(a) x-axis scatter.

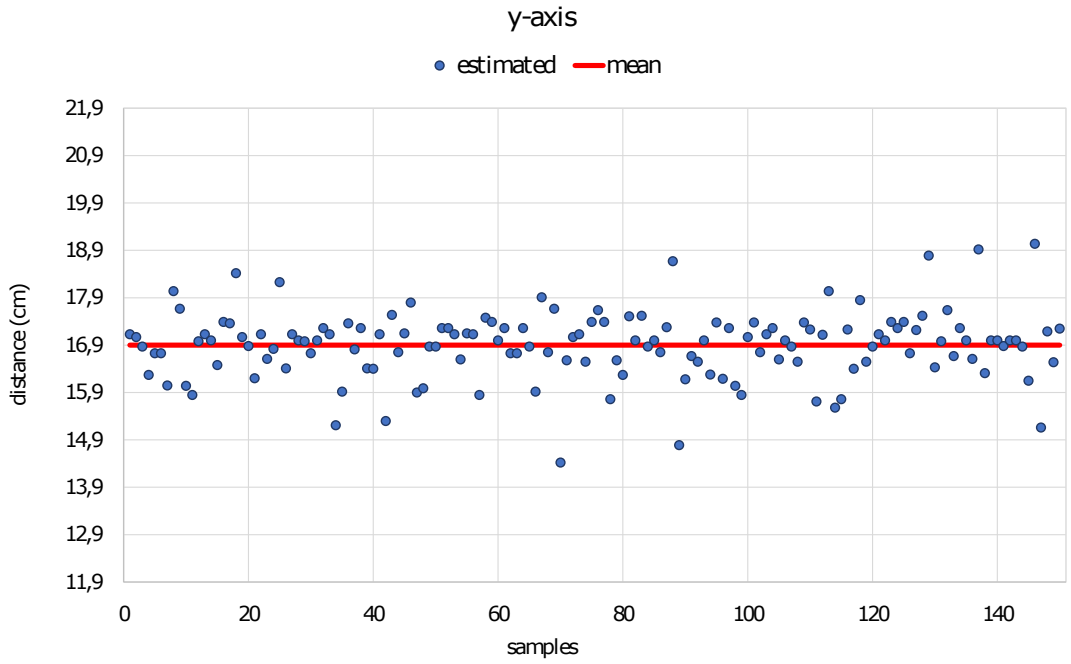

(b) y-axis scatter.

Figure F.12: Case B: Object number five positioned in center of the detection area.

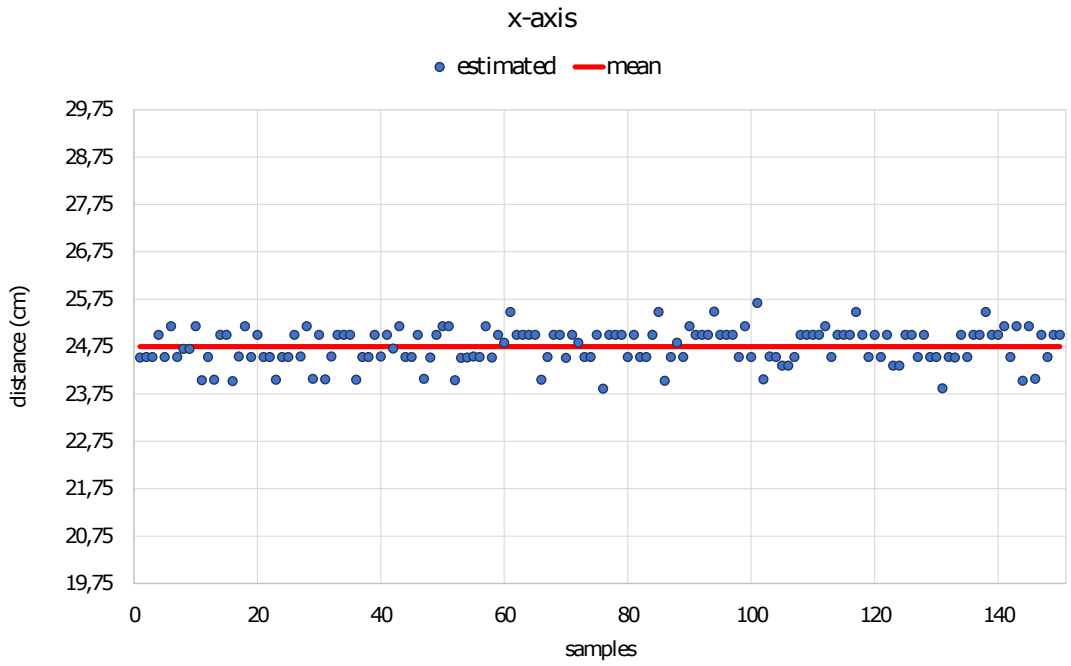

(a) x-axis scatter.

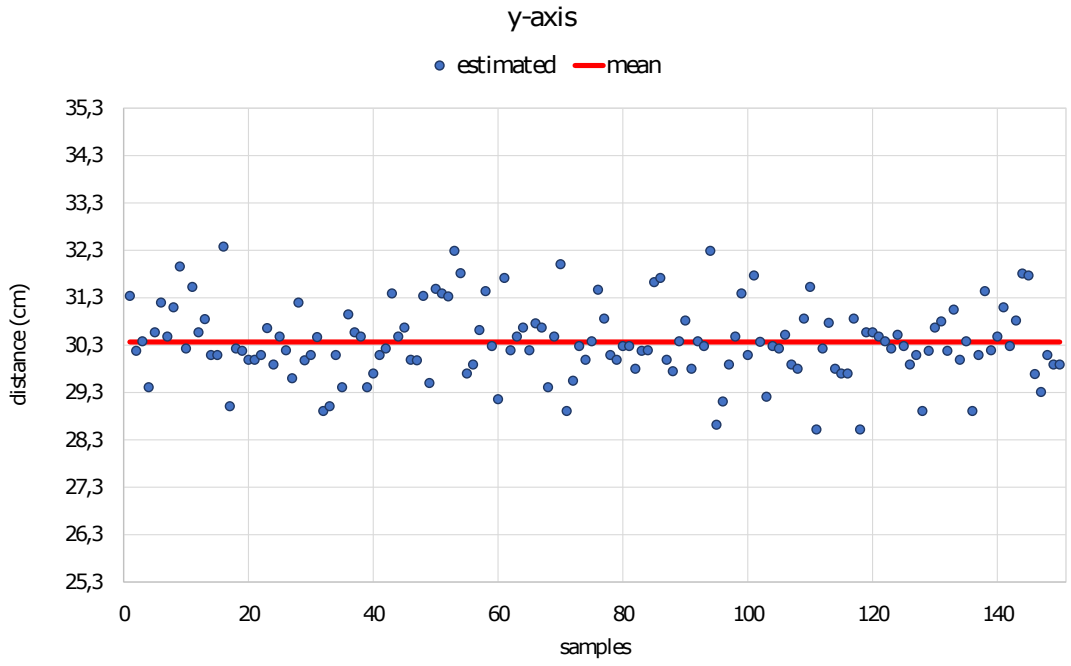

(b) y-axis scatter.

Figure F.13: Case B: Object number five positioned on left of the detection area.

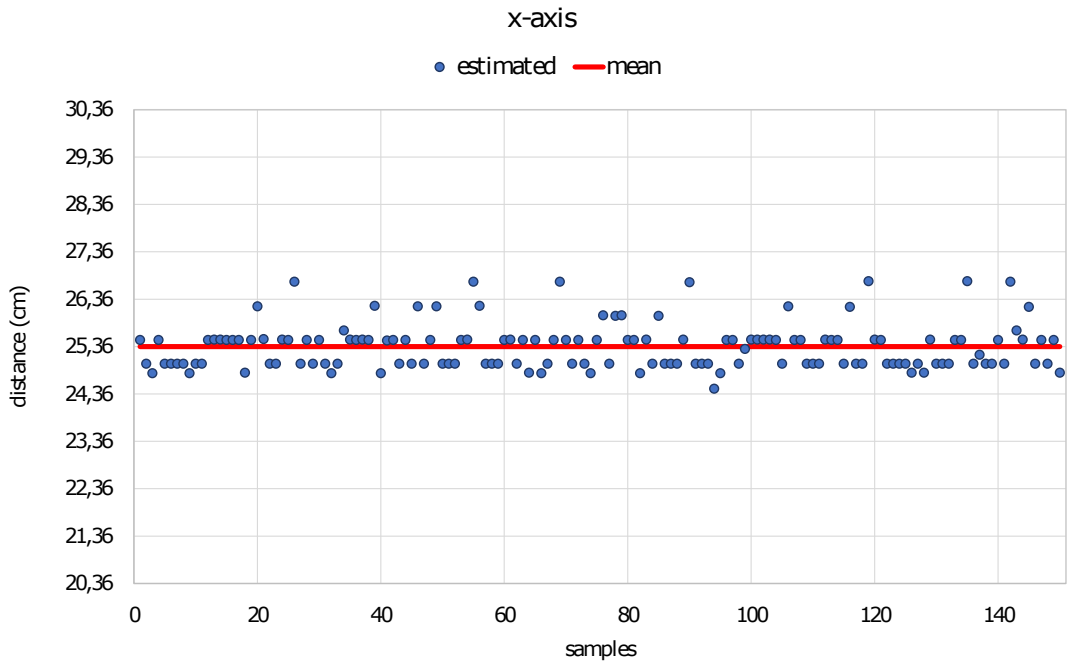

(a) x-axis scatter.

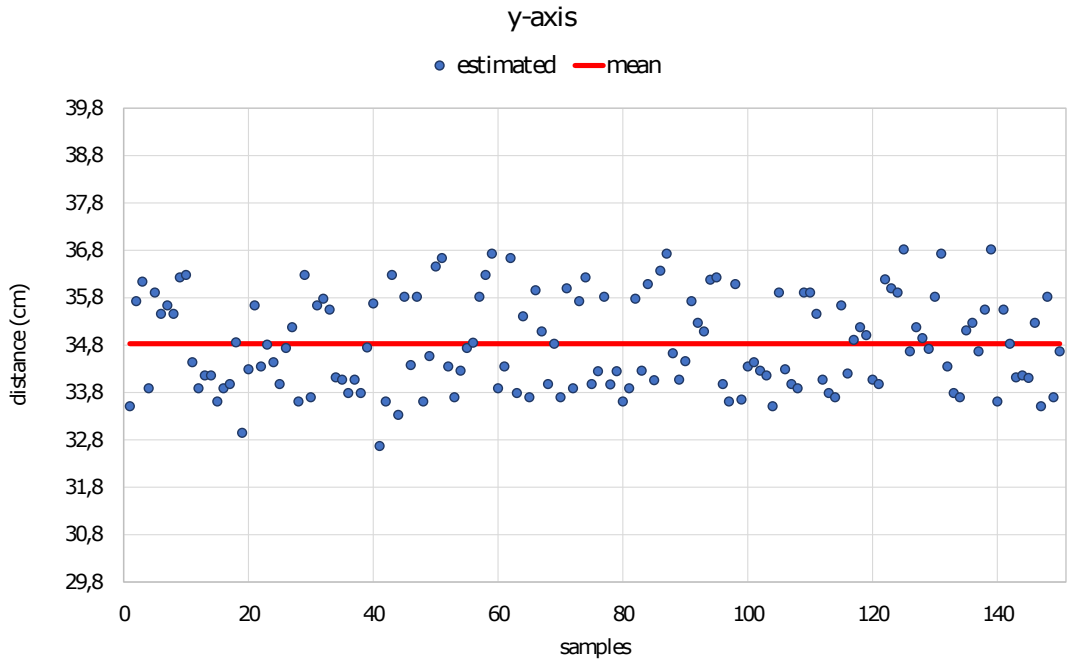

(b) y-axis scatter.

Figure F.14: Case B: Object number five positioned on right of the detection area.

Third Scenario

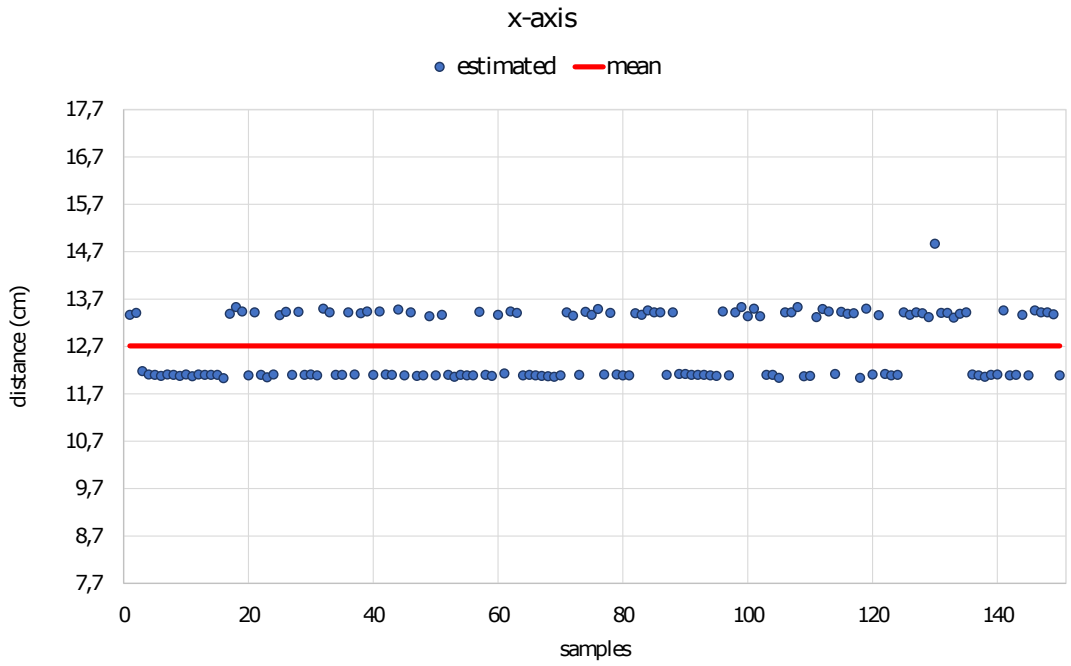

(a) x-axis scatter.

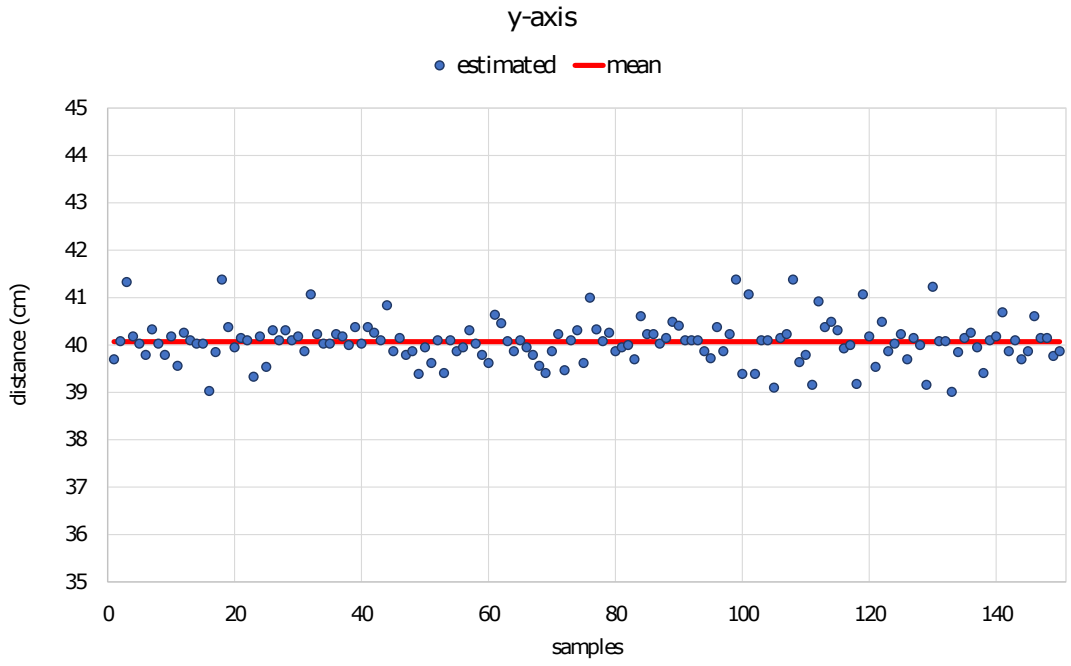

(b) y-axis scatter.

Figure F.15: Case C: First set of measurements referring to object number three (See Table 5.10).

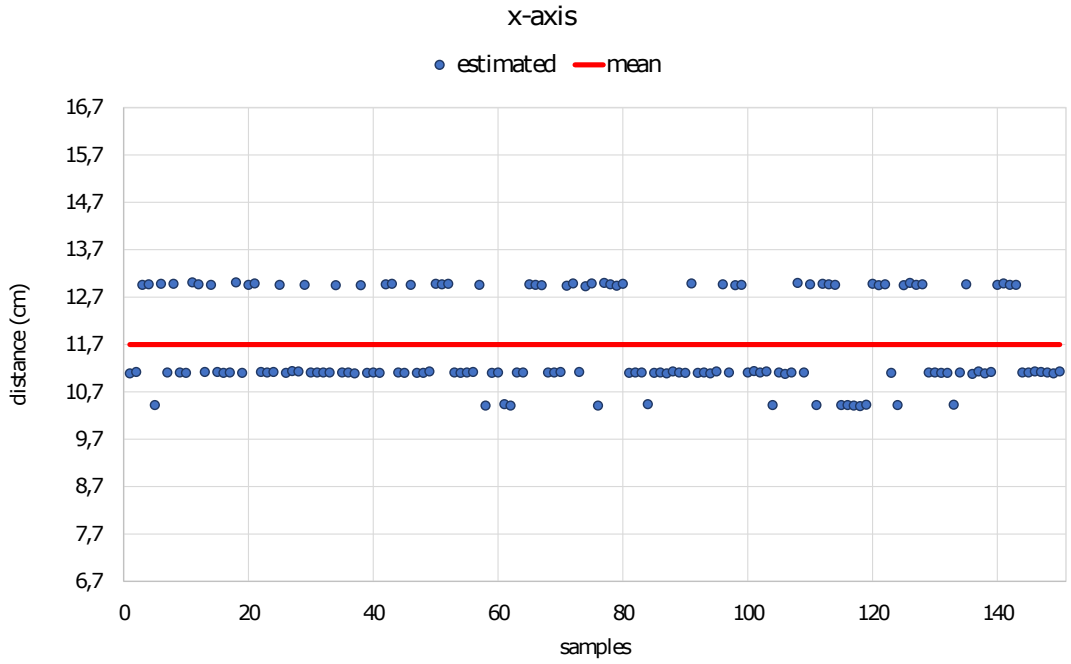

(a) x-axis scatter.

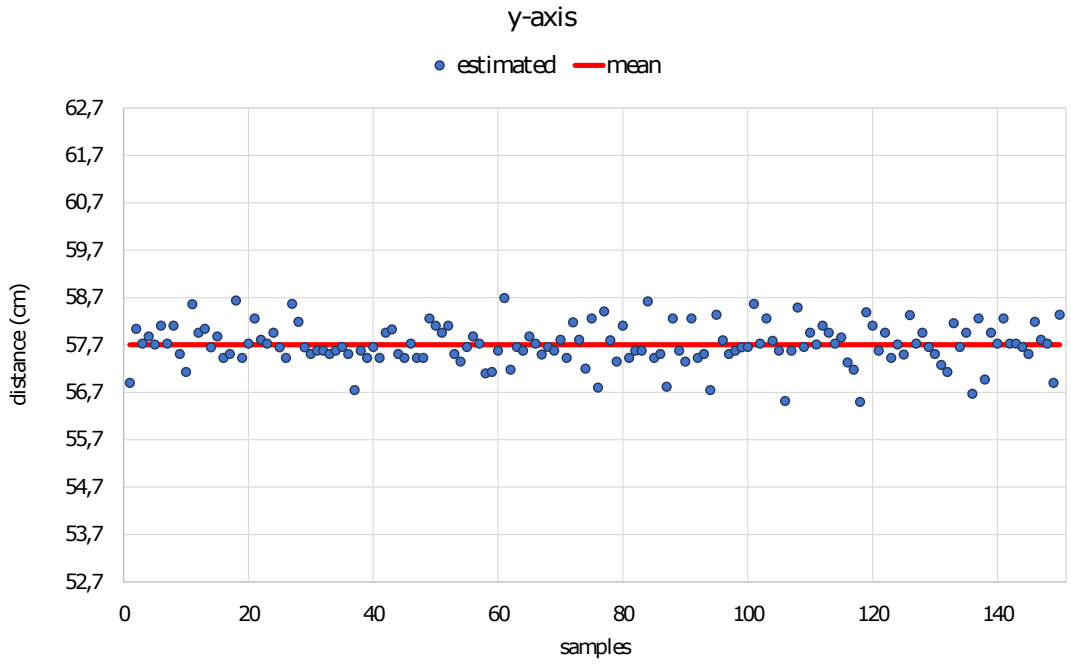

(b) y-axis scatter.

Figure F.16: Case C: Second set of measurements referring to object number five (See Table 5.10).

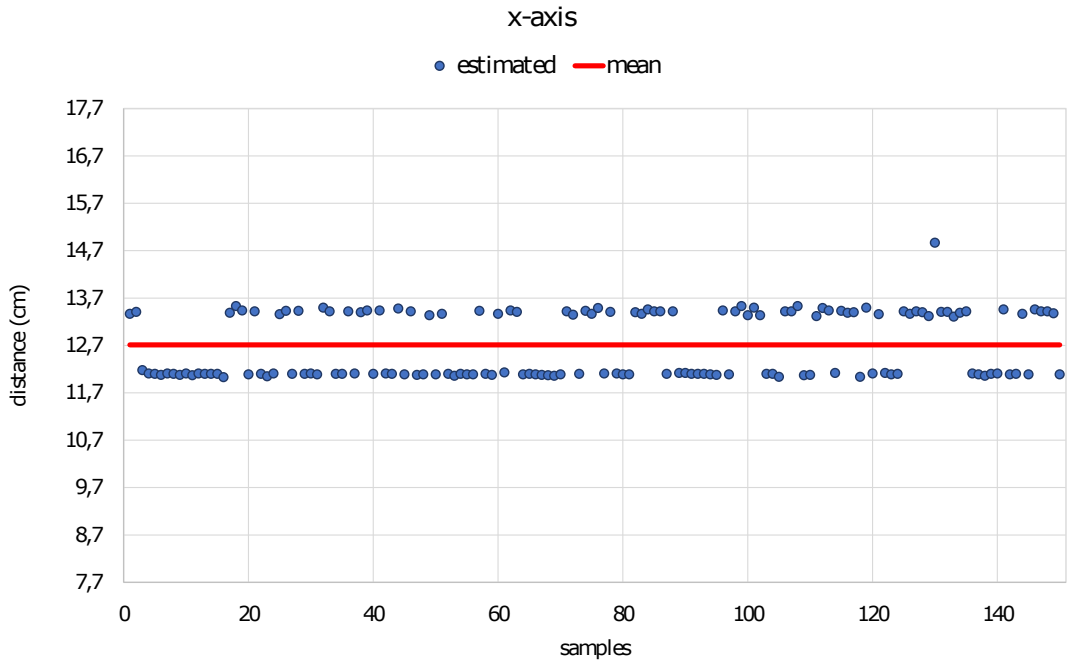

(a) x-axis scatter.

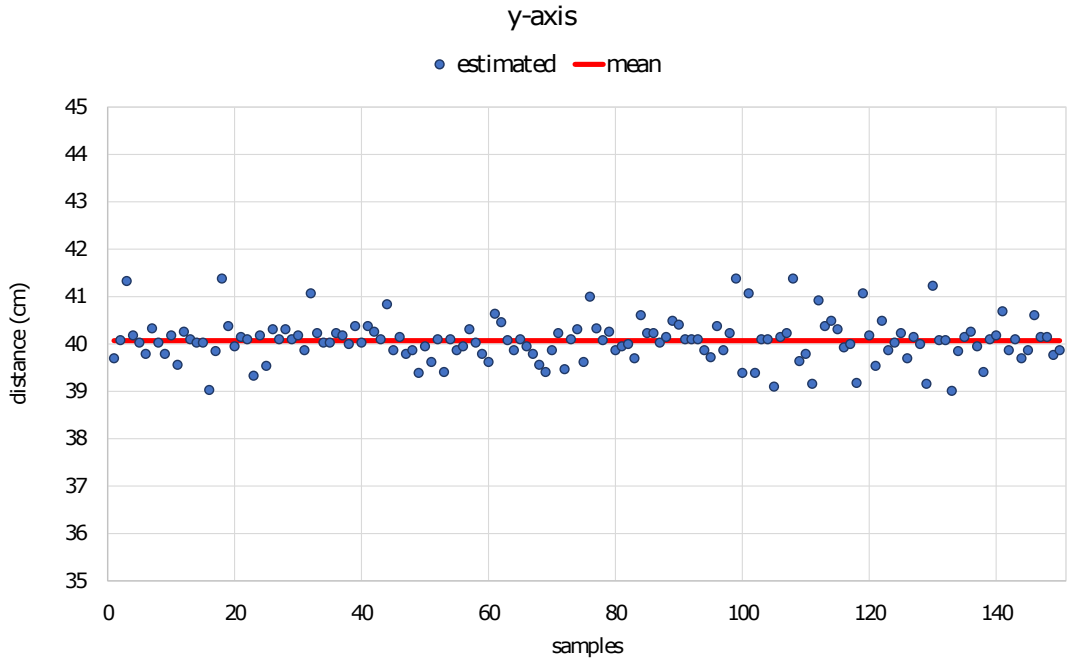

(b) y-axis scatter.

Figure F.17: Case C: Set of measurements referring to object number three closer to the system (See Table 5.11).

Appendix G

Architecture Proposal

Following is presented the technical drawing of the proposed physical structure with all dimensions in millimeter. Also, a sensor holder is designed.

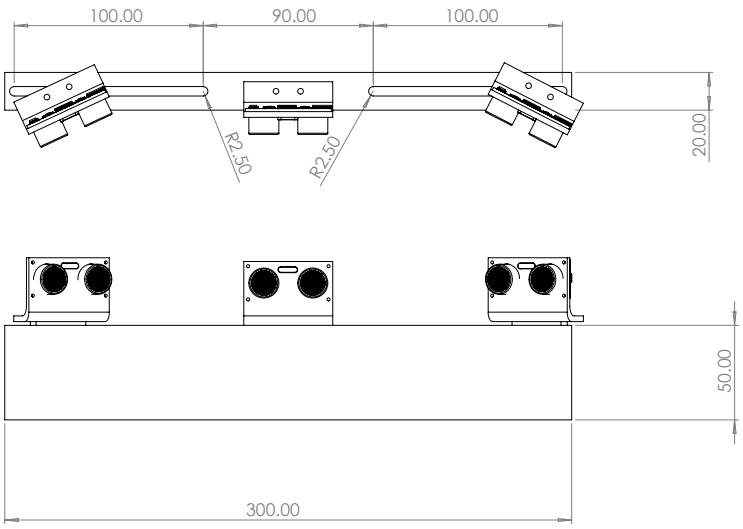

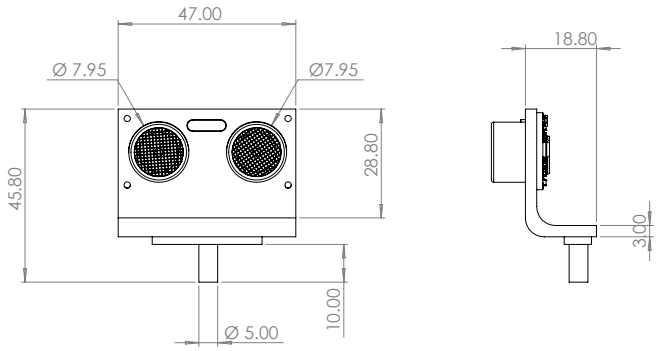
47.00
Ø 7.95
Ø7.95
45.80
28.80
10.00
Ø 5.00
18.80
3.00